

# Comments on the Review of Should wind turbines rotate in the opposite direction? - Reviewer 1

Antonia Englberger<sup>1</sup>, Julie K. Lundquist<sup>2,3</sup>, and Andreas Dörnbrack<sup>1</sup>

<sup>1</sup>German Aerospace Center, Institute of Atmospheric Physics, Oberpfaffenhofen, Germany

<sup>2</sup>Department of Atmospheric and Oceanic Sciences, University of Colorado Boulder, Boulder, USA

<sup>3</sup>National Renewable Energy Laboratory, Golden, Colorado, USA

**Correspondence:** Antonia Englberger (antonia.englberger@dlr.de)

Dear Dr. M. Paul van der Laan,

Thank you for taking the time to carefully review our paper. We read your review in detail and appreciate you sharing your own simulation results. Regarding your comments, we think there are several misunderstandings with the first version of the paper. Therefore, with the help of your comments, we performed some far-reaching changes to the manuscript. Here is a list of the major changes.

- We changed the title.
- We explained in detail the turbulence generation method we applied in the simulations.
- We included a section, introducing a simple analytical model predicting the expected changes in the spanwise velocity field in the wake by a superposition of a veering inflow with a Rankine vortex. (New section 3)
- We added additional simulations with different directional shears (including the  $0.12^\circ \text{ m}^{-1}$  value you applied in your simulation).
- We investigated the impact of the rotational frequency on the wake differences.
- We added additional plots, explaining the wake differences and its occurrence for different rotational direction of the actuator.
- We added a section comparing the numerical results predictions of the analytical model. This section explains in detail the source of the difference in the wakes between a clockwise and a counterclockwise rotating rotor in case of a veering inflow.
- We added an Appendix, verifying the application of the turbulence preserving method for this theoretical and idealized parameter study.

In the following we respond in detail to each of your comment/question.

The authors employ large-eddy simulations (LES) of a single actuator disk subjected to different stable atmospheric boundary layers to investigate the impact of the rotational direction on the potential downstream wind turbine power. The article has an interesting topic and I think it is worth publishing an in depth study about it.

We are pleased you think it is an interesting topic and it is worth publishing a detailed study about it. When we received the replies from the reviewers, we realized that we had insufficiently introduced the fairly new topic. The differences were only described and not thoroughly explained. We have corrected this oversight in the revised version.

However, I have four main concerns with this work.

First of all, the inflow is not a solution of the LES model, but simply set as an initial condition without any inflow turbulence.

This was a misunderstanding: In the paper we stated: 'A turbulent stably stratified regime in our wind-turbine simulations performed with open horizontal boundary conditions is verified by applying the parametrization of Englberger and Dörnbrack (2018). All parameters required to apply the parametrization are described in detail in Englberger and Dörnbrack (2018).' Instead, we should have explained the turbulent inflow in more detail rather than simply referring to a previous paper where this LES spin-up and inflow turbulence has been developed and successfully validated.

In the modified version we emphasized more clearly that inflow turbulence is applied on the leftmost boundary as a 2D slice at every time step. The inflow turbulence results from the turbulence parametrization of Englberger and Dörnbrack (2018), including turbulent fluctuations retrieved from a neutral boundary layer precursor simulation (Englberger and Dörnbrack, 2017) in combination with adjustable stratification-dependent parameters. In the modified version we explained this impression of turbulence on the inflow in detail (also adding the corresponding equation). Further we verify its applicability for this investigation. In the appendix we further show that the occurrence of a difference between a clockwise and a counterclockwise rotating actuator does not depend on the applied turbulence intensity, only that the degree of the differences is modified by the turbulent intensity. The difference in the flow pattern (amplification of spanwise flow in case of counterclockwise rotating rotor and weakening/reversion in case of clockwise rotating rotor under veering inflow in the NH) only depends on the mean inflow profile and the vortex component of the wind turbine.

In addition, the applied inflow turbulence impacts the wake recovery and the resulting velocity deficit of  $\approx 0.45$  at a downstream distance of  $7D$ . If these simulations had laminar inflow, as we think your comment suggests, the wake would persist much longer.

Secondly, the methodology of quantifying the impact of the rotational direction of the rotor on a downstream wind turbine is not sufficient and the reported gains in power are misleading because they only reflect a few specific cases that are rare with respect to all the flow cases that are typically present in an annual energy production calculation of a wind farm.

The reviewer identifies two issues: the first concerning the methodology and second that these impacts are rare. Regarding the first issue, we changed the selection of considered cases in comparison to the previous version. Further we introduce the

expected results by simple analysis (superposition of spanwise component of veering inflow with Rankine vortex) in a new Section 3 and compared the simulation results to the analytical expectations (new Section 5), to make the manuscript more consistent. In the revised version, we considered cases of changing the atmospheric inflow (geostrophic wind, directional shear) and the rotational frequency of the rotor. All other simulation results from the previous manuscript version are eliminated to be more consistent. With including the expected results in the analysis section (3) and comparing the simulation results to them (section 5), we hope we have proven that our methodology is now sufficient and consistent.

Regarding the second issue, we agree with the reviewer that we specifically only considered an inflow from west to east in the northern hemispheric mid-latitudes  $270^\circ$  at hub height. Because this is an idealized study attempting to understand if this effect is significant in any case, we focused on this idealized inflow scenario and varied the impact factors (geostrophic wind, directional shear, rotational frequency) to investigate the impact of each of them on the difference in the wake structure between clockwise and counterclockwise rotating actuators.

It is quite common for idealized studies to focus on specific wind conditions to understand specific phenomena, and here we explore the difference of the rotational direction impact on the wake under veering inflow conditions. We certainly do not claim to address all relevant flow cases for the annual energy production calculation in a wind farm. The considered cases in our study (regarding the geostrophic wind speed and the directional shear) are chosen from measurement papers like Walter et al. (2009), Sanchez Gomez and Lundquist (2020), ?, and Bodini et al. (2020). Of course, the measurement results are location specific. We considered three different measurement campaigns, including offshore measurements e.g. 13 months of lidar measurements in Massachusetts in (Bodini et al., 2020), as well as onshore measurements e.g. covering 3 months of lidar observations in north-central Iowa in Sanchez Gomez and Lundquist (2020) and two years of meteorological tower observations in Lubbock (Texas) in Walter et al. (2009). From these measurements we extracted the frequency of occurrence of veering vs. backing and likewise the frequency of occurrence of specific wind speeds and directional shears. In the introduction, we added a paragraph pointing out that our values are chosen in relation to these three measurement campaigns and that the percentage of occurrence of veering or specific wind speed or directional shear values is location dependent.

Maybe the reviewers reaction is related to the simple title of the study, 'Should wind turbines rotate in the opposite direction?'. This question was chosen as title for the paper as it is simple and interesting and for motivation to consider this issue. But we agree with the reviewer that our paper cannot give an answer to this question considering all relevant cases in a wind farm over a year or at any location on earth. Therefore, we change the title of our manuscript to 'Changing the rotational direction of a wind turbine under veering inflow: A parameter study.'

[Thirdly, the information provided in the article is not sufficient to redo the simulations and understand the presented results.](#)

Thank you for the comment. We listed all data to the best of our knowledge in the previous manuscript:

- $512 \times 64 \times 64$  grid points
- horizontal and vertical resolution of 5 m
- open horizontal boundaries

- 40 min simulation time
- $D = z_h = 100$  m
- inflow profiles of  $u, v, w, \theta$  in Eqs. 4, 5, 7, 8
- wind veer profile in Eq. 6
- BEM with scaled wind turbine (here we refer to Englberger and Dörnbrack (2017, parametrization B))

A detailed listing of all main properties of the simulations are given in Table 1 (wind speed, directional shear both determining the mean inflow wind field and the rotational frequency determining the strength of the vortex)

For more complex simulation inputs (wind-turbine parametrization, turbulence preserving method), we referred to previous papers where all details are listed and the method are validated and explained:

- the wind-turbine parametrization including rotor properties
  - 'A detailed description of the wind-turbine parametrization and the applied smearing of the forces, as well as all values used in the blade parametrization are given in (Englberger and Dörnbrack, 2017, parametrization B).' (See Table 5 of Englberger and Dörnbrack (2017))
- the turbulence preserving method
  - 'A turbulent stably stratified regime in our wind-turbine simulations performed with open horizontal boundary conditions is verified by applying the parametrization of Englberger and Dörnbrack (2018). All parameters required to apply the parametrization are described in detail in Englberger and Dörnbrack (2018).' (See Table 1 of Englberger and Dörnbrack (2018))

In the revised version we included the following additional information:

Regarding the wind-turbine parametrization we extend the explanation, but only concisely. For more details about the parameters and applied calculation of  $F_{WT}$  from Eq. 1 we refer to Englberger and Dörnbrack (2017, parametrization B). However, we added now the very simple analytical equation showing the same effect of amplification or reduction/reversion of the spanwise wake component. Therefore, the occurrence of the effect does not depend on the turbine type, rotor diameter, radial distribution of the forces. But of course they impact the strength of the effect. As this is a parameter study, not referring to a specific wind turbine, location etc. we did not change our wind-turbine. However, we include the turbine impact by changing the rotational frequency of the rotor to show the sensitivity to the strength of the vortex in the analytical section 3 and also the numerical simulation section 4.

Regarding the turbulence preserving method, we added a much more detailed description (see comment above).

Finally, I disagree with the main conclusion. I provided an Appendix where I have performed Reynolds-averaged Navier-Stokes simulations of two NREL-5MW wind turbines with 7D spacing subjected to an atmospheric inflow with a strong wind veer. I also see a relatively large impact of the rotation direction on the power output of the downstream wind turbine for a

specific wind direction. However, my simulations suggest the opposite of the present paper, where a clockwise rotating wind turbine in the Northern Hemisphere performs better than a counter-clockwise rotating wind turbine (subjected to a strong wind veer).

We really appreciate your effort of performing the simulations and your generosity in sharing your results. However, we do not agree with your statement that your results disagree with ours. We performed simulations with a veering over the rotor of  $0.04^\circ \text{ m}^{-1}$ ,  $0.08^\circ \text{ m}^{-1}$  and  $0.16^\circ \text{ m}^{-1}$ . According to our simulations, a counterclockwise rotating rotor results in a higher downstream velocity at 7 D in case of  $0.04^\circ \text{ m}^{-1}$  and  $0.08^\circ \text{ m}^{-1}$ . In case of  $0.16^\circ \text{ m}^{-1}$  a clockwise rotating wake has a higher downstream velocity at 7 D in comparison to a counterclockwise rotating one. Your simulation investigated it for a directional shear of  $0.12^\circ \text{ m}^{-1}$  over the rotor with the same result as our  $0.16^\circ \text{ m}^{-1}$  simulation. Therefore, we think your simulation results did not disagree with our results for the strong wind veer case.

To focus on the impact of the directional shear, we added a simulation with a directional shear of  $0.12^\circ \text{ m}^{-1}$ , corresponding to the directional shear you applied in your simulation, and likewise a simulation with a very high directional shear of  $0.20^\circ \text{ m}^{-1}$  to point out the impact of the directional shear on the results. Please see Fig. 7, 10, 11, 12, and 13 in the revised version representing the results. According to our results, for low values of the directional shear ( $0.04^\circ \text{ m}^{-1}$ ) the rotor and time averaged downwind velocity  $\overline{u_A}$  at 7 D is larger for a counterclockwise rotational direction in comparison to a clockwise one. For very high values of the directional shear ( $0.20^\circ \text{ m}^{-1}$ ) the opposite is the case. In between, there is a directional shear values with no difference in  $\overline{u_A}$  between clockwise and counterclockwise rotating actuators. According to our results (and thanks to the added simulations in the new manuscript), this is the case for a critical directional shear value  $ds_c$  with  $0.12^\circ \text{ m}^{-1} < ds_c < 0.16^\circ \text{ m}^{-1}$ . The specific value of  $ds_c$  of course depends on the turbulent intensity, the rotor diameter, the radial distribution of the forces, the wind-turbine type, the resolution, etc. But regarding the result of  $ds_c$  very close to your result with a directional shear of  $0.12^\circ \text{ m}^{-1}$ , the deviation is not unexpected for us. Especially regarding the main difference, you considered two wind turbines and we consider the available power in the wind. But also further differences, smaller geostrophic wind, different size of the WT, different radial distribution of the forces, different turbulence applied as inflow condition. Therefore, your results did not show a different result of the complete rotational direction under veering inflow topic. On the contrary, we think it supports our results. It also supports our assumption that the difference is related to the mean inflow fields as predicted by the analysis, as your result is very similar to ours despite all the differences in the atmospheric conditions (different geostrophic wind, turbulence method) and the wind turbine (rotor size, radial distribution of the forces, different rotational frequency).

This is because the initial horizontal wake deflection for clockwise rotating wind turbine (without the effect of wind veer but including a wind shear) is clockwise (as seen from above). The counter-clockwise rotating wake brings fresh momentum from above towards the right side of the wind turbine, which results in a stronger deficit on the left side, and this causes the wake to deflect clockwise as seen from above, as shown by Zahle and Sørensen (2008). The addition of wind veer in the Northern Hemisphere deflects the wake even more clockwise, which is also shown in van der Laan and Sørensen (2017).

We agree with your comments here, but they are valid in case of no veering wind, as you stated. We also apply this explanation in the work Englberger et al. (2019), explaining the difference between clockwise and counterclockwise rotating actuators in the evening boundary layer in case of no wind veer. Regarding the wake deflection in dependence of the rotational direction of

the rotor in combination with veering inflow, our results show that the wake deflection is larger in case of a counterclockwise rotating disc interacting with veering inflow, independent of the atmospheric parameters directional shear and wind speed. We explain this with the amplification of the spanwise flow component in the wake in case of a counterclockwise rotating rotor, resulting in a larger wake deflection in comparison to the weakening or even reversion which occurs in case of a clockwise rotating actuator.

Hence, I disagree with the authors conclusion. I have written a list of main and minor comments below. Since there are so many major concerns, I am afraid that I have to reject the article.

Regarding all the misunderstandings (insufficient description of turbulence generation method instead only referring to the corresponding paper, misleading title in a way we did not anticipate, misinterpretation of your simulation results with our results due to application of a directional shear value with is close to the critical value we detect in our results) we understand your recommendation to reject the previous version of this article. Your comments were really helpful to us to eliminate the misunderstandings via including a detailed description of the turbulence generation method applied, changing the title of the manuscript, adding additional simulations helping to narrow down the critical values of the directional shear, including the simple analytical equation which explained the differences seen in the simulation. Considering the extensive revisions in the presentation of the results we performed in this revised version, we hope we have addressed your concerns.

In the following we refer to your main comments:

1. Why do use a scaled down version of the DTU-10MW wind turbine? Wouldn't it be easier to either use the NREL-5MW wind turbine or the original DTU-10MW wind turbine (which is an upscaled version of the NREL-5MW wind turbine)? These reference wind turbines are made to make a comparison between scientific literature in wind energy more fair, and using a reference wind turbine allows other researchers to redo your simulations more easily.

We understand your point here. Our attempt was to apply the flow field modifications of a generalized wind turbine with a rotor diameter as well as a hub height of 100 m. As it is a parameter study, it is not related to a specific turbine, location, etc. In the revised version we also add the analytical model, which explains the difference and also that they are not turbine dependent (also occurring for a rather simple Rankine vortex).

Page 4, Line 26: Here you mention that you set different magnitudes of wind veer over the rotor area. How do you set these magnitudes? It seems that you specify them according to an initial profile from Eq. (6), without changing the physical parameters that actually influence the wind veer, i.e. the Coriolis parameter or geostrophic wind (for a constant inversion strength and atmospheric stability). If this is the case then all simulations will converge to the same wind veer if you run them long enough unless you have periodic conditions on all four lateral boundaries.

Here is a misunderstanding. We do not prescribe specific inflow profiles in a precursor simulation extending it until it reaches an equilibrium state, therefore, our results will not converge to the same wind veer. In EULAG, we apply the background/environmental wind profiles  $u_e(z)$  and  $v_e(z)$ , without Coriolis force in the simulation, and superposed the turbulence on the inflow. This tur-

bulent inflow wind field interacts with the actuator. The chosen background wind profiles determine if there is a veering or a backing wind or no wind veer at all or in case of a veering inflow the also determine the wind speed and directional shear in the simulations.

You never mention the word precursor or which boundary conditions you use, so it is unclear to me how you make sure that inflow has reached a quasi steady-state before you apply the inflow to a wind turbine wake simulation. If you do not use a precursor simulation, then the inflow will develop downstream and you cannot isolate the wake effects from the imbalance of the inflow profile. If you do use a precursor simulation for each case, then please specify all the input parameters necessary to run each case.

We should have explained the turbulence generation method in more detail. We changed this part of the paper (see general statement). We also added the stratification-dependent parameters applied in the simulations. In the revised version it says ... 'of a neutral boundary layer precursor simulation ...'. To make sure that our simulations reach steady state, we extended the simulation to 40 min, now averaging over 30 min. For the reference simulation we tested a simulation time of 1.5 h with the same result as averaging over the last 30 min.

In addition, it would make sense to plot all inflow profiles and report the wind speed and turbulence intensity (for example based on the turbulent kinetic energy) at hub height.

We thought about the comment of plotting the profiles, however, we did not include the plots basically due to three reasons: Firstly, they are idealized profiles following Eqs. 6 (streamwise component) and 8 (spanwise component). Secondly, the profiles referring to the turbulence generation method are already discussed and shown in Englberger and Dörnbrack (2018). Thirdly, the modified version of the manuscript already includes 20 figures considering the discussion of the results (as requested by the reviewers), therefore, this plot was eliminated in the end.

Furthermore, you seem to use a laminar inflow (without a roughness length), which does not make sense when modeling a wind turbine wake subjected to an atmospheric inflow.

If we understand this comment correctly, you refer to a roughness length  $z_0$  in the inflow profile? In EULAG, we do not apply a MOST surface layer parametrization.

3. Eq. (9): What is  $\eta_{mech}$  ? If you intend to calculate the electric (hypothetical) power from the mechanical (hypothetical) power, one would expect to have a 6% loss for a modern wind turbine, not 36%. In addition, it is unclear where the power in the other two dimensions are evaluated (y and z), you only mention the downstream distance. Furthermore, I would expect to the power to scale with  $U^3$  and I would take the integral of  $U^3$  over the rotor area. Please clarify. In addition, if you are not considering a second wind turbine, you are ignoring upstream effects of the downstream wind turbine. It is worth while to mention this simplification.

Our very simple power calculation is basically proportional to  $u^3$  (sorry we missed the 3 in Eq. 9) should represent the power

available in the flow which could be extracted from a downwind turbine. And the important information is only the difference of  $P$  in percent, as it is a parameter study. Our intent with this was only to give a comparison also in case of power not only of m/s, however, it was very misleading instead of helpful and the information in % could likewise be calculated from  $u$  directly. Therefore, we excluded the power completely from our revised manuscript. In the revised version we only refer to a spanwise and streamwise velocity difference between clockwise and counterclockwise rotating simulations.

4. It would be nice to report the tip speed ratio, the thrust coefficient and the power coefficient, for each case. This information is necessary to replicate your simulations.

Our representation of the wind turbine parametrization does not rely on thrust or power coefficients but rather lift and drag coefficients are applied in the calculation of the wind-turbine forces, as explained in Englberger and Dörnbrack (2017). We recognize the importance a reader is able to replicate the simulations. For reasons of space and because it is a very long manuscript anyway, we do not include all wind-turbine values applied in the BEM method. Instead, for all other wind-turbine parameters we refer to Englberger and Dörnbrack (2017). In addition, in the revised version we included the rotational frequency of each individual simulation in Table 1.

5. Table 1: This table is confusing. Why do you have both clockwise and counter-clockwise at the same row? I also get confused with the amount of cases and labeling. You also use these labels all the time in the article and it makes it hard to follow the text. Couldn't you simplify the cases and pick those that are really important for your conclusions? The intention was to read it as 'Simulation with different rotational directions of the rotor' 'clockwise' vs. 'counterclockwise' (all in capital letters and bold). This should save us one additional column stating the rotational direction and we think it is applicable as all other parameters are the same in the clockwise as well as the counterclockwise rotational direction simulations referring to one case. In the modified version we explained this in the table caption.

Regarding your comment with the labelling, we changed it to make it more intuitive with  $ds$  for directional shear,  $u$  for geostrophic wind speed, and  $\Omega$  for rotational frequency with the corresponding figures following for  $ds$  and  $u$  and values for low, high and very high in case of the rotational frequency.

Following your comment, we simplified the cases and now we only consider three parameters:  $u_g, ds, \Omega$

6. Table 1: How is it possible to get a negative and positive wind veer for the same Coriolis parameter? This seems to me that your inflow profile is not in balance with your equations because these kind of effects are typically caused by (unsteady) meso-scale phenomena, which you are not modelling, as far I can understand.

Veering or backing is defined by the inflow profile. To make it more clear that veering or backing is prescribed by the background flow field, not resulting from a precursor simulation, we excluded the Coriolis force from the simulations. The Coriolis force is only relevant for determining the mean inflow profiles (veering or backing inflow) but not its interaction with the wake is leading to the differences (this was another misinterpretation of the results).

7. I would expect the wake deflects differently for different rotor rotation directions or the wake deflects simply more for a certain rotor direction. Is this correct? It might be worthwhile to discuss and show this (for example with a wake center tracking method). In addition, if you had a downstream wind turbine in unfavourable staggered position, then the additional wake deflection could reduce the power of the downstream wind turbine.

Yes exactly. Our simulation results show that the wake deflects more in case of a counterclockwise rotating rotor operating in veering inflow (or a clockwise rotating one in backing inflow). We added horizontal lines of the streamwise velocity in the lower and the upper rotor part as well as at hub height. See Figs. 6, 13 and 17. They allow a quantitative evaluation of the differences in the wake deflection angle between counterclockwise and clockwise as it was possible from the contour plots in the original manuscript version.

We thought about your comment of unfavourable positions of a downwind turbine. In the revised version of the manuscript we elevated the  $90^\circ$  sector and time averaged grid points with and  $0 \text{ m} < r \leq R$  for the top and the bottom sector directly behind the wind turbine. Than we extracted the information at  $7D$  and added the same information at a spanwise distance of  $y = 1/2 D$  and  $-1/2 D$  at  $x = 7D$ . The results are not presented in the new manuscript (basically as it is an extension and not directly related to the analysis section), however, here we would like to show you the plot in Fig. 1. Considering the horizontal profiles in the lower and the upper rotor half at  $z = 75 \text{ m}$  and at  $z = 125 \text{ m}$  in Figs. 5, 6, and 7, the wake is deflected in the lower rotor part towards the left (right) and in the upper rotor part towards the right (left) in case of veering (backing) inflow. As the lateral wake position depends on the inflow wind angle, the spanwise wake position approaches away from  $y = 0D$  for increasing directional shear. This is presented in Fig. 1 (here). In case of no wind veer (Fig. 1(b)), there is no difference. In case of veering inflow (Fig. 1(e)), at  $y = -1/2 D$ , there is a small rotational direction difference in the bottom rotor part, and at  $y = 1/2 D$ , there is a difference in the top rotor part. The top left ( $y < 0$ ) and the bottom right rotor parts are unaffected by the rotational direction, as there is no wake in these sectors. In case of a backing wind (Fig. 1(h)) the situation is the opposite. In case of a veering inflow, increasing the geostrophic wind (Fig. 1(c)) or the directional shear (Fig. 1(f)) increases the difference in  $\bar{u}$ , especially in the top right rotor part. The same is valid for an increase of the rotational frequency (Fig. 1(i)). Decreasing the atmospheric or vortex strength, the difference decreases. Therefore, there is an impact at  $y = 0D$  and likewise in the wake affected sectors to the right or the left. In the considered idealized simulations of this work, the impact on  $\bar{u}$  has therefore the same tendency in case of staggered or unstaggered arrangements of the hypothetical downwind turbines.

8. Figure 1, why not just plot wake deficit profiles as function of the cross coordinate at different downstream distances? Now you are only looking directly behind the wind turbine, while the wake has deflected laterally (and possible vertically as well), so you are missing a lot of important information.

This is answered in point 7. in detail.

9. The streamwise velocity contour plots presented of Figures 3, 5 and 6, do not seem to resemble converged statistics. If you have converged statistics, then I expect smooth plots, see for example the low turbulence intensity case in van der Laan

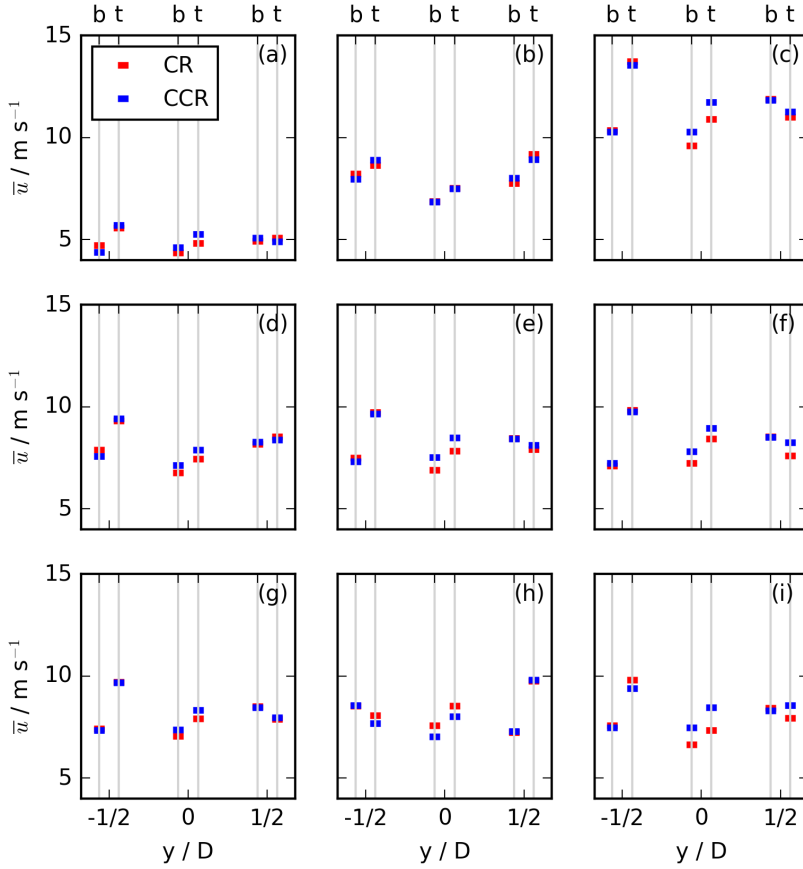


**Figure 1.** Sector averages of  $\bar{u}$  representing the top and bottom  $90^\circ$ -sectors for  $0 \text{ m} < r \leq 50 \text{ m}$  for clockwise and counterclockwise rotating actuators for the same simulations as in Fig. 19 of the manuscript at  $y=0D$  and in addition shifted by  $D/2$  in both lateral directions. The indices 'b' and 't' at the top x-axis represent the corresponding bottom or top sectors.

and Andersen (2018), where 1 hour LES results are presented. This could indicate that your LES data set is not large or long enough, or your simulation has not converged to a (quasi) steady-state, but keeps changing instead.

- We extended the reference simulation to 1.5 h and the wake structure did not change.
- In Englberger et al. (2019), simulations with both rotational directions are conducted with the inflow resulting from the stable regime of a diurnal cycle precursor simulation. In these simulations the spanwise flow component was 8 times it is chosen for this parameter study and the effect did not occur. Therefore, we refer the wake structure to the domain size. We cannot reproduce the simulations in this work on a larger spanwise domain as the applied NBL precursor simulation in the turbulence generation method limits the domain size.

- The effect not only occurs for counterclockwise rotating rotors. This is supposed to be the case as the spanwise inflow velocity is amplified in the wake. Considering a geostrophic wind of  $6 \text{ m s}^{-1}$  in CR\_u6 it also occurs. Here, the spanwise flow component decreases in comparison to the reference case, and likewise the streamwise component. Therefore, the effect seems to be additionally influenced by the streamwise wind speed.

10. Conclusion and abstract: You have to mention that the simulated power increase of 23% only reflects a specific wind direction. In other words, if you would consider multiple wind directions, then the impact of rotor rotation direction on the power (deficit) is much smaller than you report.

We modified the introduction and listed in detail that

- This difference occurs only at night.
- There are seasonal differences.
- The percentage of occurrence is location dependent
- The occurrence of specific directional shears and wind speeds is also location and also seasonal dependent.

we modified the conclusion by: This is only an idealized parameter study (turbulence is not location sensitive or result from an SBL precursor simulation). The results are not valid everywhere.

In addition, if a full wind farm is considered, I expect that the effect of rotation direction is reduced further downstream in the wind farm because of an increase in turbulence level.

Further we added a common on wind farms: 'We have assessed the wake of an individual turbine, but these results could be extended to a large farm in which the presence of upwind turbines could affect turbulence intensity, which probably affects the magnitude.'

Finally, if one would look at the effect of the rotor rotation on the wind farm annual energy production, which also consists of many flow cases, where rotor rotation has no influence, you might find that the effect of rotor rotation direction is far less than 1%. Such the study would be necessary in order to answer the question raised in the title. If your title is Should wind turbines rotate in the opposite direction? then I expect to find a thorough answer in the article. The presented simulations cannot answer this question because we need an estimate of the rotor rotation direction on the annual energy production. Regarding your comment on wind direction, there is a misunderstanding. We do not simulate a specific wind direction (for a specific location). We only simulate different directional shear values in an idealized simulation set-up. But we agree that a wind direction change occurs mainly at night and a veering wind only represents a certain percentage of this nights. (See listed modifications of the introduction.) Further, we agree with your comment on the title and changed it as explained in the general comments.

## References

- Bodini, N., Lundquist, J. K., and Kirincich, A.: US East Coast Lidar Measurements Show Offshore Wind Turbines Will Encounter Very Low Atmospheric Turbulence, *Geophysical Research Letters*, 46, 5582–5591, <https://doi.org/10.1029/2019GL082636>, 2019.
- Bodini, N., Lundquist, J., and Kirincich, A.: Offshore Wind Turbines Will Encounter Very Low Atmospheric Turbulence, in: *Journal of Physics. Conference Series*, vol. 1452, National Renewable Energy Lab.(NREL), Golden, CO (United States), 2020.
- Englberger, A. and Dörnbrack, A.: Impact of Neutral Boundary-Layer Turbulence on Wind-Turbine Wakes: A Numerical Modelling Study, *Boundary-Layer Meteorology*, 162, 427–449, <https://doi.org/10.1007/s10546-016-0208-z>, 2017.
- Englberger, A. and Dörnbrack, A.: A Numerically Efficient Parametrization of Turbulent Wind-Turbine Flows for Different Thermal Stratifications, *Boundary-layer meteorology*, 169, 505–536, <https://doi.org/10.1007/s10546-018-0377-z>, 2018.
- Englberger, A., Dörnbrack, A., and Lundquist, J. K.: Does the rotational direction of a wind turbine impact the wake in a stably stratified atmospheric boundary layer?, *Wind Energy Science Discussions*, 2019, 1–24, <https://doi.org/10.5194/wes-2019-45>, <https://www.wind-energ-sci-discuss.net/wes-2019-45/>, 2019.
- Sanchez Gomez, M. and Lundquist, J. K.: The effect of wind direction shear on turbine performance in a wind farm in central Iowa, *Wind Energy Science (Online)*, 5, 2020.
- Walter, K., Weiss, C. C., Swift, A. H., Chapman, J., and Kelley, N. D.: Speed and direction shear in the stable nocturnal boundary layer, *Journal of Solar Energy Engineering*, 131, 011 013, <https://doi.org/10.1115/1.3035818>, 2009.

# Comments on the Review of Should wind turbines rotate in the opposite direction? - Reviewer 2

Antonia Englberger<sup>1</sup>, Julie K. Lundquist<sup>2,3</sup>, and Andreas Dörnbrack<sup>1</sup>

<sup>1</sup>German Aerospace Center, Institute of Atmospheric Physics, Oberpfaffenhofen, Germany

<sup>2</sup>Department of Atmospheric and Oceanic Sciences, University of Colorado Boulder, Boulder, USA

<sup>3</sup>National Renewable Energy Laboratory, Golden, Colorado, USA

**Correspondence:** Antonia Englberger (antonia.englberger@dlr.de)

Dear Reviewer 2,

Thank you for taking the time to carefully review our paper. We read your review in detail and appreciate you sharing your own simulation results. Regarding your comments (especially your comments asking what exactly contributes to higher/smaller  $\overline{u_A}$  values), we think there are several misunderstandings with the first version of the paper. Therefore, with the help of your comments, we performed some far-reaching changes to the manuscript. Here is a list of the major changes.

- We changed the title.
- We explained in detail the turbulence generation method we applied in the simulations.
- We included a section, introducing a simple analytical model predicting the expected changes in the spanwise velocity field in the wake by a superposition of a veering inflow with a Rankine vortex. (New section 3)
- We added additional simulations with different directional shears.
- We investigated the impact of the rotational frequency on the wake differences.
- We added additional plots, explaining the wake differences and its occurrence for different rotational direction of the actuator.
- We added a section comparing the numerical results predictions of the analytical model. This section explains in detail the source of the difference in the wakes between a clockwise and a counterclockwise rotating rotor in case of a veering inflow.
- We added an Appendix, verifying the application of the turbulence preserving method for this theoretical and idealized parameter study.

In the following we respond in detail to each of your comment/question.

## General Comments

The research question of the article is interesting and well-motivated. I cannot comment on the technical set-up of the LES and the turbine model, as I have no experience with modeling, but some of the chosen simulation parameters seem questionable to me. There are several issues with the results:

(i) A presentation of the wake structure away from the hub height is missing.

We added several figures covering this. Contour plots representing the top rotor half at  $z = 125$  m and also the bottom rotor half at  $z = 75$  m (Fig. 4, 9, 11, 12, 15, 16). We also included a y-z contour plot representing the difference in the wake skewing between clockwise and counterclockwise rotating actuators (Fig. 5). Further, for a quantitative comparison we added vertical and spanwise profiles of the streamwise velocity (Fig. 6, 13, 17).

(ii) The exclusive focus on the mean streamwise velocity ignoring other quantities that affect a downstream turbine (I am not counting the power as a separate quantity here due to way it is computed).

We eliminated the power from the paper, as it leads to many misunderstandings.

In a recently submitted revised version of a previous paper Englberger et al. (2019) (attached) we apply the inflow conditions from a stable regime from a diurnal cycle precursor simulation. In that work we also focus on the turbulence in addition to the velocity components.

This work, however, is a parameter study with a very simplified setup of the numerical simulations. The applied turbulence is based on a turbulence generation method from Englberger and Dörnbrack (2018b), applying the turbulent perturbations of a neutral boundary layer precursor simulation (Englberger and Dörnbrack, 2017) in combination with adjustable-stratification dependent parameters resulting from this stable regime of Englberger and Dörnbrack (2018a), which is applied directly in Englberger et al. (2019). We apply this turbulence generation method as it provides a computationally fast testbed for wind-turbine simulations with open horizontal boundary conditions on a small domain and it also includes atmospheric characteristics in the inflow (not only random perturbation). This allows us to produce the large number of simulations in this work. We consider this method appropriate, as the occurrence of the differences between clockwise and counterclockwise rotating turbines results from the veering inflow and only the degree of the differences is modified by the turbulent intensity applied (see Appendix). Therefore, we only show velocities in the manuscript.

In the revised version, however, we also included the spanwise and vertical velocity. Further, we show vertical and horizontal profiles at different heights over the rotor of the streamwise velocity, not only the rotor averaged value as in the original manuscript version.

(iii) No physical explanation is given how the stronger rotation of the wake causes the higher entrainment, which is provided as reason for the main finding.

This is given in Englberger et al. (2019), where the turbulence profiles are presented. Here, due to the limitations of this work as listed above, it is not shown.

(iv) I am not convinced that the increased entrainment is the sole reason for the higher streamwise mean velocity across rotor of the downstream turbine and a modification of the spanwise advection influencing the shape of the wake should be investigated, too.

The main reason for the striking difference between clockwise and counterclockwise rotating rotors under veering or backing inflow presents the amplification or reduction/reversion of the spanwise flow field. To present and discuss this, we added Fig. 2. A  $y$ - $z$ -cross section plot for veering and no veering inflow simulations at  $x = 3 D$  for clockwise and counterclockwise rotating simulations. The first row presents the  $(v, w)$  vectors in the  $y$ - $z$ -plane, the second row the spanwise wake velocity  $v$ , and the third row the vertical wake velocity  $w$ . The figure shows a striking difference in the spanwise flow field between clockwise and counterclockwise rotating rotors and also in comparison to the difference between both rotational directions in case of  $\frac{\partial v_f}{\partial z} = 0$ .

The conclusions do not account for the limitations of the study and its applicability is overestimated. Therefore, the rather definitive answer to the research question provided here does not hold in my opinion (but there could be an argument to pursue the research question further).

We agree with your comment. Therefore, we added the limitations of this work to the introduction:

- Veering tends to occur only at night.
- Veer shows seasonal variability.
- The frequency of occurrence is location dependent
- The occurrence of specific directional shears and wind speeds is also location and also seasonal dependent.

and in the conclusion:

- This work is an idealized parameter study (turbulence is not location sensitive or results from an SBL precursor simulation). The results are not valid everywhere.
- Transferring the results of this study to a wind farm, the presence of upwind turbines has an effect on the turbulence intensity, which did not affect the occurrence of the difference, but its magnitude (see Appendix). Therefore, the rotational direction impact on the power production of a wind farm is another open research topic.

We also excluded any referring to a preferential rotational direction. We only stated that there are differences in the wake in case of  $\frac{\partial v_f}{\partial z} \neq 0$ . And added the limitations of this work, as it is not valid for every location etc. (see above)

Further we changed the title, excluding the question at all. The question was chosen as title for the paper as it is simple and interesting and for motivation to consider this issue. But we agree with the reviewer that our paper cannot answer this question as it is only a simplified parameter study. Therefore, we change the title of our manuscript to 'Changing the rotational direction of a wind turbine under veering inflow: A parameter study'

## Specific comments

Page 2, lines 12-14: Sentence should be narrowed to the mixed layer in absence of synoptic or mesoscale forcing.

This is no longer included in the manuscript.

Page 2, lines 17-19: From the text, it could be misunderstood that the wind veer resulting from the influence of friction is directly connected to temperature advection and lifting. Therefore, I would propose to change the sentence ("This wind veer is associated with...") to something like "Besides the surface friction, temperature advection and dynamic lifting also influence the veering of the wind".

Thank you, we changed it according to your suggestion.

Page 3, lines 9-11: Vassel-Be-Hagh and Archer, 2017 (<https://doi.org/10.1016/j.seta.2016.10.004>) studied counter-rotating rows of wind turbines in a wind farm and mentions different wake characteristics for the counter rotating turbines.

Thank you, we included the paper together with the 1.4% power increase of a wind farm with clockwise and counterclockwise rotating wind turbine rows in case of no wind veer.

Page 4, lines 9: The rotor diameter is a third of the height and the width of the simulation domain. Can this affect the wake development? Also the temperature inversion is 50 m above the top tip of the turbine, which corresponds to a very shallow boundary layer. Would a higher inversion layer have an influence on the results?

The spanwise extension of the wake probably has an influence on the streamwise velocity. The averaged x-z contour plots are not smooth for the counterclockwise rotating simulations. This is supposed to be the case as the spanwise inflow velocity is amplified in the wake. The effect not only occurs for counterclockwise rotating rotors. Considering a geostrophic wind of  $6 \text{ m s}^{-1}$  in CR\_u6 it also occurs. Here, the spanwise the the streamwise flow component did change size in comparison to the reference case. Therefore, the effect seems to be additionally influenced by the streamwise wind speed.

In Englberger et al. (2019), simulations with both rotational directions are conducted with the inflow resulting from the stable regime of a diurnal cycle precursor simulation. In these simulations the spanwise flow component was 8 times it is chosen for this parameter study and the effect did not occur. Therefore, we refer it to the domain size. We cannot reproduce the simulations in this work on a larger spanwise domain as the applied NBL recursor simulation in the turbulence generation method limits the domain size.

The shallow boundary layer is also related to the domain size of the simulations. In Englberger et al. (2019) the inversion layer starts higher above, but the impact of the rotational direction is still present.

As it is a parameter study which requires a computationally faster method in comparison to the simulations in Englberger et al. (2019) in order to run all various simulations and as the occurring difference is in agreement with the analysis predictions, the spanwise and vertical domain size limitations are not responsible for the rotational difference in the wake.

Page 4, lines 27-29: What is the reasoning for choosing the lower rotor area in contrast to the upper rotor area to modify

the type of wind veer? While it is difficult to say anything general about a stable boundary layer, at least for textbook cases the wind veer is stronger in the upper part (opposed to convective boundary layer where wind veer stronger near the surface layer). In addition, the effect is presumably larger in the upper part, because the wind speeds are higher due to wind shear.

The reason was the Ekman spiral in case it is only affecting the lower rotor region with no significant veer in the upper rotor region. See modified attached version of Engelberger et al. (2019) in Fig. 3. However, we excluded the simulations with veer limited to the lower rotor area.

As you mentioned in your summary, we investigate 'the influence of the stratification, the magnitude and structure of the wind veer, and the wind speed on this result is also investigated to some extent'. To make this study more consistent, we included the analytical predictions and prepared the numerical simulations only for the corresponding cases. In the revised version, we considered cases of changing the atmospheric inflow conditions (geostrophic wind, directional shear) and the rotational frequency. All other simulation results from the previous manuscript version are eliminated (including veer limited to the lower rotor part) to be more consistent. With including the expected results in the analysis section (3) and comparing the simulation results to them (section 5), our methodology is now more consistent.

Page 5, Eq. 8: Is 00 changed for the very stable case? Otherwise, there is an unstable layer above the hub height, because the pot. temp is 306 K at 200 m 303 K above and that would influence the dynamics for this case.

Yes, sorry this was a typo. It is no longer included in the manuscript as these simulations are eliminated.

Page 5, Eq. 9: That should be  $\overline{u_A}^3$  instead of  $\overline{u_A}$  and since all else is constant, the available power could be used instead.

Our very simple power calculation is basically proportional to  $u^3$  (sorry we missed the 3 in Eq. 9) should represent the power available in the flow which could be extracted from a downwind turbine. Our intent with this was only to give a comparison also in case of power differences in % not only of m/s, however, it was very misleading instead of helpful for reviewers. Therefore, we excluded the power completely from our manuscript. In the revised version we only refer to a spanwise and streamwise velocity difference between clockwise and counterclockwise rotating simulations. The difference in % can also be calculated from  $\overline{u_A}$ .

Page 6, lines 9-10: In Engelberger et al. (2019) — Fig. 8 it is shown that the consistent wake cases have a stronger rotation of the wake compared to the contrasting wake cases at  $x/D = 7$ . This means that the downwind turbine is receiving a stronger wind veer for the consistent cases compared to contrasting wake cases (beside the higher  $\overline{u_A}$  shown here). That stronger wind veer would presumably impact the power of a downwind turbine negatively. Maybe the downwind turbine could be viewed as a yawed turbine for the upper / lower rotor part and Eq. (9) modified to use an adapted power coefficient for each sections of the rotor.

You are right, please see Fig. 11 and 12 of the revised manuscript version of Engelberger et al. (2019) (attached). The turbulent intensity is slightly larger in case of a counterclockwise rotating rotor at 7D in all rotor heights. This would impact the hypothetical downwind turbine.

Section 3 in general: Spanwise plots of the streamwise velocity at  $x/D=7$  similar to Fig. 3, 5 and 6 should be shown and discussed. I understand that  $\overline{u_A}$  is including values above and below the hub height, but in my opinion this is not sufficient to understand the effect of the direction of the rotor rotation and wind veer on the wake structure. Further insights into the mechanism might be gained by looking at turbulent momentum transport or turbulence production, if available from the LES. A few of the following comments reiterate this comment for the specific subsections.

We included a y-z plot of the spanwise and vertical velocity (Fig. 3) and also of the streamwise velocity (Fig. 5). We also include x-y plots also in the upper and the lower rotor half in Figs. 4, 9, 10, 12, 15, 16. Further, we included vertical and horizontal profiles of the streamwise velocity at three specific rotor heights in Figs. 6, 13, and 17. The turbulence profiles are shown in the previous study of Englberger et al. (2019), where the 2D slices of all three wind components as well as the potential temperature are applied as upstream inflow condition at each time step. As this is a very simplified parameter study and due to the applied turbulence generation method, we decided showing the turbulence profiles is not helpful.

Page 9, lines 12 — 15: I have three questions on this. First, after a look at the model from Englberger et al. (2019), I do not yet understand the distinction between entrainment and wake recovery and why entrainment is considered as the explanation for the observations. Second, do the authors have any notion why the entrainment is larger for the consistent wake case in a physical sense? For example, whether the consistent wake cases have larger gradients of the absolute value of the wind vector due to the rotation, which might facilitate a stronger turbulent momentum transport. Is the turbulent momentum transports from the LES available to investigate this?

To give an explanation for the difference we updated both manuscript versions (also Englberger et al. (2019)) including a very simple analytical equation, which is the superposition of the spanwise veering inflow equation with the spanwise component of a Rankine vortex (Eq. 17). This shows that the amplification of the spanwise flow component in case of a counterclockwise rotating rotor in case of veering inflow in the NH is responsible for the difference in comparison to a clockwise rotating rotor in which the spanwise flow component is weakened/reversed due to the superposition of the vortex component. This different behaviour of the spanwise flow component impacts the streamwise flow and results in larger turbulent intensity values in case of a counterclockwise rotating rotor. The larger turbulence resulting from the amplification of the wake in case of a counterclockwise rotating rotor results in a larger entrainment rate and therefore in a more rapid wake recovery in comparison to the clockwise rotating case.

Third, I wonder whether a more pronounced ellipsoidal wake cross-section might contribute to a higher  $\overline{u_A}$  beside entrainment? Looking at Fig. 6 in Engelberger et al. 2019, an increase of the veer in the wake by the consistent wake cases could make the wake more ellipsoidal. This in turn could cause parts of the wake missing the rotor area of the downstream turbine and increase  $\overline{u_A}$ , too.

In fact there are two differences contributing. The larger wake deflection angle and the larger spanwise wake width in case of a counterclockwise rotating rotor result in larger  $\overline{u_A}$  values.

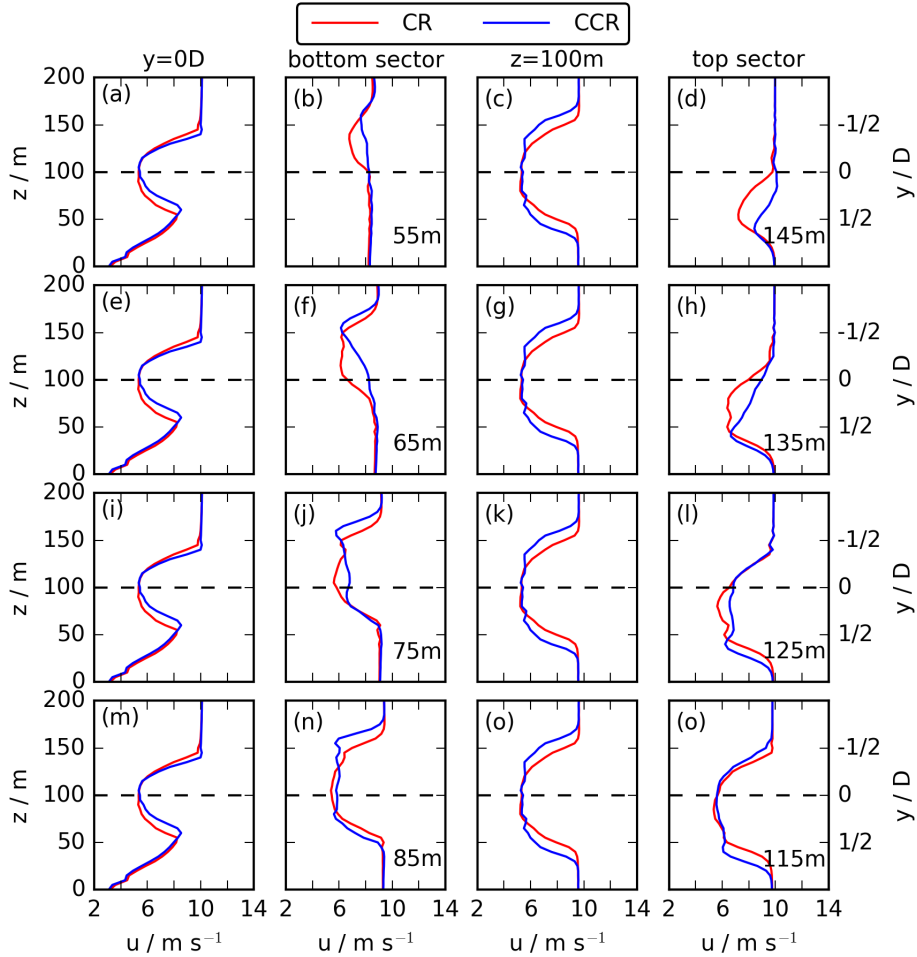


**Figure 1.** Vertical (first column) and horizontal profiles at different heights for the CR and CCR reference cases.

To show this in the paper, we added a similar figure as in Englberger et al. (2019) for both rotational directions in this work (see Fig. 5). The different lateral elongation of the wake can lead to this assumption for the outer part of the top and bottom sectors. To investigate it in more detail, we also include vertical and horizontal profiles of  $\bar{u}$  at specific heights. According to the vertical profile (Fig. 6a), this can be assumed. Looking at the upper and lower rotor half profiles (Fig. 6b, d), the streamwise velocity is larger in case of a counterclockwise rotating rotor. Looking at the same plot in Fig. 1 (only added in this response, not in the paper) at  $z = 55$  m or 145 m in the first row, at  $z = 65$  m or 135 m in the second row and at  $z = 85$  m or 115 m in the fourth row, the difference increases for increasing the radial distance to the nacelle. Therefore, in the top and bottom sector this will certainly contribute to  $\overline{u_A}$ . This increase in  $\overline{u_A}$  in case of a counterclockwise rotating rotor is related to the larger wake deflection angle in case of a counterclockwise rotating wake.

Further, looking at the profile at  $z = 100$  m, and also at 85 m and 115 m, the spanwise wake width is larger in case of a counterclockwise rotating rotor. This difference, which is especially pronounced in the right and left sectors, also contribute to the larger  $\overline{u_A}$ -values in case of counterclockwise rotating actuators.

The larger  $\overline{u_A}(a)$  values in Fig. 7 are therefore a result of the larger wake deflection angle and the larger spanwise wake width in case of a counterclockwise rotating simulation comparing the reference case CR and CCR.

Page 9, lines 27-29: Linking stability directly to the time of day requires the assumption of a radiation driven diurnal cycle of the boundary layer with the absence strong synoptic or meso-scale forcing. The same for page 12, lines 8-11.

We agree. As including different levels of the atmospheric stability is rather complex and it is not explained by the simple analytical equation, we postponed this results and will investigate them in more detail in the future.

Fig. 4: Panel b is quite busy. Would it be possible to make this figure a four panel figure and separate the weak, moderate and strong wind veer cases in one panel and the cases with only the lower rotor area affected by wind veer in a second panel? That would be also more consistent with the subsection structure used in the text.

We agree. As we eliminated a few of the simulation, we only result with one figure showing  $\overline{u_A}$ . The corresponding figure 7(e) includes the same amount of profiles as old figure 4(b), however, now the only consider a different amount of directional shear and therefore the lines are not crossing etc. as before. Due to these changings, we leave the result for all simulations with varying the directional shear in one panel as it makes it easier for the reader to see the difference in the wake if the directional shear is changed.

Page 12, lines 6-9: I believe the phrasing of this sentence is unfortunate, because it could be misunderstood that the power improvement of the downstream turbine itself becomes larger with longer duration (the percentage values from the previous sentence increase over time).

We agree that it could be misunderstood. We eliminate this sentence as the potential temperature varying simulations are not longer included.

Page 12, lines 18-21: This sentence explains the difference between CR and CCR, but not the difference between CCR\_th60 and CCR\_th15/CCR. The faster wake recovery for more stable stratification (and presumably a subsequently lower turbulence intensity) for the consistent wake cases is still counter intuitive to me. Do the authors have any explanation what is causing that behavior?

As the investigation with different background potential turbulent profiles is rather complex and cannot explained with the simply analytic equation, it is excluded from this paper and we will investigate it in more detail in the future.

Page 12, lines 25: As for the comment on page 9, lines 12-15, I believe it is possible that an increased ellipsoidal wake shape with increasing wind veer might have a pronounced effect on  $\overline{u_A}$  beside entrainment. Vertical cross-sections of the streamwise

velocity and plots of the momentum transport could be used to investigate. Maybe some insights into the curious decrease for the strong wind veer case might be gained from them, too.

To investigate this in more detail, we perform two additional simulations with a directional shear of  $0.12^\circ \text{ m}^{-1}$  and  $0.20^\circ \text{ m}^{-1}$ . According to our results there is a critical directional shear value  $ds_c$  with  $0.12^\circ \text{ m}^{-1} < ds_c < 0.16^\circ \text{ m}^{-1}$ . Below this critical values, the  $\overline{u_A}$ -value is larger for a counterclockwise rotating rotor, whereas above it is larger in case of a clockwise rotating one.

The new figure 13 gives some insight into this. An increase of the directional shear increases the wake deflection angle. However, increasing the directional shear to high values of  $0.16^\circ \text{ m}^{-1}$  and even very high values of  $0.20^\circ \text{ m}^{-1}$  results in a larger streamwise velocity close to the nacelle, contributing to larger values especially in the left and the right  $90^\circ$  sectors (last two rows of Fig. 13). This overcomes the larger streamwise velocity values in the top and bottom sectors in Fig. 13 at 75 m and 125 m respectively. Therefore, the more rapid wake recovery for large directional shear values results in larger  $\overline{u_A}$ -values in case of clockwise rotating discs.

In the paper it is explained with: 'In the clockwise as well as the counterclockwise rotating actuator simulations (Figs. 10 - 12) the wake recovers more rapidly if directional shear increases. A larger directional shear represents a larger resolved turbulence source due to an increase of  $\frac{\partial v_f}{\partial z}$ , and, therefore, the simulations with higher directional shear values result in higher entrainment rates and a more rapid wake recovery.'

Page 13, line 1-2: Is this amplified the turbulence production occurring at specific regions of the wake? Could the terms of the TKE budget provide any insights into the cause of the higher entrainment (if they can be computed from the LES)?

This has to be tested in LESs applying precursor simulations of the SBL for different directional shears. This is one of our planned next steps.

Page 15, lines 5-6: I would always expect a larger  $\overline{u_A}$  for an increased inflow wind speed if the efficiency of the upwind turbine is not changing (as it is the case here) and I am not seeing where the entrainment is entering the picture from the results. Is that sentence referring to the relative difference between CR / CCR and CR\_u14 / CCR\_u14?

Yes we agree with your expectation. A larger wind speed has an effect on the streamwise wake elongation. Yes, the specific sentence is referring to the relative difference between CR/CCR and CR\_u14/CCR\_u14.

Section 3.6 and Fig. 7: I like this section bringing everything together and the figure is very informative, but I had a hard time reading the first two paragraphs of this section due to the amount of simulation abbreviations. Since the simulations can be deduced from the Fig. 7, perhaps the text could focus on the physical meanings. E.g. "The blue square shows a power increase by 4% for counterclockwise rotating turbines compared to a clockwise rotating ones for a weakly stable stratification." instead of "The point 'th15' represents a power increase by 4% at 7D for CCR\_th15 in comparison to CR\_th15".

Thank you. Actually, due to all new figures we extracted this figure and also the text. See Fig. 2 (only here) as updated version.

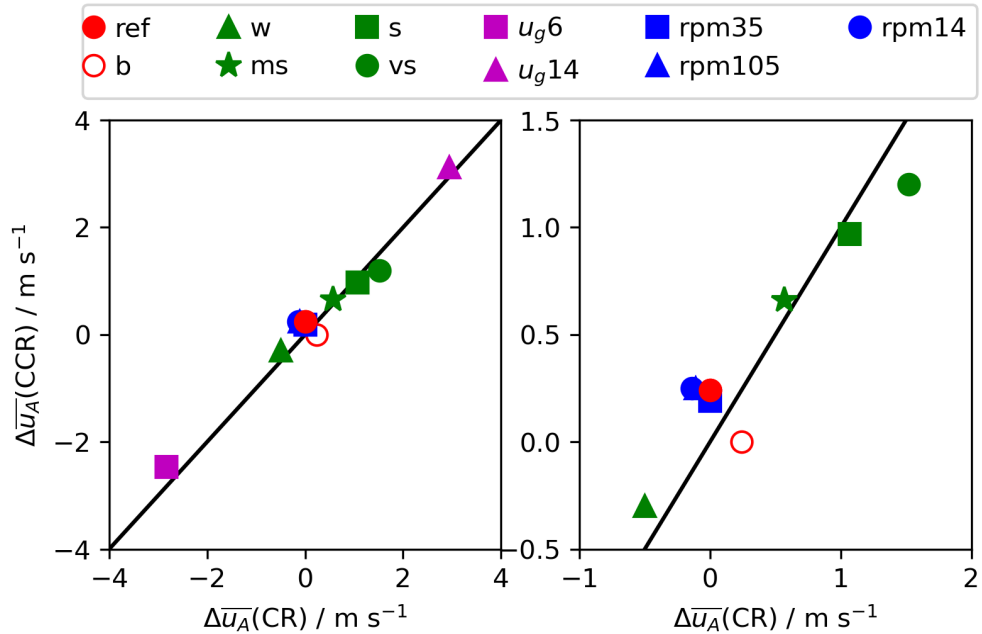


**Figure 2.** Coloured contours of the streamwise velocity  $\bar{u}_{i,j,k_*}$  in  $\text{m s}^{-1}$  for different geostrophic winds at  $z=75$  m. The black contours represent the velocity deficit  $VD_{i,j,k_*}$  at the same vertical location.

Page 17, line 6-7: It should be specified that the power of the waked downstream turbines is considered here (it could be misunderstood that the power of the upwind turbine improves, too).

Thank your for this hint. As we excluded power and only discuss the velocity of one wind turbine, no misunderstandings like that should be possible.

Page 17, lines 22-24: How much of that cumulative capacity is located in wind farms, where wake effects can occur? (in contrast to isolated turbines where it would not matter).

This is an interesting question. In the GEWC there is no distinction between offshore and onshore. As we extracted the power and the discussion about any preferential rotational direction, we also extracted the NH and SH comparison of installed capacity.

Page 17, lines 28-29: I believe there is a need for further studies on some aspects to this question:

We agree and added are complete paragraph about this:

'To explore a more comprehensive assessment of the wake impact, further investigations would be interesting. The investigation of the non-linearity of the interaction process, numerical simulations applying the turbulence of a SBL precursor

simulation for different strengths of stratification and directional shears, or even considering a low-level jet at the rotor height. Topography could influence the wake dynamic explored here. We have assessed the wake of an individual turbine, but these results could be extended to a large farm in which the presence of upwind turbines could affect turbulence intensity, which probably affects the magnitude. However, an important point will be to prove the theoretically predicted effect resulting from superposition of inflow veer with the vortex component on the wake with measurements. ’

1: This conclusion is based on numerical simulations with simplified a very simplified estimation of the downstream turbine power. A verification with experiments for real wind turbines would be a reasonable call. 2: Unstable and neutral stratification of the boundary layer is not regarded in this study, but can be subject to wind veer as well. 3: Real wind turbines have an induction zone that modify the flow further from the simulation results. 4: Besides the higher streamwise velocity investigated here, the wake structure could see further changes (turbulence intensity, veer, shear), which could impact a downstream turbine. 5: It is possible that two important categories of wind farm locations have a different veering/backing ratios then considered here. Offshore wind parks in proximity to a coast due to the baroclinicity between land and sea. Wind farms located on a ridge due to topography and baroclinicity.

1: The power is eliminated and we now stated in the conclusion: ’However, an important point will be to prove the theoretical effect resulting from superposition of inflow veer with the vortex component on the wake with measurements.’

2: We only focus on veering and backing in nighttime situations following Walter et al. (2009).

3: We agree, this will modify the streamwise velocity at the downwind turbines location. Here, however, we compare the streamwise velocities for both rotational directions with no downwind turbine in both cases. Therefore, the difference between clockwise and counterclockwise is comparable.

4: We investigated more aspects in the revised version of the paper with including the horizontal and vertical profiles of  $u$ .

5: We listed possible differences related to topography and location in the conclusion in the revised version of the manuscript.

## References

- Englberger, A. and Dörnbrack, A.: Impact of Neutral Boundary-Layer Turbulence on Wind-Turbine Wakes: A Numerical Modelling Study, *Boundary-Layer Meteorology*, 162, 427–449, <https://doi.org/10.1007/s10546-016-0208-z>, 2017.
- Englberger, A. and Dörnbrack, A.: Impact of the diurnal cycle of the atmospheric boundary layer on wind-turbine wakes: a numerical modelling study, *Boundary-layer meteorology*, 166, 423–448, <https://doi.org/10.1007/s10546-017-0309-3>, 2018a.
- Englberger, A. and Dörnbrack, A.: A Numerically Efficient Parametrization of Turbulent Wind-Turbine Flows for Different Thermal Stratifications, *Boundary-layer meteorology*, 169, 505–536, <https://doi.org/10.1007/s10546-018-0377-z>, 2018b.
- Englberger, A., Dörnbrack, A., and Lundquist, J. K.: Does the rotational direction of a wind turbine impact the wake in a stably stratified atmospheric boundary layer?, *Wind Energy Science Discussions*, 2019, 1–24, <https://doi.org/10.5194/wes-2019-45>, <https://www.wind-energ-sci-discuss.net/wes-2019-45/>, 2019.
- Walter, K., Weiss, C. C., Swift, A. H., Chapman, J., and Kelley, N. D.: Speed and direction shear in the stable nocturnal boundary layer, *Journal of Solar Energy Engineering*, 131, 011 013, <https://doi.org/10.1115/1.3035818>, 2009.

# Comments on the Review of Should wind turbines rotate in the opposite direction? - Reviewer 3

Antonia Englberger<sup>1</sup>, Julie K. Lundquist<sup>2,3</sup>, and Andreas Dörnbrack<sup>1</sup>

<sup>1</sup>German Aerospace Center, Institute of Atmospheric Physics, Oberpfaffenhofen, Germany

<sup>2</sup>Department of Atmospheric and Oceanic Sciences, University of Colorado Boulder, Boulder, USA

<sup>3</sup>National Renewable Energy Laboratory, Golden, Colorado, USA

**Correspondence:** Antonia Englberger (antonia.englberger@dlr.de)

Dear Reviewer 3,

Thank you for taking the time to carefully review our paper. We read your review in detail and appreciate you sharing your own simulation results. Regarding your comments, we think there are several misunderstandings with the first version of the paper. Therefore, with the help of your comments, we performed some far-reaching changes to the manuscript. Here is a list of the major changes.

- We changed the title.
- We explained in detail the turbulence generation method we applied in the simulations.
- We included a section, introducing a simple analytical model predicting the expected changes in the spanwise velocity field in the wake by a superposition of a veering inflow with a Rankine vortex. (New section 3)
- We added additional simulations with different directional shears.
- We investigated the impact of the rotational frequency on the wake differences.
- We added additional plots, explaining the wake differences and its occurrence for different rotational direction of the actuator.
- We added a section comparing the numerical results predictions of the analytical model. This section explains in detail the source of the difference in the wakes between a clockwise and a counterclockwise rotating rotor in case of a veering inflow.
- We added an Appendix, verifying the application of the turbulence preserving method for this theoretical and idealized parameter study.

## Referee comments

The authors argue that counter-clockwise rotation wind turbines in northern hemisphere (as opposed to clockwise as is currently done) can lead to a power increase of 11% in the downwind turbine due to constructive interactions between the axial vorticity in the wake and veered Ekman layer, especially when strong stable stratification is present. While I am fascinated by the overall theme of this research, I do not feel that the authors have done a thorough investigation to corroborate their hypothesis. While the paper uses a provocative title and well written, I hesitant in recommending publication at this time since I have the following serious concerns regarding the quality of the numerical simulations performed.

The intent of the manuscript was not to be provocative. The question was chosen as title for the paper as it is simple and interesting and for motivation to consider this issue. But we agree with the reviewer that it could lead to misunderstandings. Therefore, in the revised version, we changed the title to 'Changing the rotational direction of a wind turbine under veering inflow: A parameter study'

Further, there seem to be some misunderstandings with the simulations. The simulations in this manuscript are wind turbine simulations performed under prescribed wind and turbulence conditions. In the parameter study presented in this work, we applying a very simplified set-up with a turbulence generation method. This is not a stable boundary layer input applied in the wind-turbine simulations. But we agree the manuscript could give the impression as we talk about veering wind in a stably stratified regime. In the revised version of the manuscript we only talk about a veering inflow or a backing inflow or no veer at all. Further, we added a detailed explanation of the turbulence generation method, instead of only referring to the corresponding paper. We also added the basic equation for this. The modification should make it clear that no SBL LES is performed. Further, we rerun all simulations as implicit LES also excluding the Coriolis force. With that we would like to make clear that it is only an idealized parameter study, and the Coriolis force has only an effect on the prescribed inflow wind field whether the resulting differences between clockwise and counterclockwise rotating turbines not results from an interaction effect of the vortex with the wake. It is not affected by the Coriolis force interacting with the wake and deflecting it.

We apply the turbulence parametrization instead of the SBL precursor simulation as it provides a computationally fast testbed for wind-turbine simulations on a small domain. Regarding the large number of performed simulations, it would be computationally very expensive running them all as SBL simulation and a resolution refinement down to 0.25 m is not possible with the current supercomputer resources we can use. Especially considering the effect that the simulations with varying wind speed and directional shear would require different precursor simulations to conduct the SBL wind-turbine simulations.

This parameter study with a very simplified numerical setup was the first attempt to investigate the impact of the atmospheric parameters (geostrophic wind speed and directional shear) and the impact of the vortex parameter (rotational frequency) on the wake differences between clockwise and counterclockwise rotating actuators. The results allow us to identify which SBL precursor simulations are required to investigate the interesting cases in detail in future simulations.

1. The Ekman layers being simulated are highly stratified with very high gradient Richardson numbers. TKE based eddy-viscosity SGS closures are notoriously terrible at stably stratified layers; see the work by Sullivan et. al, (JAS, 2016) where they show grid sensitivities up to 0.25m for similar states of stratification. You must show that the Ozmidov scale is larger than the grid scale, especially for your strongest stratification case for me to accept the accuracy of the SBL simulated using your SGS closure. This is not done in the current version of the manuscript.

The presented simulations represent a wind-turbine simulation with prescribed wind and turbulence conditions. It is not an SBL simulation with a rather fine resolution close to the ground. To make this clear, we rerun all simulations as ILES excluding the SGS closure. The applied resolved turbulence develops from small fluctuations impressed on the flow field by our 'turbulence preserving method'.

2. Since much of the argument made in the paper relies on axial vorticity, the authors need to present a strong case showing that the axial vorticity captured by their grid resolution and actuator-line parameterization is correct. A grid convergence study might help, although I remain skeptical regarding whether actuator lines can correctly represent axial vorticity. There is substantial discussion on this topic in open-literature.

There is a misunderstanding, we did not apply an actuator line technique, we run the simulations with an actuator disc approach. The disc is resolved with 21 grid points. Following Ivanell et al. (2008), Wu and Porté-Agel (2011), and Gomes et al. (2014), the minimum number of grid points to result in the same resolution independent wake structure for actuator disc models is 10 grid points in vertical and spanwise direction.

3. There is new evidence that suggests that ignoring the horizontal component of Earth's rotation (as the authors have done) has a significant quantitative impact on wakes of large turbines representing small Rossby numbers. See the recent work by Howland et al. (2020, JFM) on this topic. Even at approx.. 45deg. Latitudes, I would speculate the direction of wind (Westerly vs Easterly) would affect the power of the downwind turbine by similar order of magnitude as shown by the authors for CW vs CCW rotation.

In the present study, we only consider the Coriolis force as cause for the inflow profiles. To make this clear, we rerun all simulations without a Coriolis force.

These only recently published results, however, are rather interesting and we will include the horizontal component of the Coriolis force in the fine resolved SBL WT simulations we plan to perform next.

## References

- Gomes, V. M. M. G. C., Palma, J. M. L. M., and Lopes, A. S.: Improving actuator disk wake model, in: The science of making torque from wind. Conference series, vol. 524, p. 012170., 2014.
- Ivanell, B. S., Mikkelsen, R., and Henningson, D.: Validation of methods using EllipSys3D, pp. 183–221., Technical report, KTH, TRITA-MEK 2008:12, 2008.
- Wu, Y. T. and Porté-Agel, F.: Large-Eddy Simulation of Wind-Turbine Wakes: Evaluation of Turbine Parametrisations, *Boundary-Layer Meteorol*, 138, 345–366, 2011.

# ~~Should wind turbines rotate in~~ Changing the opposite rotational direction ? ~~of a wind turbine under veering inflow: A parameter study~~

Antonia Englberger<sup>1</sup>, Julie K. Lundquist<sup>2,3</sup>, and Andreas Dörnbrack<sup>1</sup>

<sup>1</sup>German Aerospace Center, Institute of Atmospheric Physics, Oberpfaffenhofen, Germany

<sup>2</sup>Department of Atmospheric and Oceanic Sciences, University of Colorado Boulder, Boulder, USA

<sup>3</sup>National Renewable Energy Laboratory, Golden, Colorado, USA

**Correspondence:** Antonia Englberger (antonia.englberger@dlr.de)

**Abstract.** ~~Wind~~ All current-day wind turbine blades rotate in clockwise direction ~~seeing as seen~~ from an upstream ~~position.~~ This perspective. ~~The choice of the~~ rotational direction impacts the wake ~~in a stably stratified atmospheric boundary layer, in which if~~ the wind profile ~~is characterised by a veering or a backing wind~~ changes direction with height. Here, we ~~challenge the arbitrary choice of the rotational direction of the blades by investigating the interaction of the rotational direction with~~ investigate the respective wakes for veering and backing winds in both hemispheres by means of large-eddy simulations. ~~Likewise we~~ We quantify the sensitivity of the wake to the strength of ~~stratification, the strength and type of~~ wind veer, ~~and~~ the wind speed, and the rotational frequency of the rotor in the Northern Hemisphere. A veering wind in combination with counterclockwise rotating blades ~~would result in a power output increase of 11.5% for a downwind turbine~~ results in a larger streamwise velocity output, a larger spanwise wake width, and a larger wake deflection angle at the same downwind distance in comparison to a clockwise rotating ~~upwind~~ turbine in the Northern Hemisphere. In the Southern Hemisphere, the ~~power output of a downwind turbine would decrease by the same value if the upwind~~ same wake characteristics occur if the turbine rotates counterclockwise. These ~~wake differences~~ downwind differences in the wake result from the ~~interaction of a veering or a backing wind with the rotational direction of the near wake. In the common case of a clockwise rotating rotor and a veering wind in the Northern Hemisphere, or similarly a backing wind in the Southern Hemisphere, the rotational direction differs in the far wake compared to the near wake. In contrast, if a counterclockwise rotating rotor interacts with a veering wind in the Northern Hemisphere or a backing wind in the Southern Hemisphere, the rotational direction of the near wake persists throughout the entire wake. Under veering wind conditions in the Northern Hemisphere, enhancing the thermal stability or increasing the strength of the veering wind further enlarges the power output difference up to 23%. The positive impact on the potential power production can be explained by an intensified entrainment of the ambient air and the more rapid wake recovery under shared wind conditions~~ amplification or weakening/reversion of the spanwise wind component due to the effect of the superimposed vortex of the rotor rotation on the inflows shear. An increase of the directional shear or the rotational frequency of the rotor under veering wind conditions increases the difference in the spanwise wake width and the wake deflection angle between clockwise and counterclockwise rotating blades. ~~actuators, whereas the wind speed lacks a significant impact.~~

*Copyright statement.* The copyright of the authors Antonia Englberger and Andreas Dörnbrack for this publication are transferred to Deutsches Zentrum für Luft- und Raumfahrt e. V., the German Aerospace Center. This work was authored [in part] by the National Renewable Energy Laboratory, operated by Alliance for Sustainable Energy, LLC, for the U.S. Department of Energy (DOE) under Contract No. DE-AC36-08GO28308. Funding provided by the U.S. Department of Energy Office of Energy Efficiency and Renewable Energy Wind Energy Technologies Office. The views expressed in the article do not necessarily represent the views of the DOE or the U.S. Government. The U.S. Government retains and the publisher, by accepting the article for publication, acknowledges that the U.S. Government retains a nonexclusive, paid-up, irrevocable, worldwide license to publish or reproduce the published form of this work, or allow others to do so, for U.S. Government purposes.

## 1 Introduction

Most modern industrial-scale wind turbines rotate clockwise, as seen from a viewer looking downwind. Traditional Danish windmills turned counterclockwise ~~due to (Maegaard et al., 2013), who preferred~~ the thin end of the laths pointing towards the left on the blades as they were built by right-handed millers. This rotational direction was adapted by the wind-turbine pioneer Christian Riisager and ~~also by subsequently by the company~~ Tvind. In 1978, Erik Grove-Nielson designed the first ~~5-m-5-m~~ fibreglass blades. He and his wife Tove ~~decided for chose~~ a clockwise rotational direction of the blades ~~purportedly~~ to distinguish their product from Tvind. ~~Therefore, the first modern wind turbines rotated in both directions.~~ Descendants of the Riisager wind turbine (Wind Matic and Tellus) rotate counterclockwise ~~and while those~~ of Grove-Nielson (Vestas, Bonus (now Siemens), Nordtank and Enercon) ~~rotate~~ clockwise. Three of the four clockwise rotating blade manufacturers became market leaders in the international wind power industry, and the clockwise rotating blades, eventually, became the global standard (Maegaard et al., 2013). The clockwise blade rotation is, therefore, ~~barely~~ a historical coincidence without ~~any~~ physical motivation.

~~Rotating blades are faced by~~ Rotating blades encounter a variety of wind conditions. In a convective regime during daytime above the surface layer, there is no significant change of the incoming wind direction or wind speed with height and the inflow conditions are ~~rather~~ uniform over the whole rotor area. A nocturnal stably stratified regime, however, often generates wind profiles with changing magnitude (vertical wind shear) and direction (wind veer) (Lindvall and Svensson, 2019). Vertical variations of both quantities reflect the balance between Coriolis force and friction. Friction affects the lowest part of the wind profile and contributes as internal friction in the flow while the rotational direction of the wind vector in the Ekman spiral aloft depends on the hemisphere. In the Northern Hemisphere (NH) (Southern Hemisphere (SH)), winds tend to rotate clockwise (counterclockwise) with height (Stull, 1988). ~~This veering wind is associated with warm air advection and dynamic lifting. It changes in cases of cold air advection or dynamic sinking into~~ Veer occurs on many nights both onshore (Walter et al., 2009; Rhodes and Lundquist, 2013; Sanchez Gomez and Lundquist, 2020b) and offshore (Bodini et al., 2020, 2019). According two years of meteorological tower measurements in Lubbock (Texas) (Walter et al., 2009) and three months of lidar observations in north-central Iowa (Sanchez Gomez and Lundquist, 2020b), veer occurs in well over 70% of those SBL occurrences ( $\approx 76\%$  in Walter et al. (2009) and  $\approx 78\%$  in Sanchez Gomez and Lundquist (2020b)). In the remaining 22% (Sanchez Gomez and Lundquist, 2020b) to 24% (Walter et al., 2009), a backing wind ,which occurs. A backing wind is char-

acterized by a counterclockwise (~~clockwise~~)-wind direction change with height in the NH(~~).~~. ~~In addition, frontal passages or topographically-driven phenomena such as drainage flows may modify this typical background veer (Walter et al., 2009; Bodini et al., 2019~~

The frequency of occurrence of a veering wind depends on many criteria. A wind direction change with height occurs mainly at night. Secondly, seasonal differences occur. Thirdly, the frequency of occurrence of veering or backing is location specific. In Lubbock (Texas) (Walter et al., 2009) and in north-central Iowa (Sanchez Gomez and Lundquist, 2020b), a veering wind occurs in three out of four nights. In their global climatology of veer based on radiosonde data, Lindvall and Svensson (2019) find stronger veer (or backing for the SH) in midlatitudes (see their Fig. 3). Of course, topography can change the frequency of occurrence significantly. Each location has its own percentage values of the occurrence of a veering wind. In this study, a directional shear of  $0.08^\circ \text{ m}^{-1}$  is applied in the reference case, as it corresponds to the mean of the frequency of occurrence of a veering inflow in Walter et al. (2009). Further, seasonal dependence occurs (Bodini et al., 2019, 2020). The longer lasting nights during winter are characterised by smaller mean values of the directional shear (minimum winter values in December of  $0.03^\circ \text{ m}^{-1}$  (Bodini et al., 2020, Fig. 4) according to 13 months of offshore lidar measurements in Massachusetts). The shorter nights during summer, however, are characterised by larger mean values of the directional shear (maximum summer values in June of  $0.095^\circ \text{ m}^{-1}$  (Bodini et al., 2020, Fig. 4)). The occurrence of a specific directional shear (e.g.  $ds = 0.08^\circ \text{ m}^{-1}$ ) for a specific wind speed (in between  $9 \text{ m s}^{-1}$  and  $11 \text{ m s}^{-1}$ , similar to the reference case used here) is much larger during winter (85% of the veering cases are characterized by  $ds < 0.08^\circ \text{ m}^{-1}$ ) in comparison to the summer (45% (Bodini et al., 2020, Fig. 5)).

The wind turbine's wake characteristics in a veering wind regime differ for counterclockwise and clockwise rotating blades as shown by Englberger et al. (2019). The rotational direction (Englberger et al., 2019). The induced vortex component of the near wake is mainly's flow is determined by the rotation of the blades, whereas. The wake rotates opposite to the blade rotation due to aerodynamics and design of the wind-turbine blades (Zhang et al., 2012). In contrast, the rotational direction of the far wake is determined by the Ekman spiral. If a northern hemispheric Ekman spiral interacts with clockwise rotating blades, the spanwise flow component in the wake weakens or even reverses due to a superposition with the vortex of the near wake and attenuates to the inflow in the far wake. In this case, the near wake's counterclockwise rotation diminishes and becomes clockwise in the far wake. After this reversion or likewise in the case of a reduction of the spanwise wake component, the wake's rotation strength intensifies downwind. Conversely, if the same flow inflow interacts with counterclockwise rotating blades, the near wake rotates in a clockwise direction. In contrast to the former case, spanwise flow component is amplified in the near wake, because the rotational direction persists in the whole wake, as the stably-stratified regime in the results also in a clockwise flow rotation of the far wake. However, the and the wake's rotation strength weakens downwind.

The modification of the spanwise flow component also impacts the streamwise velocity in the wake. It affects the velocity deficit in the near wake, the streamwise wake elongation of the wake, the spanwise wake width, and the deflection angle of the wake (Englberger et al., 2019). There also exists a rotational direction impact is rather small on the streamwise velocity component in a flow regime without significant vertical wind shear and wind veer (Vermeer et al., 2003; Shen et al., 2007; Sanderson, 2009; Vassel-Be-Hagh and Archer (2017) simulated a wind farm similar to Lillegrund in Sweden with alternative rotational direction

of the rotors, starting with clockwise in the first row. Including wind shear but no wind veer in the height of the rotor (Vermeer et al., 2003; Shen et al., 2007; Sande, 2009; Kumar et al., 2013; Hu et al., 2013; Yuan et al., 2014; Mühle et al., 2017; Englberger et al., 2019) inflow conditions, the power output was 1.4% larger in comparison to only clockwise rotating rotors in the wind farm. However, compared to the wake differences for clockwise and counterclockwise rotating rotors in a flow regime with wind veer, the differences are small in the case of no wind veer (Englberger et al., 2019). Therefore, the 1.4% in Vassel-Be-Hagh and Archer (2017) can be considered as a lower limit, the consideration of veer amplifies this difference.

This interaction of the rotational direction of a wind turbine with a veering wind suggests that a preferential rotational direction of a wind turbine in a stably stratified on each hemisphere could exist. The term 'preferential' refers to the positive impact on a downwind turbine's inflow velocity (less perturbed and higher magnitude) and, therefore, its potentially larger power output.

We investigate the relationship between the upstream wind profile and the direction of the turbine rotation by using large-eddy simulations (LESs). Both clockwise and counterclockwise rotating actuators are embedded in stably stratified atmospheric flows representing a veering as well as a backing wind for the and also for the . In addition, we investigate inflow for both hemispheres. In the case of a veering inflow in the NH, we carry out a parameter study investigating the impact of the rotational direction of the blades for different strengths of the stably stratified regime, for different amounts of wind direction changes with height, for different rotor parts affected by the veering wind, and also for different wind speeds. Altogether, 24 combinations of rotor rotation and inflow wind conditions in a stably stratified are simulated.

magnitude of the geostrophic wind, the directional shear, and the rotational frequency of the rotor. The results of the rotational direction impact on the wake are interpreted for all simulations with a theoretical analysis considering a Rankine vortex representation of the wake. To our knowledge, this is the first parameter study which investigates the impact of the interactions of wake rotational direction in combination with an Ekman spiral on wake characteristics, which are relevant for the performance of a downwind turbine and for wind turbine control strategies (Fleming et al., 2019).

The previous study Englberger et al. (2019) lays the groundwork for this study, describing in detail the rotational direction impact in veer. Our previous study (Englberger et al., 2019) lays the groundwork for this investigation, describing in detail the rotational direction impact in a stably-stratified regime under veered inflow conditions and in an evening boundary layer regime under non-veered conditions (in the Northern Hemisphere). Further, that work explains the physical mechanism responsible for the rotational direction impact of the blades on the wake by simple analysis of a linear superposition of the veering inflow wind field with a Rankine vortex.

This paper is organised as follows. The numerical model EULAG and the wind-turbine simulation setup, and the metrics applied in this work are described in Sect. 2. The analysis predictions are introduced in Sect. 3. The corresponding idealized simulations investigating the rotational direction impact on the wake follows follow in Sect. 3, investigating the difference of a veering wind and a backing wind on both hemispheres, the impact of the strength of stratification, the strength of the veering wind, the type of the veering wind, and the wind speed for a veering wind in the . A conclusion is given 4. A comparison of the simulation results to the analysis predictions is given in Sect. 5 and a conclusion follows in Sect. 4-6.

## 2 Numerical Model Framework

### 2.1 The Numerical Model EULAG

The ~~dry flow through a wind turbine is simulated with the multiscale geophysical~~ wind-turbine simulations, with prescribed wind and turbulence conditions, are conducted with the flow solver EULAG (Prusa et al., 2008). ~~A~~ For a comprehensive description and discussion of EULAG ~~can be found in we refer to~~ Smolarkiewicz and Margolin (1998) and Prusa et al. (2008).

The Boussinesq equations for a flow with constant density  $\rho_0 = 1.1 \text{ kg m}^{-3}$  are solved for the Cartesian velocity components  $u, v, w$  and for the potential temperature perturbations  $\Theta' = \Theta - \Theta_{BL}$  (~~Smolarkiewicz et al., 2007~~),  $\Theta_e$  (~~Smolarkiewicz et al., 2007~~)

$$\frac{d\mathbf{v}}{dt} = -\nabla \left( \frac{p'}{\rho_0} \right) + \mathbf{g} \frac{\Theta'}{\Theta_0} + \mathcal{V} \underline{-2\Omega(\mathbf{v} - \mathbf{v}_{BL})} + \beta_v \frac{\mathbf{F}_{WT}}{\rho_0}, \quad (1)$$

$$\frac{d\Theta'}{dt} = \mathcal{H} - \mathbf{v} \nabla \Theta_{BL} f, \quad (2)$$

$$\nabla \cdot (\rho_0 \mathbf{v}) = 0, \quad (3)$$

~~where with  $\Theta_e$  representing the environmental/background state and  $\Theta_0$  represents representing~~ the constant reference value of 300 K ~~and  $u_{BL}, v_{BL}, w_{BL}$ , and  $\Theta_{BL}$  are height dependent environmental states.~~ In Eqs. (1), (2) and (3),  $d/dt$ ,  $\nabla$  and  $\nabla \cdot$  represent the total derivative, the gradient and the divergence, respectively. The quantity  $p'$  represents the pressure perturbation with respect to the environmental state ~~and~~. Further,  $\mathbf{g}$  represents the vector of acceleration due to gravity. The subgrid-scale terms  $\mathcal{V}$  and  $\mathcal{H}$  symbolise viscous dissipation of momentum and diffusion of heat ~~and~~. ~~the Coriolis force is represented by the angular velocity vector of the earth's rotation.~~  $\mathbf{F}_{WT}$  corresponds to the turbine-induced force ~~and~~  $\beta_v$  to the rotational direction. All following simulations are performed without an explicit subgrid-scale closure as implicit LES (Grinstein et al., 2007), to remove any question of the influence of the subgrid-scale closure on the results. Further, we apply a free-slip vertical boundary condition.

The turbine-induced forces ( $\mathbf{F}_{WT}$ ) in Eq. (1) are parametrized with the blade element momentum (BEM) method as ~~rotating actuator disc with both rotational directions  $\beta_v$ . All following simulations are performed with a TKE closure (Schmidt and Schumann, 1989; actuator disc, including a nacelle and excluding the tower. The BEM method enables the calculation of the steady loads, thrust, and power for different wind speeds and rotational speeds of the blades. The airfoil data of the 10 MW reference wind turbine from DTU (Bak et al., 2013) are applied, whereas the radius of the rotor as well as the chord length of the blades are scaled to a rotor with a diameter of 100 m. For a more detailed description of the wind-turbine parametrization and all values used in the wind-turbine parametrization we refer to parametrization B of Englberger and Dörnbrack (2017).~~

The actuator disc rotates in clockwise or counterclockwise direction, depending on the choice of  $\beta_v \in \{-1, 1\}$ . The rotor rotation is not directly simulated, instead, the rotor forces are exerted directly on the velocity fields in Eq. (1). A clockwise rotating rotor initiates a counterclockwise wake rotation and vice versa, following conservation of angular momentum (Zhang et al., 2012)

In this work, a common clockwise rotor rotation 'cr' is defined as  $\beta_v = 1$  and  $\beta_w = -1$  and a counterclockwise rotor rotation 'ccr' as  $\beta_v = -1$  and  $\beta_w = 1$ , with  $\beta_u = 1$  in both cases.

## 2.2 Setup of the Wind-Turbine Simulations

Wind-turbine simulations on  $512 \times 64 \times 64$  grid points with a horizontal and vertical resolution of 5 m and open **horizontal** boundaries are performed for **a stably stratified lasting 20** veering and non-veering inflow lasting 40 min. The rotor of the wind turbine has a diameter  $D$  as well as a hub height  $z_h$  of 100 m and is located at 300 m **in  $x$ -direction** downwind from the inflow boundary and centred in the spanwise  $y$ -direction.

**24** wind-turbine simulations explore the combinations of the incoming wind field and the rotational direction of the wind-turbine rotor. They are listed in Table 1. The simulations are initialized with the zonal velocity profile-

$$10 \quad \underline{u_{BL}(z) = u_g * \left( 1 - \exp\left(-\frac{z\sqrt{f/\kappa}}{\sqrt{2}}\right) \right)},$$

A veering wind profile can be described by the Ekman spiral 2

$$u_{Ekman}(z) = u_g \cdot (1 - \exp(-z\gamma) \cos(z\gamma)), \quad (4)$$

$$v_{Ekman}(z) = u_g \cdot (\exp(-z\gamma) \sin(z\gamma)), \quad (5)$$

following Stull (1988), with a geostrophic wind  $u_g$ , ~~the Coriolis parameter  $f$~~  and

$$15 \quad \underline{\gamma = \sqrt{\frac{f}{2\kappa}}}$$

representing a Coriolis parameter  $f = 1.0 \times 10^{-4} \text{ s}^{-1}$ , and an eddy viscosity coefficient  $\kappa$ .

Wind direction change between two heights is defined as directional shear. As we assume the directional shear to be an impact factor for the interaction process of a rotating system with veering inflow, a modified version of the Ekman spiral is applied as  $v_f$  in the simulations in this work. Further, the negative vertical gradient of the streamwise velocity in the supergeostrophic component of the Ekman spiral is not considered in  $u_f$ .

The simulations are initialized with the streamwise velocity profile

$$u_f(z) = u_g * (1 - \exp(-z\gamma)), \quad (6)$$

with an eddy viscosity coefficient  $\kappa = 0.06 \text{ m}^2 \text{ s}^{-1}$ , following Shapiro and Fedorovich (2010). The corresponding meridional spanwise velocity profile is

$$25 \quad \underline{v_{BLf}(z) = 0} \quad (7)$$

in the case of no veering inflow with  $\frac{\partial v_f}{\partial z} = 0$ , and

$$\underline{v_f(z) = u_{BLf}(z) * \tan \cdot \tan(\phi_{wind}(z))} \quad (8)$$

in the case of veering inflow with  $\frac{\partial v_f}{\partial z} \neq 0$  with a given directional shear

$$ds = \frac{\Delta\phi}{100 \text{ m}}, \quad (9)$$

with  $-\frac{z}{D}\phi_{50 \text{ m}}$  and  $\phi(z) = \pm 2\Delta\phi(1 - \frac{z}{D})$

(10)

in the lowest 200 m and constant above. The influence of the Coriolis force on the flow field is only included in the simulations via Eqs. 6, 8. Note that no Coriolis force is applied in the numerical model (Eq. 1).

In the incoming wind conditions we consider on For  $u_f$  and  $v_f$ , we consider the NH ( $f > 0$ ) and the SH ( $f < 0$ ), a veering ( $\frac{\partial\phi_{wind}}{\partial z}\Delta\phi \ll 0$  in NH,  $\frac{\partial\phi_{wind}}{\partial z}\Delta\phi \gg 0$  in SH), and a backing ( $\frac{\partial\phi_{wind}}{\partial z}\Delta\phi \gg 0$  in NH,  $\frac{\partial\phi_{wind}}{\partial z}\Delta\phi \ll 0$  in SH) wind. In the reference simulation (with a veering wind on in the NH, the wind direction change over the rotor radius is  $\Delta\phi = 4^\circ$  with  $v_{BL}(z_h)$ ), the directional shear is  $0.08^\circ \text{ m}^{-1}$  with  $v_f(z_h) = 0$ . The initial vertical velocity is

$$w_{BLf}(z) = 0 \quad (11)$$

in all simulations. The flow components  $u_f$ ,  $v_f$ , and  $w_f$  are used for specifying the initial conditions. The pressure solver in EULAG further applies  $u_f$  and  $v_f$  as boundary conditions. The potential temperature is

$$\Theta_e(z) = \Theta_0 + \frac{3 \text{ K}}{200 \text{ m}} z \quad (12)$$

in the lowest 200 m and 303 K above.

15 For a veering wind in the NH, we further modify the strength of  $\Delta\phi$  over the rotor with  $2^\circ$ ,  $4^\circ$ , and  $8^\circ$  corresponding to a weak ( $w$ ) modify the geostrophic wind, the directional shear and the rotational frequency of the rotor. We sample winds with a geostrophic wind component of  $u_g = 6 \text{ m s}^{-1}$ ,  $u_g = 10 \text{ m s}^{-1}$  (reference simulation), and  $u_g = 14 \text{ m s}^{-1}$ , referred to with the acronyms u6 and u14 in the simulation nomenclature. Further, we apply a directional shear of  $0.04^\circ \text{ m}^{-1}$ ,  $0.08^\circ \text{ m}^{-1}$ ,  $0.12^\circ \text{ m}^{-1}$ ,  $0.16^\circ \text{ m}^{-1}$ , and  $0.20^\circ \text{ m}^{-1}$  corresponding to weak (ds4), moderate ( $m$ ), or strong ( $s$ ) veer. We also test the rotational direction sensitivity towards the rotor section interacting with  $\Delta\phi$  reference simulation), moderate to strong (ds12), strong (ds16) and very strong (ds20) shear. As additional parameter, the rotational frequency ranges from  $\Omega \neq 0.058^\circ \text{ s}^{-1}$ ,  $\Omega \theta$ , limited to the lower rotor part ( $l$ ) or extended over the entire rotor ( $e = 0.12^\circ \text{ s}^{-1}$ ,  $\Omega = 0.175^\circ \text{ s}^{-1}$ , to  $\Omega = 0.23^\circ \text{ s}^{-1}$ , corresponding to low ( $\Omega$ ), moderate (reference simulation), high ( $\Omega h$ ), and very high ( $\Omega v h$ ) in the simulation nomenclature.

This work is a parameter study investigating the impacts of the inflow (directional shear, wind speed) and the geostrophic wind  $u_g$  with  $10 \text{ m s}^{-1}$  and  $14 \text{ m s}^{-1}$ .

The potential temperature in the reference simulation is rotating system (rotational frequency) on the the wake. The wake's impact by the rotational direction of the rotor depends on the mean wind profile, which is determined by the geostrophic wind (Eqs. 6, 8) and the directional shear (Eq. 9). Turbulence modifies the strength of the wakes, but not the occurrence (Appendix and Section 5). Therefore, we perform the simulations as implicit LES with no explicit subgrid-scale closure model. Moreover, we apply the turbulence parametrization by Englberger and Dörnbrack (2018b) to perturb the flow field during the numerical integration. This turbulence parametrization provides a computationally fast method for wind-turbine simulations with open horizontal boundary conditions on a small domain. It includes stability-dependent atmospheric characteristics in the inflow. This makes the method very suitable for parameter studies. We superimpose upon the inflow wind field turbulent fluctuations of a neutral boundary layer precursor simulation (Englberger and Dörnbrack, 2017), as represented by term I in Eq. 13, where  $\mathbf{u}_p|_{i^*,j,k}$  is the velocity vector of a neutral boundary layer equilibrium state at each grid point  $i, j$ , and  $k$ .

$$\Theta_{BL}(z)\mathbf{u}_p^*|_{i=1,j,k}^\delta = \Theta_{\alpha_0} + \frac{3K}{200m} z \cdot \alpha_{i^*,j,k} \cdot \left( \mathbf{u}_p|_{i^*,j,k} - \frac{1}{n \cdot m} \sum_{i=1}^n \sum_{j=1}^m \mathbf{u}_p|_{i,j,k} \right) \underline{I}. \quad (13)$$

in the lowest 200 m and 303 K above. We test the rotational direction sensitivity towards the strength of the stably stratified and preformed simulations. The indices of the grid points are denoted by  $i = 1 \dots n$ ,  $j = 1 \dots m$ , and  $k = 1 \dots l$  in the  $x$ ,  $y$ , and  $z$  directions, respectively. The star refers to a streamwise shift by one grid point at every time step  $\delta$  with  $1.5 \text{ K } i^* \neq 200 \text{ m}$  and  $6 \text{ K } i + \delta$ , whereas  $i^* \neq 200 \text{ m}$  corresponding to weakly (*th15*) and strongly (*th60*) stably stratified regimes in addition to the moderate regime (*th30*) of the reference simulation.  $[1, n]$  and  $\delta^*$  represents the passed number of timesteps. The prefactor  $\alpha_0$  represents the amplitude of the turbulence perturbations and  $\alpha_{i^*,j,k}$  represents adjustable stratification-dependent parameters for convective and stable regimes as well as the transitions between them. The stratification-dependent parameters were retrieved from a 30-h diurnal cycle simulation from Englberger and Dörnbrack (2018a).

We consider two different rotational directions. In the following simulations we apply a nighttime representations using values of  $\alpha = 0.3$ ,  $\alpha_u = 0.15$ ,  $\alpha_v = 0.24$ , and  $\alpha_w = 0.13$  (Englberger and Dörnbrack, 2018b, Table 1). A rather similar set-up including the turbulence parametrization has been applied in Englberger and Lundquist (2020).

## 2.3 Metrics

For the investigation of the rotational direction impact on the wake, the following characteristics are calculated from the simulation results: the spatial distribution of the time-averaged discrete streamwise velocity  $\overline{u_{i,j,k}}$ , the time-averaged discrete

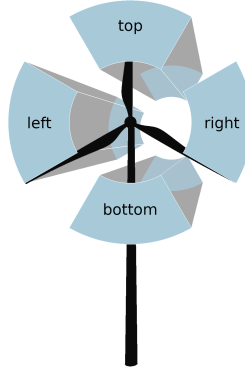


**Figure 1.** Schematic illustration of the top sector, the bottom sector, as well as the left and right sectors, defined from a view looking downwind towards the wind turbine on the disc.

spanwise velocity  $\overline{v_{i,j,k}}$ , and the streamwise velocity deficit

$$VD_{i,j,k} \equiv \frac{\overline{u_{1,j,k}} - \overline{u_{i,j,k}}}{\overline{u_{1,j,k}}} \quad (14)$$

The characteristics are averaged over the last 30 min of the 40-min wind-turbine simulation. The 30-min temporal average is calculated online in the numerical model according to the method of Fröhlich (2006, Eq. 9.1).

- 5 In the following, the quantities  $\overline{u_{i,j,k}}$  and  $\overline{v_{i,j,k}}$  are evaluated and discussed for top and bottom sectors. They result from a division of the rotor blades. As the forces  $\mathbf{F}_{WT}$  acting on the velocity components in area into four sections of  $90^\circ$ , as shown in Fig. 1, including all grid points with a distance  $r$  from the rotor center  $0 \text{ m} < r \leq R$ . The left and right sectors are defined from a view looking downwind towards the wind turbine on the disc.

### 3 Theoretical analysis

- 10 In this section, simple analytic relations are evaluated for three different inflow conditions (no veer, veering wind, backing wind) and in the case of a veering inflow, also for three different parameters (wind speed, directional shear, rotational velocity). The approach follows Englberger et al. (2019) and is modified to allow different directional shear values.

A rotating system can be described by a Rankine vortex with the radial dependence  $r$  and the rotational velocity  $\omega$ : 1

$$\overline{v_v(z)} = \pm \omega r \sin(\vartheta) \quad (15)$$

15  $\overline{w_v(z)} = \mp \omega r \cos(\vartheta) \quad (16)$



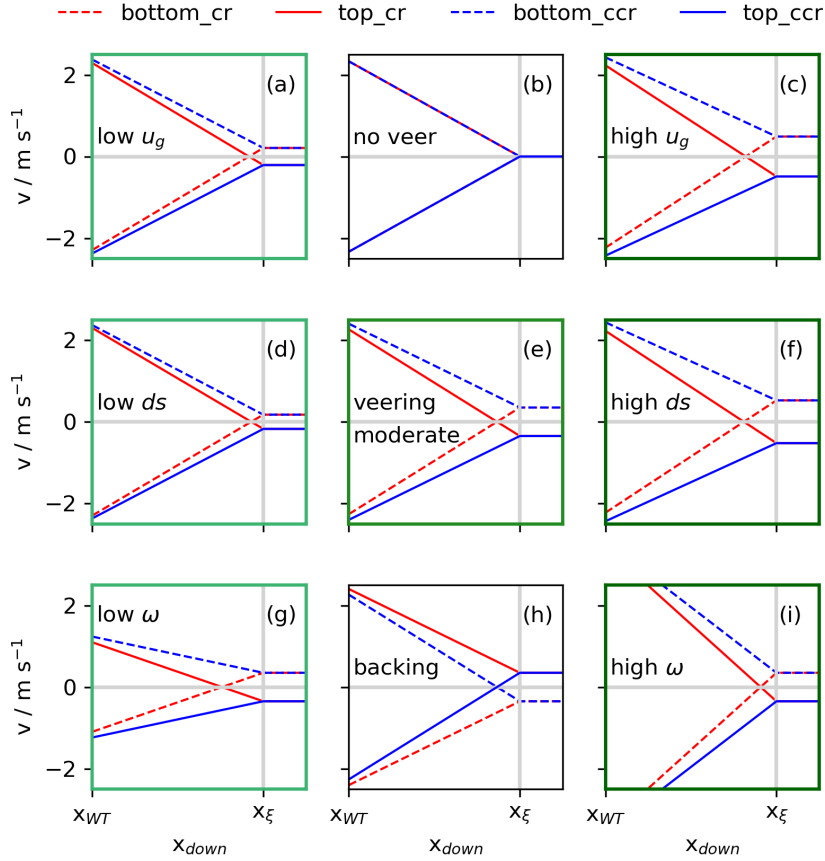


**Figure 2.** Representations of  $v(z = 75\text{m}, x_{down})$  at the rotor center in lateral position as bottom and  $v(z = 125\text{m}, x_{down})$  as top (Eq. 17) for a clockwise (cr) and a counterclockwise (ccr) rotating rotor in the case of no veer in (b), a veering wind in (e), and a backing wind in (h). In the case of a veering wind in (e), moderate parameters of  $u_g = 10 \text{ m s}^{-1}$ ,  $ds = 0.08^\circ \text{ m}^{-1}$ , and  $\omega = 0.12^\circ \text{ s}^{-1}$  are applied. In the left and right column, only one parameter is changed compared to the veering wind situation in (e). Applying low parameters  $u_g = 6 \text{ m s}^{-1}$  in (a),  $ds = 0.04^\circ \text{ m}^{-1}$  in (d), and  $\omega = 0.058^\circ \text{ s}^{-1}$  in (g), and applying high parameters  $u_g = 14 \text{ m s}^{-1}$  in (c),  $ds = 0.12^\circ \text{ m}^{-1}$  in (f), and  $\omega = 0.175^\circ \text{ s}^{-1}$  in (i).

lower rotor half and  $v_v(z_h + R/2, x_{down}) = +\omega r \sin(90^\circ) = \omega r > 0$  in the upper rotor half. However, if '-' is applied in Eq. 17,  $v_v(z_h - R/2, x_{down}) = -\omega r \sin(270^\circ) = \omega r > 0$  in the lower rotor half and  $v_v(z_h + R/2, x_{down}) = -\omega r \sin(90^\circ) = -\omega r < 0$  in the upper rotor half. The sign '+' corresponds to a counterclockwise wake rotation which arises from a clockwise rotor rotation  $\mathcal{C}R$  and (Zhang et al., 2012), whereas the sign '-' corresponds to a clockwise wake rotation arising from a counterclockwise

5 rotor rotation  $\mathcal{C}C\mathcal{R}$ . Simulations with ccr.

In the case of a clockwise rotating rotor  $CR$  corresponding to, the rotor competes against the veer effect with  $v_v(z_h - R/2, x_{down}) < 0$  superpositioning  $v_f(z_h - R/2) > 0$  and  $v_v(z_h + R/2, x_{down}) > 0$  superpositioning  $v_f(z_h + R/2) < 0$ . In both the top and bottom half of the rotor, the spanwise component of the inflow  $v_f$  is weakened by the vortex component  $v_v$ , or even reversed, if  $|v_v| > |v_f|$ . Approaching downwind, the impact of  $v_v$  decreases and  $v(z, x_{down})$  approaches  $v_f(z)$  at  $x_{down} = x_\xi$  with  $v_v(z, x_\xi) = 0$ .

In the case of a counterclockwise rotating near wake are comparable to the  $CCW$  simulations in Englberger et al. (2019), rotor, the wake vortex intensifies the inflow with  $v_v(z_h - R/2, x_{down}) > 0$  superpositioning  $v_f(z_h - R/2) > 0$  and simulations with a counterclockwise rotating rotor  $CCR$  corresponding to a clockwise rotating near wake are comparable to  $CW$  (Englberger et al., 2019)  $v_v(z_h + R/2, x_{down}) < 0$  superpositioning  $v_f(z_h + R/2) < 0$ . The vortex intensifies the inflow  $v_f(z_h)$  in all rotor heights. Approaching downwind, the impact of  $v_v$  decreases and  $v(z, x_{down})$  approaches  $v_f(z)$  at  $x_{down} = x_\xi$  with  $v_v(z, x_\xi) = 0$ . At  $x_{down} = x_\xi$ , the situation is independent of the vortex and the wake has completely recovered.

The different behaviour of the spanwise wake component is presented in Fig. 2(e). In the case of  $cr$ , the vortex component weakens the spanwise inflow component, resulting in a reversion of the sign of  $v(z, x_{down})$  behind the rotor at  $x_{down} < x_\xi$ . In the case of  $ccr$ , however, the vortex component intensifies the spanwise inflow component. At  $x_\xi$ , both rotational directions show the same result, approaching towards the inflow conditions.

Figure 2(h) represents the situation for a backing wind. Only  $\phi(z)$  (Eq. 10) and, therefore, the flow component  $v_f(z)$  (Eq. 8) changes sign in both the top and bottom half of the rotor. The vortex component  $v_v(z \pm R/2, x_{down})$  is not inflow dependent. Therefore, the wake behaviour of  $ccr$  ( $cr$ ) in the case of backing wind is comparable to  $cr$  ( $ccr$ ) under veering inflow, resulting in a decrease (intensification) of  $v_f(z)$  in the wake, following Eq. 17 with a '-' in Eq. 10.

The turbine-induced forces  $\mathbf{F}_{WT}$  are calculated with the BEM-method, including nacelle at the center grid point. This analysis shows a rotational direction dependent downwind behaviour of the spanwise flow component in the case of  $\frac{\partial v_f}{\partial z} \neq 0$ . The superposition of the Rankine vortex with a veering inflow (and likewise the backing wind) has three impacts. The veering inflow is determined by the geostrophic wind  $u_g$  and the directional shear  $ds$  over the rotor height. The vortex component is determined by the rotational velocity  $\omega$  of the rotor. The impact of  $u_g$ ,  $ds$  and excluding the tower. For the airfoil data, the 10 MW reference wind turbine from DTU (Bak et al., 2013) is applied, whereas the radius of the rotor as well as the chord length of the blades are scaled down to the rotor with a diameter of 100 m. The rotation frequency is set to 7 rpm. A detailed description of the wind turbine parametrization and the applied smearing of the forces, as well as all values used in the blade parametrization are given in Englberger and Dörnbrack (2017, parametrization B). A turbulent stably stratified regime in our wind turbine simulations performed with open horizontal boundary conditions is verified by applying the parametrization of Englberger and Dörnbrack (2018b). All parameters required to apply the parametrization are described

in detail in Englberger and Dörnbrack (2018b). A rather similar set-up, including the wind turbine parametrization and the parametrization of  $\omega$  on the expected mean behaviour of the spanwise wake component is presented in Fig. 2 for low values of the parameters in the left row and high values in the right row, whereas Fig. 2(e) represents the veering case for moderate parameter values.

5 A decrease of  $u_g$  (Fig. 2(a)) or  $ds$  (Fig. 2(d)) and likewise an increase of  $u_g$  (Fig. 2(c)) or  $ds$  (Fig. 2(f)) impacts the mean value of the spanwise wake field. Decreasing the atmospheric parameter values (Fig. 2(a), (d)), the values of  $v_f(z_h \pm R/2)$  also decrease, leading to a downwind shift of the sign-changing point of  $v(z, x_{down})=0$  (compare Fig. 2(a), (d) to (e)). A further decrease of  $v_f(z \pm R/2)$  approaching  $v_f(z \pm R/2)=0$  of the non-veering inflow case, results in Fig. 2(b). An increase of  $u_g$  (Fig. 2(c)) or  $ds$  (Fig. 2(f)) results in an increase of  $v_f(z \pm R/2)$  and an upward shift of the sign-changing point. If  
10 the atmospheric parameter values increase (decrease), the difference in the slope of the spanwise component between cr and ccr also increases (Fig. 2(c), (f)) (decreases (Fig. 2(a), (d))). Likewise, the slope in the case of cr increases for high values (Fig. 2(c), (f) in comparison to low values (Fig. 2(a), (d)), whereas in the case of ccr, the slope decreases for larger values of the inflow parameters (Fig. 2(c), (f) vs. (e) vs. (a), (d)). This behaviour can be interpreted as an increase of the difference in the wake between cr and ccr if the atmospheric parameters increase.

15 The rotational velocity  $\omega$  controls the magnitude of the spanwise vortex component. A decrease of  $\omega$  (Fig. 2(g)) and likewise an increase (Fig. 2(i)) also influences the mean value of the spanwise wake field, especially in the near wake. A decrease of  $\omega$  decreases  $v(z, x_{down})$  directly behind the rotor (Fig. 2(g)), whereas an increase results in an increase of  $v(z, x_{down})$  in the near wake (Fig. 2(i)). Larger values of  $\omega$  lead to a less rapid wake recovery in the near wake.

As a veering wind in the NH is comparable to a backing wind in the SH (following the definition via Eq. 10), all panels in  
20 Fig. 2 are also valid for the SH with red lines representing ccr\_SH and blue lines representing cr\_SH and dashed lines referring to the top rotor part and solid lines to the bottom rotor part.

## 4 Idealized simulations: Rotational Direction Impact on the Wake

### 4.1 Veering vs. No Veering Inflow

The analysis of the preceding section predicts a rotational direction impact on the spanwise velocity component  $v$  (and likewise  
25 the vertical component  $w$ ) in the wake under veering (or backing) inflow, whereas the wake characteristics in the case of no veer are independent of the rotational direction of the rotor. This rotational direction impact is investigated by LESs with veering and no veering inflow, with the simulation CR, CCR, CR\_NV, and CCR\_NV conducted with the parameters as listed in Table 1. The interactions between the wake rotation and the inflow are embodied in Fig. 3 in the crossstream and

vertical velocities at  $x = 3D$ . The first two columns represent CR and CCR in the case of veering inflow, whereas the last two columns correspond to no wind veer in the incoming flow field. The top row (Fig. 3(a)-(d)) represents the vectors  $(v, w)$ . The evolution of  $v$  and  $w$  is represented in the second row ((e)-(h)) for  $v$  and in the third row ((i)-(l)) for  $w$ . In the case of no wind veer, the sign of  $v$  is opposite in the upper and the lower rotor half for CR\_NV and CCR\_NV (Fig. 3(g), (h)), as predicted by the turbulent stably stratified regime, have been applied and explained in more detail in Englberger et al. (2019) and Englberger and Lundquist (2020) analysis (Eq. 17). The same is valid for the sign of  $w$  (Fig. 3(k), (l)). The numerical model shows a clockwise rotating wake in the case of CCR\_NV (while looking downwind (Fig. 1)), and a counterclockwise rotating wake in the case of CR\_NV.

Under veering inflow, the simulated wake rotates clockwise in the case of CCR (Fig. 3(b)) and counterclockwise in the case of CR (Fig. 3(a)), similar to the no veer case (Fig. 3(d), (c)). However, in comparison to the no veer case, the strength of rotation differs and is much more pronounced in the case of CCR (Fig. 3(b)) in comparison to CR (Fig. 3(a)). This rotation arises from the spanwise velocity component, as the vertical velocity (Fig. 3(i), (j)) is comparable to the non-veering cases (Fig. 3(k), (l)). The positive and negative perturbations in  $v$  have the same positive and negative patterns in CR (Fig. 3(e) vs. (g)) and CCR (Fig. 3(f) vs. (h)) as in CR\_NV and CCR\_NV in the corresponding rotor sector at  $x = 3D$ , however, with smaller  $|v|$  values in the upper and lower rotor sector in the case of CR and larger  $|v|$  values in the case of CCR. This simulated amplification of the spanwise flow component in the case of CCR (Fig 3(f)) and weakening up to a reversion of the sign in the wake region at  $x = 3D$  in the case of CR (Fig. 3(e)) is in agreement with the predictions of the analysis (Eq. 17) and Fig. 2.

List of all performed simulations in this study for a clockwise and a counterclockwise rotor rotation. Here,  $b$  represents a backing wind and  $v$  a veering wind.  $th15$  a low stably stratified regime and  $th60$  a strongly stably stratified one.  $e$  and  $l$  correspond to the rotor position, which is affected by wind veer (entire ( $e$ ) rotor or lower ( $l$ ) rotor half).  $s$  and  $w$  corresponds to a strong or a weak wind veer and  $u14$  to a higher geostrophic wind speed of  $14 \text{ m s}^{-1}$ .  $\phi_{wind}$  results from Eq. 10. The simulations  $CR$  and  $CCR$  correspond to both reference simulations with opposite rotational direction with  $CR_v_{NH}_{th30}_{em}_{u10}$  and  $CCR_v_{NH}_{th30}_{em}_{u10}$ . All  $_{-}$  to  $CR$  and  $CCR$  correspond to the differences between the corresponding simulation and its reference simulations  $CR$  and  $CCR$ .

## 5 Rotational Direction Impact on the Wake

In the following, the impact of the rotational direction of the rotor towards different atmospheric conditions is systematically investigated. Here, we consider the 10-min time and rotor area averaged streamwise velocity  $\overline{u_A}$ . It is further used to calculate

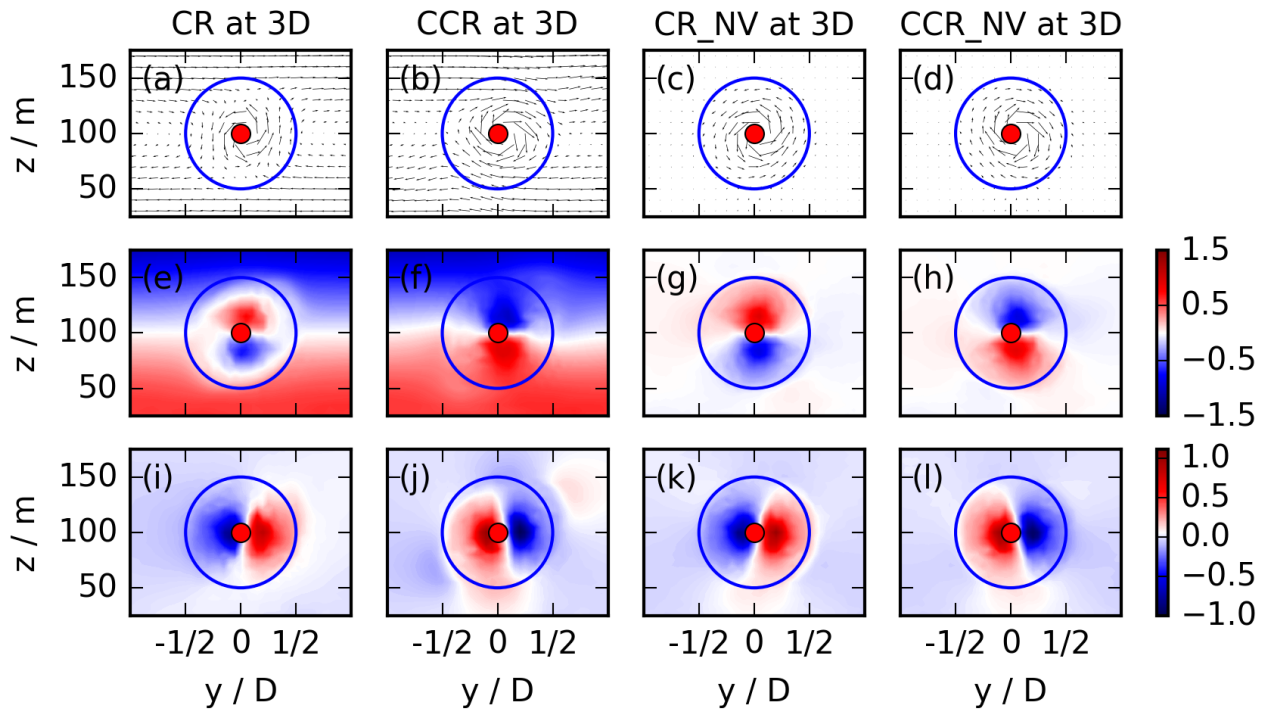


**Figure 3.**  $y$ - $z$ -cross sections for veering and no veering (NV) inflow simulations at  $x=3D$  for CR (first column), CCR (second column), CR\_NV (third column), and CCR\_NV (last column). The first row ((a)-(d)) presents the  $(v, w)$  vectors in the  $y$ - $z$ -plane, the second row ((e)-(h)) the spanwise wake velocity  $v$ , and the third row ((i)-(l)) the vertical wake velocity  $w$ . The blue circle represents the circumference of the actuator disc. This picture is looking downwind on the wake (Fig. 1, corresponding to the left sector for  $y < 0D$  and the right sector for  $y > 0D$ ).

the power produced by a hypothetical downwind turbine up to  $10D$  downstream with

$$P = \frac{1}{2} \rho_0 c_p \eta_{mech} A \overline{u_A}$$

where  $\rho_0$  is the density of the air,  $c_p$

A downwind distance of  $x=0.5$ ,  $\eta_{mech}=3$  0.64 and  $A$  the area of the rotor (Manwell et al., 2002)  $D$  is visualized in Fig. 3 because a significant spanwise vortex impact on the spanwise flow component in the wake can be expected. In the following,

5  $\overline{u_A}$  and  $P$  are evaluated and discussed at all downwind positions from 4 special emphasis is placed at  $x/D$  to  $10/D$ , with special emphasis at  $7D$ , as which is often considered a typical downwind distance for a hypothetical waked wind turbine in numerical

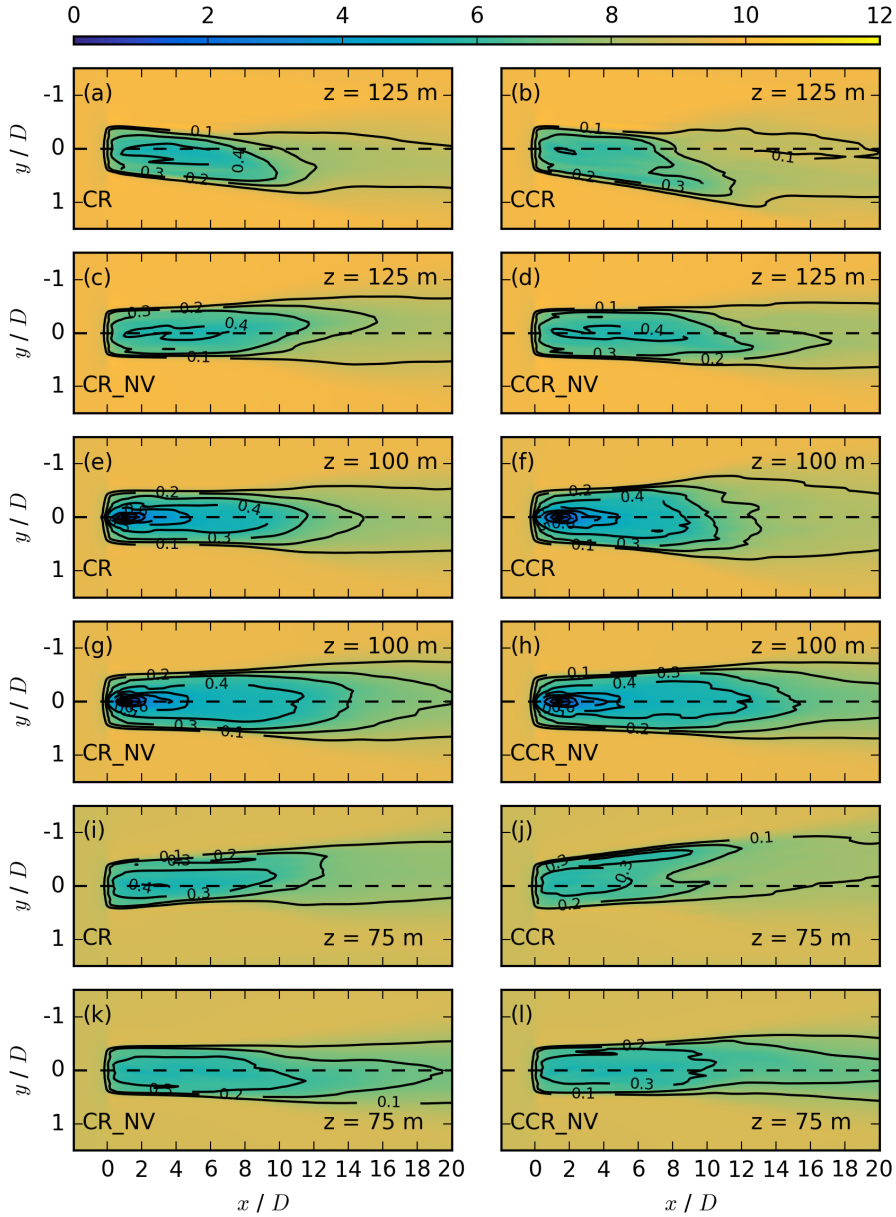


**Figure 4.** Contours of the streamwise velocity  $\overline{u_{i,j,k}}$  in  $\text{m s}^{-1}$  at  $z = 125$  m in the first two rows, at  $z = 100$  m the the third and fourth row, and at  $z = 75$  m in the last two rows for the simulations CR, CCR, CR\_NV and CCR\_NV, each averaged over 30 min. The black contours represent the velocity deficit  $VD_{i,j,k}$  at the same vertical location.

simulation studies (e.g. Gaumond et al. (2014); Abkar et al. (2016)). Further, we use the velocity deficit, defined according to

$$VD_{i,j,k} = \frac{\overline{u_{i_1,j,k}} - \overline{u_{i,j,k}}}{\overline{u_{i_1,j,k}}},$$

**Table 1.** List of all performed simulations in this study for a clockwise (leftmost column) and a counterclockwise (rightmost column) rotor rotation. The parameters  $u_g$ ,  $ds$ , and  $\Omega$  refer to both rotational directions, whereas the only difference e.g. between CR and CCR in the first line is the rotational direction. Further,  $\_NV$  represents no wind veer,  $\_b$  a backing wind,  $\_ds$  refers to varying the directional shear,  $\_u$  refers to varying the geostrophic wind, and  $\_{\Omega}$  refers to varying the rotational frequency in the corresponding simulations.

SIMULATIONS WITH DIFFERENT ROTATIONAL DIRECTIONS OF THE ROTOR			
CLOCKWISE	$\phi_{wind}(150\text{ m})\phi_{wind}(50\text{ m})\frac{\partial\Omega}{\partial z}u_g$	$f_{ds}$	$\Omega$
CR	$-4^\circ-4^\circ-3\text{ K}/200\text{ m}-10\text{ m s}^{-1}$	$10\text{ m s}^{-1}-0.08^\circ\text{ m}^{-1}$	$>0-0.12^\circ\text{ s}^{-1}$
CR_bNV	$4^\circ-4^\circ-3\text{ K}/200\text{ m}-10\text{ m s}^{-1}$	$>0^\circ\text{ m}^{-1}$	CCR_b CR_v_SH $4^\circ-4^\circ-3\text{ K}/200\text{ m}-10\text{ m s}^{-1}-0.12^\circ\text{ s}^{-1}$
CR_SHb	$-4^\circ-4^\circ-10\text{ m s}^{-1}$	$3\text{ K}/200\text{ m}-0.08^\circ\text{ m}^{-1}$	$10\text{ m s}^{-1}-0.12^\circ\text{ s}^{-1}$
CR_th15ds4	$-4^\circ-4^\circ-1.5\text{ K}/200\text{ m}-10\text{ m s}^{-1}$	$>0$	CCR_th15CR_th60 $-4^\circ-0.04^\circ\text{ m}^{-1}$ $4^\circ-0.12^\circ\text{ s}^{-1}$
CR_ds12	$10\text{ m s}^{-1}$	$>0-0.12^\circ\text{ m}^{-1}$	CCR_th60CR_es $0.12^\circ\text{ s}^{-1}$
CR_ds16	$8^\circ-10\text{ m s}^{-1}$	$3\text{ K}/200\text{ m}-0.16^\circ\text{ m}^{-1}$	$10\text{ m s}^{-1}-0.12^\circ\text{ s}^{-1}$
CR_ewds20	$-2^\circ-2^\circ-10\text{ m s}^{-1}$	$3\text{ K}/200\text{ m}-0.20^\circ\text{ m}^{-1}$	$10\text{ m s}^{-1}-0.12^\circ\text{ s}^{-1}$
CR_lsu6	$-8^\circ-0^\circ-6\text{ m s}^{-1}$	$3\text{ K}/200\text{ m}-0.08^\circ\text{ m}^{-1}$	$10\text{ m s}^{-1}-0.12^\circ\text{ s}^{-1}$
CR_lmu14	$-4^\circ-0^\circ-14\text{ m s}^{-1}$	$3\text{ K}/200\text{ m}-0.08^\circ\text{ m}^{-1}$	$10\text{ m s}^{-1}-0.12^\circ\text{ s}^{-1}$
CR_u14 $\Omega$	$-4^\circ-4^\circ-3\text{ K}/200\text{ m}-10\text{ m s}^{-1}$	$14\text{ m s}^{-1}-0.08^\circ\text{ m}^{-1}$	$>0-0.058^\circ\text{ s}^{-1}$
CR_es_u14 $\Omega$ h	$-8^\circ-10\text{ m s}^{-1}$	$8^\circ-0.08^\circ\text{ m}^{-1}$	$3\text{ K}/200\text{ m}-0.175^\circ\text{ s}^{-1}$
CR_ $\Omega$ vh	$>0-10\text{ m s}^{-1}$	$0.08^\circ\text{ m}^{-1}$	$0.23^\circ\text{ s}^{-1}$

calculated at the discrete grid points  $x_i$ ,  $y_j$ , and  $z_k$  with  $i_1$  corresponding to the first upstream grid point. At  $x = 7D$ , the vortex impact is much smaller compared to  $x = 3D$  (Fig. 3), resulting in an increase of the impact of the atmospheric flow.

#### 4.1 Veering Wind vs. Backing Wind on both Hemispheres

The comparison of simulations  $CR$  and  $CR_b$  reveals the difference in  $\overline{u_A}$  and  $P$  between a veering and a backing wind on the in case of a clockwise rotating rotor. As the rotational direction has a significant impact on the spanwise flow component at  $x = 3D$  (Fig. 3), an impact on the streamwise flow component is also expected. The numerical results for the streamwise velocity component are presented for veering ( $CR$ ,  $CCR$ ) and non-veering ( $CR_{NV}$ ,  $CCR_{NV}$ ) inflow by  $x-y$  cross sections of the streamwise velocity in the top half of the rotor disc at  $z = 125\text{ m}$  (Fig. 7a shows larger  $\overline{u_A}$  values if a backing wind ( $CR_b$ ) interacts with a clockwise rotating rotor in comparison to a veering wind ( $CR$ ). In addition, the difference of  $\overline{u_A}$  between a backing and a veering wind increases downwind up to  $\Delta\overline{u_A}4(a) \approx (d)$ , at hub height at  $z = 0.5\text{ m s}^{-1}$  at  $10D$ . Considering a counterclockwise rotating rotor in  $CCR$  and  $CCR_b$ ,  $\Delta\overline{u_A}$  is the same for  $CR$  and  $CCR_b$  and likewise for

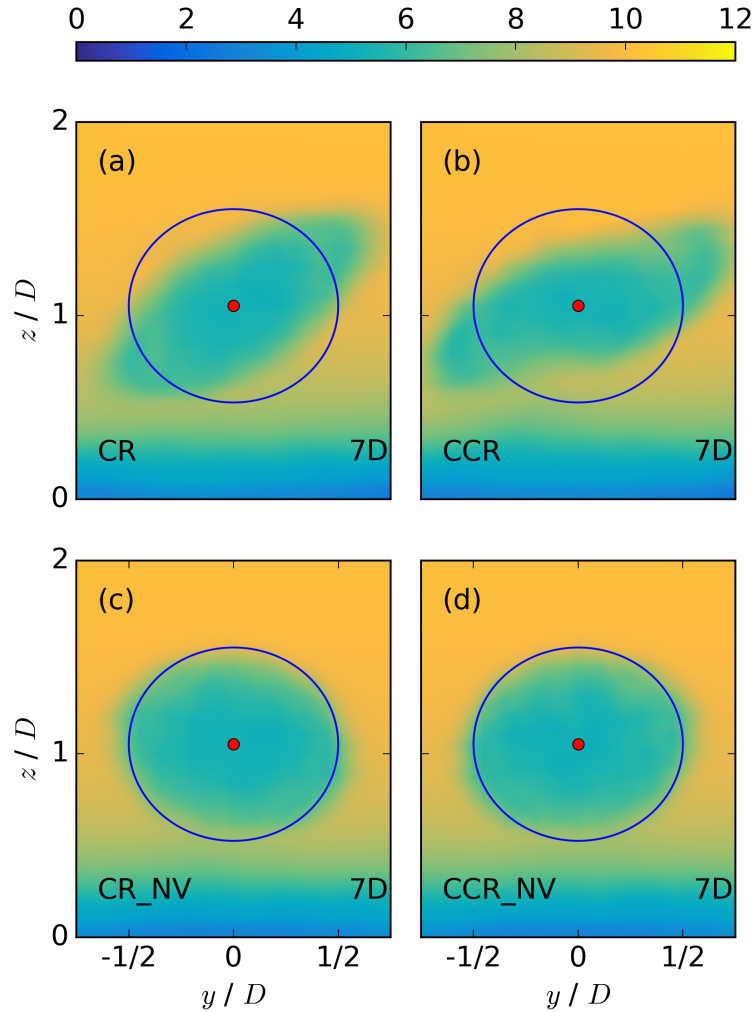


**Figure 5.** Contours of the streamwise velocity  $\overline{u_{i,j,k}}$  in  $\text{m s}^{-1}$  at a downward position of  $x = 3 D$  behind the rotor of for CR in (a), CCR in (b), CR\_NV in (c), and CCR\_NV in (d). The blue circle represents the circumference of the actuator disc.

*CCR and CR\_b.* This results in larger  $\overline{u_A}$ -values and  $P$ -values in *CCR*-100 m (Fig. 4(e) - (h)), and in the bottom half of the rotor disc at  $z = 75$  m (Fig. 4(i) - (l)).

The effect of wind veer on the streamwise velocity component of clockwise rotating wind turbines is investigated by comparing CR to CR\_NV, in Fig. 4(a) vs. (c) at  $z = 125$  m, (e) vs. (g) at  $z = 100$  m, and (i) vs. (k) at  $z = 75$  m. Inflow veer causes a more rapid wake recovery at all heights, based on comparison of the velocity deficit contours. Because enhanced

5  $\frac{\partial v_i}{\partial z} \neq 0$  in the case of veering wind, it provides a source of resolved turbulence resulting in higher entrainment in compari-

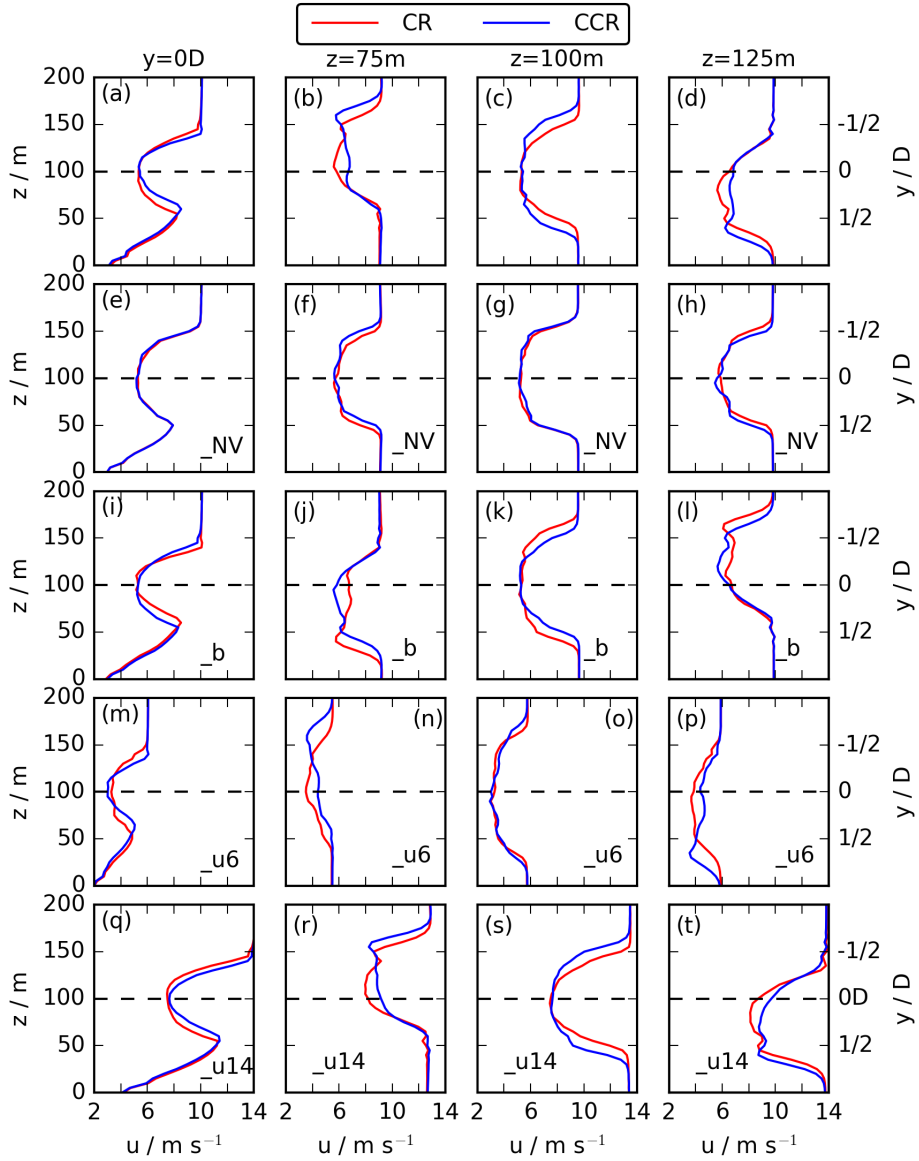


**Figure 6.** Vertical (first column) and horizontal profiles at  $z = 75$  m (second column),  $z = 100$  m (third column), and  $z = 125$  m (fourth column) of the 30 min averaged streamwise velocity at  $x = 7D$  downwind of the actuator for CR and CCR in (a) - (d), CR\_NV and CCR\_NV in (e) - (h), CR\_b and CCR\_b in (i) - (l), CR\_u6 and CCR\_u6 in (m) - (p), and CR\_u14 and CCR\_u14 in (q) - (t).

son to ~~CCR\_b~~. For a hypothetical ~~7~~ the no-veer case. Further, inflow wind veer causes wake deflection in both the top half (Fig. 4(a) vs. (c)) and the bottom half (Fig. 4(i) vs. (k)) of the rotor disc. The wake in the veered simulation CR is deflected

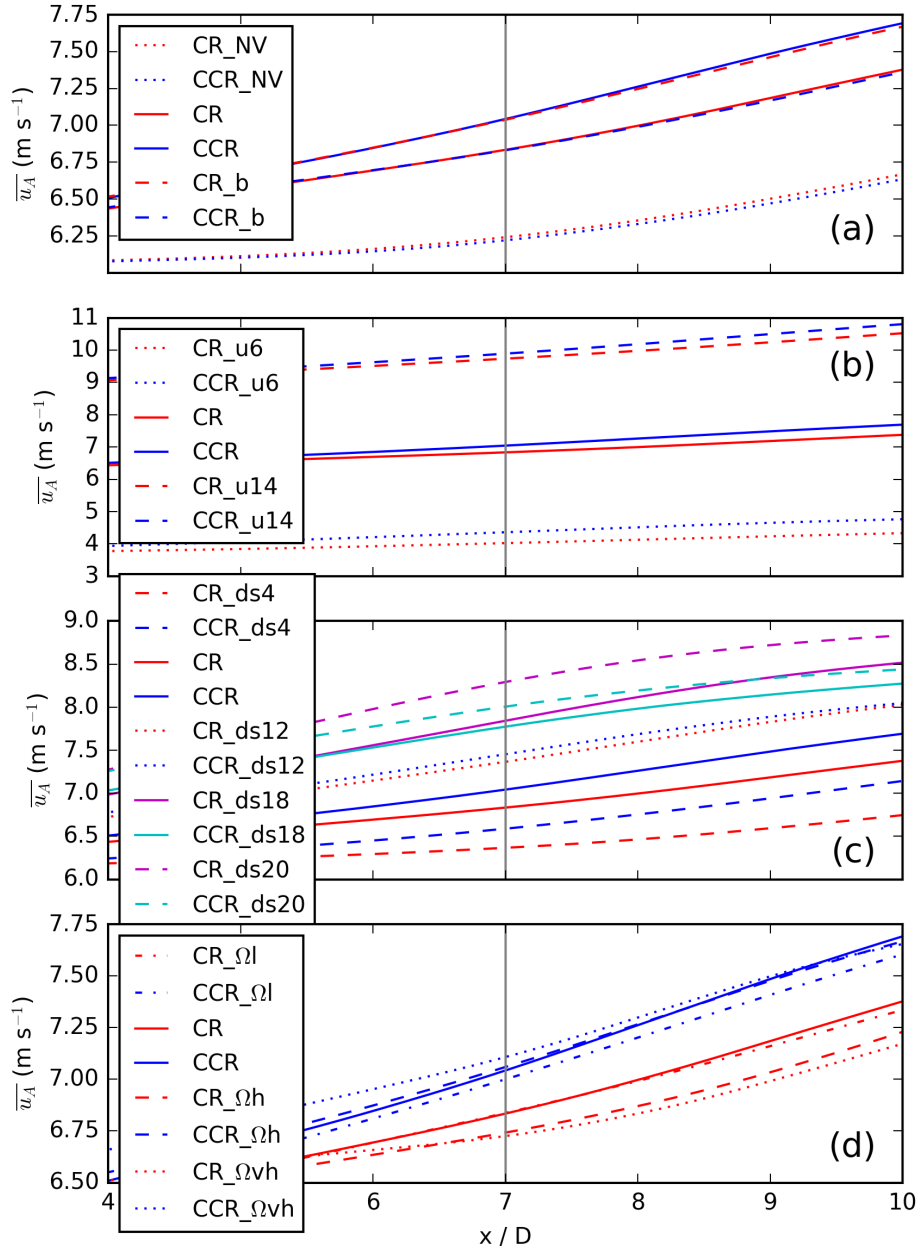


**Figure 7.** The rotor and time averaged streamwise velocity  $\overline{u_A}$  presented for a downwind region of  $[4D; 10D]$  with special emphasis at  $x = 7D$  for the simulations CR\_NV, CCR\_NV, CR, CCR, CR\_b and CCR\_b in (a), for different geostrophic wind values in (b), for different directional shears in (c), and for different rotational frequencies in (d).

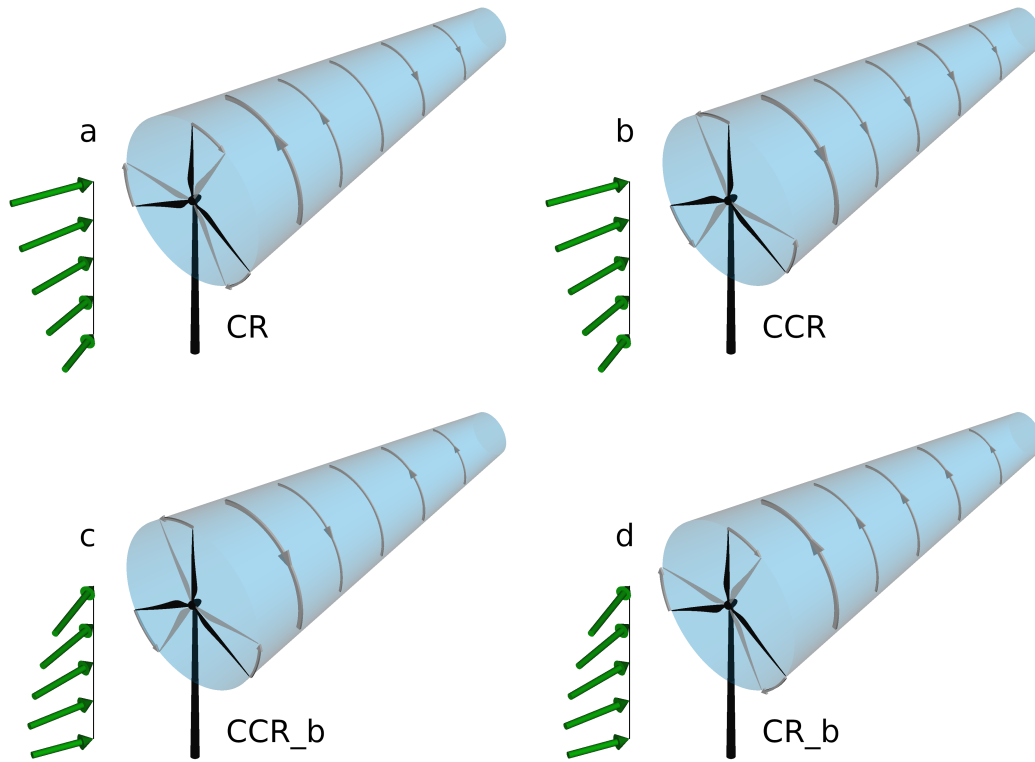


**Figure 8.** Schematic illustration of the rotational direction of the wake for the cases: Clockwise blade rotation CR with veering wind in NH (corresponding to backing wind in SH) in (a), counterclockwise blade rotation CCR with veering wind in NH in (b), counterclockwise blade rotation with backing wind CCR\_b in NH (corresponding to veering wind in SH) in (c), and clockwise blade rotation with backing wind CR\_b in NH in (d).

towards the right ( $y \geq D$ ) downwind turbine, this leads to an 11.5% increase in power in case of a veering wind interacting with counterclockwise rotating blades or if a backing wind interacts with clockwise rotating blades.

The rotor averaged streamwise velocity  $\overline{u_A}$  and the power  $P$  of a hypothetical downwind turbine are presented for a downstream region of  $[4D; 10D]$  for a veering and a backing wind in the in  $a$ , for a veering and a backing wind in the in  $b$ , and for all eight simulations together in  $c$ .

- 5 The same investigation is shown in Fig. 7b for the . Here, we also consider a veering and a backing wind with both rotational directions of the rotor, resulting in the simulations  $CR_v_{SH}$ ,  $CCR_v_{SH}$ ,  $CR_{SH}$ , and  $CCR_{SH}$ . The downstream behaviour and likewise  $\Delta \overline{u_A}$  are similar but opposite to the results in the . The power output of a hypothetical downwind turbine at  $7 \geq D$  would also be larger by 11.5%, however, on the , in case of a veering wind and clockwise rotating blades or a backing

wind-interacting with counterclockwise rotating blades. The minor difference near  $100D$  downwind between  $CR_{v\_SH}$  and  $CCR_{SH}$  and likewise between  $CCR_{v\_SH}$  and  $CR_{SH}$  in  $D$  (left ( $y < 0D$ )) in the upper (lower) rotor part (Fig. 7b) results from the applied parametrization of Englberger and Dörnbrack (2018b), as the inflow wind field was extracted from a diurnal cycle LES on the (Englberger and Dörnbrack, 2018a). This assumption is supported by the following aspects: the difference is not prevalent in the northern hemispheric simulations in Fig. 7a, and the difference emerges far downstream, starting at  $x \approx 4D$  (Fig. 4(i)). In the non-veered simulation  $CR_{NV}$ , the wake is only slightly deflected towards the left in the top-tip sector (Fig. 4(c)) and towards the right in the bottom-tip sector (Fig. 4(k)). This effect is caused by the rotation of the rotor, which transports higher momentum air counterclockwise, resulting in a wake deflection to the left at  $z \geq 8125$  m (Fig. 4(c)). Consequently, the opposite situation prevails at  $z = 75$  m (Fig. 4(k)). As the inflow veer contribution to wake deflection is much larger compared to the effect of a clockwise rotating rotor, the wake deflection changes from left in  $CR_{NV}$  (Fig. 4(c)) to the right in  $CR$  (Fig. 4(a)) in the upper rotor half and vice versa in the lower rotor half.

As a next step, the rotational direction impact in the non-veered simulations  $CR_{NV}$  and  $CCR_{NV}$  is investigated (Figs. 4(c) vs. (d), (g) vs. (h), and (k) vs. (l)). The impact of the ~~disc~~ rotational direction on the wake structure is rather small in comparison to the ambient flow field impact and it also increases approaching  $10D$ :

Schematic illustration of the rotational direction of the wake for the cases: Clockwise blade rotation with veering wind in  $NH$  ( $CR$ ) and with backing wind in  $SH$  ( $CR_{SH}$ ) in (a), counterclockwise blade rotation with veering wind in  $NH$  ( $CCR$ ) and backing wind in  $SH$  ( $CCR_{SH}$ ) in (b), counterclockwise blade rotation with backing wind in  $NH$  ( $CCR_b$ ) and veering wind in  $SH$  ( $CCR_{v\_SH}$ ) in (c), and clockwise blade rotation with backing wind in  $NH$  ( $CR_b$ ) and veering wind in  $SH$  ( $CR_{v\_SH}$ ) in (d).

In Fig. 7c, all eight simulations are shown. Here, the results of simulations  $CCR$ ,  $CR_b$ ,  $CR_{v\_SH}$ , and  $CCR_{SH}$  overlap and, likewise, the ones for  $CR$ ,  $CCR_b$ ,  $CCR_{v\_SH}$ , and  $CR_{SH}$ . The resulting flow fields of the wakes are schematically shown in is limited to the wake deflection differences at the upper (Fig. 4(c), (d)) and the lower (Fig. 8. The combinations of  $\frac{\partial \phi_{wind}}{\partial z} < 0$  and a clockwise blade rotation  $D$  and result from the rotational direction of the rotor. These differences in the non-veered simulations agree with results of Vermeer et al. (2003), Shen et al. (2007), Sanderse (2009), Kumar et al. (2013), Hu et al. (2013), Yuan et al. (2014), Mühle et al. (2017), and Englberger et al. (20

The rotational direction impact on the wake structure under veering inflow is investigated by a comparison of  $CCR$  to  $CR$  (Fig. 4(b) vs. (a), (f) vs. (e), and (j) vs. (i)). In  $CCR$ , the wake recovers more rapidly (Fig. 8a) or  $\frac{\partial \phi_{wind}}{\partial z} > 0$  and a counterclockwise blade rotation (Fig. 8c) result in contrasting rotational directions of the near and far wake, referred to hereafter as 'contrasting wake cases'. The combinations of  $\frac{\partial \phi_{wind}}{\partial z} < 0$  and a counterclockwise blade rotation 4(f) vs. (e) and

30 the wake deflection angle is larger (Figs. 4(b) vs. (a) and (j) vs. (i)) in comparison to CR. Further, the wake width is larger in the spanwise direction in CCR in comparison to CR (Fig. 8b) or  $\frac{\partial \phi_{wind}}{\partial z}$  4(b) vs. (a), (f) vs. (e), and (j) vs. (i)).

The differences in the spanwise wake width and the wake deflection angle are investigated in more detail with the  $y \sim 0$  and a clockwise blade rotation ( $z$  crosssections at  $x = 7D$  in Fig. 8d), however, result in a rotational direction of the wake which persists in the whole wake, referred to hereafter as 'consistent wake cases'. This contrasting and consistent behaviour of the rotational direction in the wake is valid on both hemispheres.

The 10-min time averaged streamwise velocity, representing the simulation from 10 min to 20 min, is plotted at hub height in Fig. ?? for all eight cases together with the velocity deficit (Eq. 14) as contour. The structures of the four contrasting wake cases (left row) resemble each other with narrower wakes. Similarly, the four consistent wake cases (right row) resemble each other with wider wakes. The entrainment of ambient air in the consistent wake cases is slightly less rapid in the near wake in comparison to the contrasting wake cases, whereas it is substantially enhanced in the far wake. This results in the higher  $\overline{u_A}$  value in the consistent wake cases and an increase of  $\Delta \overline{u_A}$  approaching downstream with rather similar values in the near wake for 5 for veering inflow (CR in (a), CCR in (b)) and no wind veer (CR\_NV in (c), CCR\_NV in (d)) with both rotational directions of the actuator. In the case of no veering inflow, the simulated wake at  $x = 7D$  retains the shape of the rotor (Fig. 5(c)). In the case of a veering inflow, however, the wake in the lower rotor half is shifted to the left and in the upper rotor half to the right (Fig. 5(a)). The striking difference between veering and non-veering inflow simulations in combination with a clockwise rotating actuator corresponds to the inflow profile (Eqs. 6, 8), where a veering inflow is characterized by a wind component from right to left for  $z < 4100$  m and from left to right for  $z > 100$  m, whereas the spanwise inflow velocity is zero in the case of no veer in all rotor heights. The skewed wake structure under veering inflow resembles those of the simulations of Abkar and Porté-Agel (2016), Vollmer et al. (2017), Bromm et al. (2017), Churchfield and Srinivas (2018), and Englberger and Dörnbrack (2018a).

Further, we compare the differences between a clockwise and a counterclockwise rotating actuator for non-veering and veering inflow. In the case of no wind veer, the simulated wake structures of CCR\_NV (Fig. 5(d)) and CR\_NV (Fig. 5(c)) show no striking difference. In the case of veering inflow, however, the skewed wake structure differs in CR and CCR (Fig. 5(a), (b)). Whereas the wake is elliptical in CR, this shape is stretched in the rotor region in CCR. This difference in shape explains the difference in the spanwise wake width at hub height (Fig. 4(f)) and also in the lower (Fig. 7) 4(j)) and the upper (Fig. 4(b)) rotor part. The wake structure dependence on the rotational direction of the rotor concurs with the results in outside the rotor region also differs between Fig. 4 of Englberger et al. (2019).

Coloured contours of the streamwise velocity  $\overline{u_{i,j,k_h}}$  in  $\text{m s}^{-1}$  at hub height  $k_h$ , averaged over the last 10 min, for *CR* in (a), *CCR* in (b), *CCR\_b* in (c), *CR\_b* in (d), *CCR\_v\_SH* in (e), *CR\_v\_SH* in (f), *CR\_SH* in (g), and *CCR\_SH* in (h). The black contours represent the velocity deficit  $VD_{i,j,k_h}$  at the same vertical location.

5 (a) and (b). Due to the elongation of the elliptical structure in *CCR* in the rotor region (Fig. 4(b)), and approximately the same vertical wake extension in *CCR* and *CR*, the wake deflection angle increases in the case of *CCR* (Fig. 5(b) vs. (a)), as shown in the lower rotor half in Fig. 4(j) vs. (i) and also in the upper rotor half in Fig. 4(b) vs. (a).

The evolving different wake structures result in a larger power output of the consistent wake cases in comparison to the contrasting wake cases of a downwind turbine of roughly 11% at  $x = 7D$  approaching even to 19% at  $10D$ . Figure 6 represents the vertical profiles at  $y = 0D$ . Considering the much higher frequency of occurrence of a veering wind in comparison to a backing wind ( $\approx 3.8$  times more frequent according to two years of meteorological tower measurements in Lubbock (Texas) (Walter et al., 2009)), a counterclockwise rotating rotor in the (and a clockwise rotating rotor in the ) would increase the power production for awaked turbine downwind.

#### 4.1 Strength of Stratification

The impact of the stable stratification is tested for three different regimes, a weakly stably stratified atmosphere in *CR\_th15*, 15 a moderate stably stratified atmosphere in *CR*, and a strongly stably stratified atmosphere in *CR\_th60*. The tested lapse rates are representative compared =  $0D$  in (a), and spanwise profiles of  $u$  at  $z = 75$  m in (b), at  $z = 100$  m in (c), and at  $z = 125$  m in (d) for both rotational directions *CR* and *CCR*. The heights correspond to Fig. 2 in Walter et al. (2009). The impact on  $\overline{u_A}$  is presented in 4. Figure 6(e) - (h) represent the non-veering inflow simulations *CR\_NV* and *CCR\_NV*. Whereas the vertical and spanwise profiles of *CR* and *CCR* in the case of no inflow veer (*\_NV*) are almost overlapping (Fig. ??a. In case of a 20 common clockwise rotating rotor, the wake lasts longer in stronger stratification 6(e) - (h)), there is a difference in the case of veering inflow (Fig. 6(a) - (d)). Firstly, the streamwise wake elongation difference of Figs. 4(f) vs. (e) is represented by larger  $u$ -values in the lower and the upper rotor half in the case of *CCR* in Fig. ?. The wake recovers faster in *CR\_th15* compared to *CR* and further *CR* recovers faster compared to *CR\_th60*. This differences in  $\overline{u_A}$  translates in a 19% larger power output of a hypothetical downwind turbine in an during the evening transition (*CR\_th15*) in comparison to the power output at night 25 where the surface fluxes are at its minimum (*CR\_th60*). Following the increase of the recovery rate from *CR\_th60* to *CR* to *CR\_th15*, it would result in an increase of 6(b) and (d). The larger wake deflection angle in *CCR* in comparison to *CR* (Fig. 4 (b) vs. (a) and (j) vs. (i)) is represented by a larger spanwise distance of the minimum of  $u$  from  $y = 0D$  in case of *CCR* in the power output for decreasing the strength of stratification.

The rotor-averaged streamwise velocity  $\overline{u_A}$  and the power  $P$  of a hypothetical downwind turbine are presented for a downstream region of  $[4D; 10D]$  for different thermal stratifications in  $a$ , for different strength of wind veer and rotor areas affected by the veering wind in  $b$ , and for different wind speeds in  $c$ .

Considering the same stratification with a counterclockwise rotating rotor in  $CCR_{th15}$ ,  $CCR$ , and  $CCR_{th60}$  in lower (Fig. 6(b)) and the upper (Fig. 6(d)) rotor half. This spanwise difference of  $u_{min}$  is accompanied by larger  $u$ -values in the case of CCR for  $y < -1/2 D$  in the lower rotor part (Fig. 6(b)) and for  $y < 1/2 D$  in the upper rotor part (Fig. 6(d)). Secondly, the difference in the spanwise wake width is represented in all three heights by a larger  $\Delta L_y$  with smaller  $u$ -values in CCR in the outermost region of the left and the right sectors in comparison to CR (Fig. ??a, the values of downwind wind speed  $\overline{u_A}$  are rather similar and nearly independent of the stratification. Only in the strongly stratified regime  $CCR_{th60}$ , the 6(b) - (d)).

As final step, the difference in the wake is summarized by the 30-min time and rotor area averaged streamwise velocity  $\overline{u_A}$ . Figure 7(a) represents the difference between clockwise and counterclockwise rotating rotors for a veering inflow and in the case of no wind veer from  $x = 4D$  to  $10D$ . At  $x = 7D$ ,  $\overline{u_A}$ -value slightly increases is  $0.24 \text{ m s}^{-1}$  larger in the counterclockwise rotating rotor simulation CCR in comparison to the weakly (4%) and moderate (3%) regimes, resulting in a maximum power output of a hypothetical downwind turbine at night where the surface fluxes approaching its minimum. However, the impact of stratification is roughly five times smaller in comparison to the one for clockwise rotating wind turbines.

This wake behaviour results in a larger potential power output of a downwind turbine in case of a counterclockwise rotating rotor of 4% in the weakly stably stratified case, of 11.5% in the moderate stably stratified case, and of 23% in the strongly stably stratified situation at 7CR, whereas there is no difference between CCR\_NV and CR\_NV. According to Fig. 6(a) D. A counterclockwise blade rotation will not only enhance the power output, it will further increase the accumulated power output during the rather long nights with approximately constant surface fluxes (9 h (Walter et al., 2009, Fig. 2), 11 h (Blay-Carreras et al., 2014; Abkar et al., 2016; Englberger and Dörnbrack, 2018a, Fig. 1)). In addition, counterclockwise blade rotation would also increase the power output during the morning boundary layer regime. This regime is strongly affected by the previous nocturnal stability with an even smaller entrainment rate before the surface fluxes become positive due to the incoming solar radiation (Englberger and Dörnbrack, 2018a, Fig. 4) (d), these larger  $\overline{u_A}$ -values in the case of CCR result from larger  $u$ -values in the upper and lower sector related to the larger wake deflection angle in the case of CCR, which compensates for the larger  $u$ -values in the outer region of the left and right sectors resulting from a larger spanwise wake width in the case of CCR.

The previous investigations show a striking dependence of the rotational direction of the rotor on the wake under veering inflow, which is qualitatively well explained by the analysis. A schematic illustration of the deceleration or even reversion of

the spanwise flow if a clockwise rotating rotor CR interacts with a veering wind is presented in Fig. 8(a). The amplification of the spanwise flow in the case of a counterclockwise rotating rotor CCR interacting with veering inflow is presented in Fig. 8(b).

#### 4.1 Veering Wind vs. Backing Wind

The contrasting power production between the clockwise and the counterclockwise rotating simulations can be explained by means of According to the analytical results (Fig. ??). The wake structure in the clockwise rotating blade simulations  $CR\_th15$  in *a*,  $CR$  in *c*, and  $CR\_th60$  in *e*, behaves as known from previous studies: a less rapid wake recovery and an elongated wake for a stronger stably stratified regime (Abkar and Porté-Agel, 2014; Abkar et al., 2016; Vollmer et al., 2016; Englberger and Dörnbrack, 2018). In contrast, the wake structures are rather similar in  $CCR\_th15$  in *b* and in  $CCR$  2(*e*) vs. (*h*), the spanwise component  $v$  in the wake is expected to be comparable for a clockwise rotating rotor in veering inflow and a counterclockwise rotating rotor in backing inflow, as well as a clockwise rotating rotor in backing inflow and a counterclockwise rotating rotor in veering inflow. The wake characteristics resulting from a backing wind with both rotational directions are investigated in the simulations  $CR\_b$  and  $CCR\_b$  and compared to the veering wind cases  $CR$  and  $CCR$  in Fig. 9. The parameters applied in the corresponding simulations are listed in Table 1.

The behaviour in the upper and the lower rotor part in Fig. 9 can directly be compared after mirroring at  $y=0D$ , an effect resulting from the opposite sign of the directional shear and  $\Delta\phi$  in Eqs. 9 and 10. A strong similarity is prevalent in the streamwise velocity component at hub height (Fig. 9(*f*), (*g*) and (*e*), (*h*)), in *d*. Only the wake width of  $CCR\_th60$  in *f* differs slightly from  $CCR\_th15$  and  $CCR$ . A significant difference in the wake elongation, as in the  $CR$  simulations, however, can not be detected in the  $CCR$  simulations. This significant difference in the entrainment process results from the different behaviour in the wake rotation approaching downstream between the contrasting wake cases  $CR$  and the consistent wake cases  $CCR$  lower rotor half (Fig. 9(*i*), (*l*) and (*j*), (*k*)) as well as in the upper rotor half (Fig. 8) and is responsible for an increase of a downwind turbines power output up to 23% for counterclockwise rotating blades instead of clockwise ones.

#### 4.2 Strength of Veering Wind

The impact of the strength of wind veer over the rotor is investigated for  $\Delta\phi$  values of  $2^\circ$  9(*a*), (*d*) and (*b*), (*c*). The more rapid wake recovery and the larger spanwise wake width for  $CCR$  and  $CR\_b$  in comparison to  $CR$  and  $CCR\_b$  are present in all rotor heights. The larger wake deflection angle in the upper and the lower rotor half in  $CCR$  (Fig. 9(*b*), (*j*)) is also comparable to  $CR\_b$  (Fig. 9(*c*), (*k*)), whereas the smaller wake deflection angle in  $CR$  (Fig. 9(*a*),  $4^\circ$ , and  $8^\circ$ , corresponding to a weak (*w*), moderate (*m*), or strong (*s*) change in  $CR\_es$ ,  $CR$ , and  $CR\_ew$  and plotted (i)) is comparable to  $CCR\_b$  (Fig. 9(*d*), (*l*)).

The qualitative comparison in Fig. ???. If the strength of veer increases, 6(i) - (l) shows the differences from Fig. 9 between CR\_b and CCR\_b in the case of streamwise wake elongation, spanwise wake width and the wake deflection angle. Further, comparing the backing wind situation (Fig. 6(i) - (l)) to the corresponding  $\overline{u_A}$ -value increases. Again, this effect is related to a more rapid entrainment of ambient air into the wake. Considering a counterclockwise rotating rotor, the power output in the weak case would be 13% larger at 7 veering wind situation (Fig. 6(a) - (d)), CR\_b corresponds to CCR and CCR\_b to CR in the vertical (Fig. 6(i) vs. (a)) and at hub height (Fig. 6(k) vs. (c)). After mirroring at  $y=0$  D CR\_b corresponds to CCR and likewise CCR\_b to CR in the lower and the upper rotor part (compare Fig. 6(j) to (b) and (l) to (d)).

Expressing the differences between a backing and a veering wind from both rotational directions of the rotor by the quantity  $\overline{u_A}$  in comparison to a clockwise rotating one. In the moderate case it would increase by 11%. In the strong case, however, it would slightly decrease by 3%. According to Fig. 3 in Walter et al. (2009), 7(a), the  $\overline{u_A}$ -values are  $0.24 \text{ m s}^{-1}$  larger if a backing wind (CR\_b) interacts with a clockwise rotating rotor in comparison to a veering wind of  $2^\circ$  has the highest measured occurring frequency of 9% and a veering wind of  $4^\circ$  has a frequency of 6%. A veering wind of  $8^\circ$ , which would slightly decrease the power output for changing the rotational direction of the rotor, however, occurs only 3% of the time. The probability of occurrence for an even higher wind veer corresponding to a higher power output for (CR). Similarly, the  $\overline{u_A}$  values are larger if a backing wind interacts with a counterclockwise rotating rotor (CCR\_b). Therefore,  $\Delta\overline{u_A}$  is the same for CR and CCR\_b and likewise for CCR and CR\_b.

The northern hemispheric results of CR and CCR are comparable to southern hemispheric CR\_b and CCR\_b situations, whereas the northern hemispheric results of CR\_b and CCR\_b correspond to CR and CCR on the SH. The schematic illustration of a backing wind interacting with both rotational directions is presented in Fig. 8(c), (d) with an amplification of the spanwise wind component in the case of a backing wind and a clockwise rotating rotor in comparison to CR\_b (Fig. 8(d)) and a weakening/reversion in the case of a counterclockwise rotating one decreases up to 1% for  $\Delta\phi$  rotor CCR\_b (Fig. 8(c)).

## 4.2 Wind Speed

Wind speed may also affect the veering inflow (Eq. 8 via Eq. 6), modifying the spanwise velocity component. There is no significant impact of  $u_g = (6, 10, 14^\circ) \text{ m s}^{-1}$  on the wake elongation, the spanwise wake width, and the wake deflection angle between clockwise and counterclockwise rotating actuators. Therefore, the contour plots are not shown. Only a qualitative comparison is presented in Fig. 6(m)-(p) for  $u_g = 6 \text{ m s}^{-1}$  and in Fig. 6(q)-(t) for  $u_g = 14 \text{ m s}^{-1}$ . The occurrence of a wake width as well as the wake deflection angle difference between clockwise and counterclockwise rotating actuators from the reference case  $u_g = 10 \text{ m s}^{-1}$  (Fig. 6(b)-(d)) is independent of  $u_g$ . Only for smaller velocity values ( $u_g = 6 \text{ m s}^{-1}$  (Fig. 6(n)-(p)), the differences are less pronounced.

Coloured contours of the streamwise velocity  $\overline{u_{i,j,k_h}}$  in  $\text{m s}^{-1}$  at hub height  $k_h$ , averaged over the last 10 min, for *CR\_ew* in (a), *CCR\_ew* in (b), *CR* in (c), *CCR* in (d), *CR\_es* in (e), and *CCR\_es* in (f). The black contours represent the velocity deficit  $VD_{i,j,k_h}$  at the same vertical location.

The difference in the power values between the clockwise and the counterclockwise rotating simulations in the strong, moderate, and weak veer cases can be explained by means of comparison to clockwise ones.

### 4.3 Directional Shear

The directional shear is the second contributing parameter to the veering inflow (Eq. 8), modifying the spanwise velocity component resulting from analysis. The impact of all five directional shear values from Table 1 on the wake is investigated at hub height (Fig. 10), in the upper (Fig. 11), and in the lower (Fig. 12) rotor half. In the clockwise rotating blade simulations *CR\_ew* in a, *CR* in c, and *CR\_es* in e, as well as the counterclockwise rotating actuator simulations (Figs. 10-12) the wake recovers more rapidly if the strength of wind veer increases, due to amplified turbulence production and, therefore, directional shear increases. A larger directional shear represents a larger turbulence source due to an increase of  $\frac{\partial v_f}{\partial x}$ . Therefore, the simulations with larger directional shear values result in higher entrainment rates and a more rapid wake recovery. Our simulated dependence of the wake recovery on the amount of wind veer for clockwise rotating simulations is comparable to the numerical results in Fig. 11 of Bhaganagar and Debnath (2014). Considering the corresponding counterclockwise rotating blade simulations *CCR\_ew* in b, *CCR* in d, and *CCR\_es* in f, the amount of wind veer

The magnitude of directional shear affects the wake elongation, however, the difference between strong, moderate, and weak wind veer is much smaller in comparison to the corresponding *CR* simulations. In detail, the dependence of the rotor direction, but, not to the same extent in clockwise rotating simulations in comparison to counterclockwise rotating ones. The wake elongation in *CR\_ew* CR\_ds4 is much longer in comparison to *CCR\_ew* CCR\_ds4 (Figs. 10-12(a) vs. (b)). It is still larger in *CR* CR in comparison to *CCR*. These differences between the *CR* and the *CCR* simulations result in the larger power output of 13% in the strong veer *CCR* cases and of 11% in the moderate veer *CCR* cases CCR (Figs. 10-12(c) vs. (d)). A further increase of the directional shear finally results in a similar wake recovery of *CR*\_ds12 and *CCR*\_ds12 (Figs. 10-12(e) vs. (f)) and a slightly more rapid wake recovery of *CR*\_ds16 in comparison to *CCR*\_ds16 (Figs. 10-12(g) vs. (h)). Comparing the very strong directional shear cases *CR*\_ds20 and *CCR*\_ds20 (Figs. 10-12(i) vs. (j)), the wake recovery is significantly faster in *CR*\_ds20. Further, the difference between *CR\_ew* and *CR* CR\_ds4 and *CR* is larger in comparison to *CCR\_ew*

and  $CCR$ . Both wake elongation trends continue for an increasing amount of veer. It finally results in a faster wake recovery of  $CR_{es}$  in comparison to  $CCR_{es}$ , which is responsible for the slightly larger power output of  $CR_{es}$  in comparison to  $CCR_{es}$ .  $CCR_{ds4}$  and  $CCR$  (Figs. 10-12(a), (c) and (b), (d)). This trend continues for increasing directional shear.

#### 4.4 Type of Veering Wind

Another difference between clockwise and counterclockwise rotating actuators is the spanwise wake width (Fig. 10(c) vs. (d)). The impact of the directional shear on the spanwise wake width at hub height results in an increase of the difference of the spanwise wake width between a clockwise and a counterclockwise rotating simulation (Fig. 10(a), (c), (e), (g), (i) vs. (b), (d), (f), (h), (j)). In addition, the rotor section (entire rotor  $e$ , lower rotor half  $l$ ) interacting with a veering wind is investigated by comparing  $CR$  to  $CR_{lm}$  and  $CR_{es}$  to  $CR_{ls}$  in wake deflection angle increases for increasing values of the directional shear. The difference of larger wake deflection angles in the case of a counterclockwise rotating actuator in the upper and the lower rotor part is also prevalent for all directional shear values (right column of Figs. 11, 12(b), (d), (f), (h), (j)). Further, large values of the directional shear in combination with a counterclockwise rotating actuator leads to a break up of the wake (Fig. ??b). Due to less mixing, the  $\overline{u_A}$ -value is much smaller in  $CR_{lm}$  in comparison to  $CR$  (16%) and likewise in  $CR_{ls}$  in comparison to  $CR_{es}$  (49%). Considering  $CCR_{lm}$ , 11, 12(h), (j)). This erosion could be related to high spanwise velocity values in the case of  $CCR_{ds16}$  and  $CCR_{ds20}$  due to amplification of the inflow and the vortex spanwise component, which is not the case in  $CR_{ds16}$  and  $CR_{ds20}$  (Fig. 12, 11(g), (i)).

For a quantitative investigation of the directional shear impact on the differences in the wake between clockwise and counterclockwise rotating actuators, vertical and horizontal profiles at  $x = 7D$  for all five cases of different directional shear values are presented in Fig. 13. Considering the vertical profile through  $y = 0D$  (left column of Fig. 13), the vertical wake extension decreases if the directional shear increases, as the wake deflection is influenced by the incoming wind direction at each height (Churchfield and Srinivas, 2018; Tomaszewski et al., 2018; Bodini et al., 2017; Englberger and Lundquist, 2020). This dependency of wake veer on wind veer is also represented at  $z = 75$  m (Fig. 13(b), (f), (j), (n), (r)) and at  $z = 125$  m (Fig. 13(d), (h), (l), (p), (t)), where the wake deflection angle is additionally influenced by the rotational direction impact on  $\overline{u_A}$  is rather similar as in the corresponding full wake  $CCR$  simulations (7% vs. 11%). Further, considering  $CCR_{ls}$ ,  $\overline{u_A}$  increases in comparison to  $CCR_{lm}$  due to a higher entrainment rate. However, compared to  $CR_{es}$  and  $CCR_{es}$ , here the  $\overline{u_A}$ -value is still larger in of the actuator. The wake deflection angle is larger if the actuator rotates counterclockwise, independent of the values of directional shear.

The directional shear impact on the spanwise wake width is investigated via the profiles of Fig. 13. Especially at hub height (Fig. 13(c), (g), (k), (o), (s)), the wake width decreases if the directional shear increases. This effect can be related to the

increase in skewness in the wake for an increasing directional shear. Comparing clockwise and counterclockwise rotating actuators, the spanwise wake width is larger in the case of a counterclockwise rotating rotor, resulting in an additional power gain of 4% for a counterclockwise rotating rotor instead of a clockwise rotating one. This is related to less turbulent mixing as the veering wind is only limited to the lower rotor half in  $CR_{1s}$  actuator, independent of the directional shear value.

5 Considering the rotor-averaged values  $\overline{u_A}$  in Fig. 7(c), the rotor-averaged wind speeds are larger for a weak wind veer in the counterclockwise rotating actuator simulations (CCR\_ds4) in comparison to the clockwise rotating ones (CR\_ds4). As the wind veer increases, the difference in  $\overline{u_A}$  between clockwise and counterclockwise rotating disc simulations decreases. In the case of a moderate to strong wind veer,  $\overline{u_A}$  is only slightly larger for the clockwise rotating rotor CR\_ds12. Approaching an even higher directional shear in the strong and very strong wind shear cases, this difference between CR\_ds16 and CCR\_ds16 and likewise between CR\_ds20 and CCR\_ds20 increases, whereas now the rotor-averaged wind speeds are larger for clockwise  
10 rotating actuators in comparison to ~~the entire rotor in  $CR_{es}$~~  counterclockwise ones.

#### 4.4 Wind Speed

~~The impact of the wind speed is investigated in~~ Independent of the directional shear, the streamwise velocity values at  $x = 7D$  are larger in the case of a counterclockwise rotating actuator in the top and the bottom sector (Fig. 13 second and fourth column). The difference between counterclockwise and clockwise rotation increases in the radial direction away from the  
15 nacelle (not shown). This is related to the larger wake deflection angle in the counterclockwise rotating case in comparison to the clockwise case. Also independent of the directional shear, the streamwise velocity values are larger in the case of a clockwise rotating actuator in the left and right sectors (Fig. ??e. Here, the geostrophic wind is increased from  $10 \text{ m s}^{-1}$  to  $14 \text{ m s}^{-1}$  in the simulations  $CR_{u14}$  and  $CR_{es\_u14}$  for both rotational directions. Increasing the wind speed 13 third row). This is an effect of the narrower wake width in the case of a clockwise rotating actuator. If the directional shear is small, the  
20 larger  $u$ -values of counterclockwise rotating actuators in the top and bottom sectors are compensating for the larger  $u$ -values in the case of a clockwise rotating actuator in the right and left sectors. If the rotational direction is very high, the opposite is the case.

#### 4.4 Rotational Frequency

The rotational frequency contributes to the wind-turbine forces in Eq. 1 and modifies the spanwise velocity component (Eq. 17).  
25 The wake impact of the four rotational frequency values from Table 1 is presented at hub height (Fig. 14), at  $z = 125 \text{ m}$  (Fig. 15), and at  $z = 75 \text{ m}$  (Fig. 16). In comparison to the impact of a change of the atmospheric parameters, which was mainly limited to the far wake, the rotational frequency also significantly impacts the near wake. An increase of the rotational frequency

results in a larger entrainment rate and, therefore, in larger  $\overline{u_A}$  values at the same downstream position. In case of moderate veer, the power output is 11% larger for counterclockwise rotating blades and minimum value of the velocity deficit (Figs. 15 and 16(g), (h) vs. (a), (b)) and a less rapid wake recovery (Figs. 15 and 16(g), (h) vs. (a), (b)). As the rotational frequency increases, the wake structure differs more between clockwise and counterclockwise rotating actuators. The difference in the spanwise wake width increases for an increasing rotational frequency at all heights. Further, an increase in the rotational frequency results in a slightly larger downwind wake extension in the case of a clockwise rotating actuator at all heights. In the case of a counterclockwise rotating actuator, however, an increase in the rotational frequency results in a similar downwind wake extension of  $VD$  (Eq. 14).

A wake splitting pattern exists in the upper (Fig. 15(f), (h)), as well as in the lower rotor part (Fig. 16(f), (h)) for large rotational frequency values. The pattern is similar to the break up of the wake for large directional shear values interacting with a counterclockwise rotating actuator in CCR\_ds16 and CCR\_ds20 (Fig. 11, 12(h), (j)). The occurrence of the pattern in combination with high rotational frequency values could also be related to a very large spanwise flow component, now resulting from a large contribution of the vortex. An additional simulation (not shown) with  $u_g = 10 \text{ m s}^{-1}$  and 4% for  $u_g$ ,  $ds = 14 \text{ m s}^{-1} 0.20^\circ \text{ m}^{-1}$ . In case of strong veer, however, the power output of the combination of  $u_g$  and  $\Omega = 10 \text{ m} 0.23 \text{ s}^{-1}$  reinforces the slitting pattern of Figs. 12 and 11(h), (j), supporting our assumption as to why the splitting occurs only for counterclockwise rotating actuators. Further, a similar but less distinctive wake splitting pattern for a counterclockwise rotating actuator was observed in the veer affected lower rotor half with  $ds = 0.28^\circ \text{ m}^{-1}$  and  $CR$  decreases the power output by 3% and the combination with  $u_g \Omega = 14 \text{ m s}^{-1} 0.12 \text{ s}^{-1}$  by, see Fig. 10(f) by Englberger et al. (2019).

For a quantitative investigation of the rotational frequency impact on the wake differences between clockwise and counterclockwise rotating rotors, the vertical and horizontal profiles at  $x = 7\%$ . Therefore,  $D$  are presented for all four cases in Fig. 17. Considering the vertical and spanwise profiles at  $z = 100 \text{ m}$  (Fig. 17 first and third column), the rotational direction decrease of  $u$  results from larger wind-turbine forces due to an increase of wind speed does not clearly impact the power output difference. The behaviour is determined by the strength of the veering wind with an increase in the strong veer case and a decrease in the moderate veer case  $\Omega$ . The difference in the wake deflection angle (Fig. 17 second and fourth column) and in the spanwise wake width (Fig. 17 second, third, and fourth column) between clockwise and counterclockwise rotating discs increases for increasing  $\Omega$ . An increase of  $\Omega$  further results in two  $u$ -minima in the lower (Fig. 17(j), (n)) and the upper (Fig. 17(l), (p)) rotor half and a larger decrease of  $u$  approaching  $r = R$  at hub height (Fig. 17(k), (o)) in the counterclockwise rotating simulations.

in the or a corresponding backing wind in the

## 4.5 Summary

Power output difference of a hypothetical downwind turbine at a downstream distance of  $7D$ , if the upwind turbine rotates counterclockwise instead of the common clockwise blade rotation (deviation from 1:1 line) and likewise the power difference for the CR and the CCR simulations  $\alpha$  in comparison to ref (x-axis:  $P(CR_\alpha)/P(CR)-1$ ; y-axis:  $P(CCR_\alpha)/P(CR)-1$ ), with  $\alpha = (b, th15, th60, es, ew, ls, lm, u14, es\_u14)$ . 'b' represents a backing wind, 'th15' and 'th60' the weakly and the strongly stably stratified regimes, 'es' and 'ew' the strong and weak wind veer cases with veer over the entire rotor, and 'ls' and 'lm' the strong and moderate wind veer cases with veer limited to the lower rotor part. 'u14' and 'es\_u14' represent the cases with an increase of the geostrophic wind.

~~The relation~~ The increase of  $u$  in the lower and upper sector compensates for the decrease in the left and right sector for increasing  $\Omega$  in the case of counterclockwise rotating discs (Fig. 17), resulting in larger values of  $\overline{u_A}$  in Fig. 7(d) for all counterclockwise rotating simulations. The  $\overline{u_A}$ -difference between clockwise and counterclockwise rotating blades is shown  
 10 actuators increases for an increasing rotational frequency, which is related to the splitting of the wake.

## 5 Comparison to Analytic Model

The idealized numerical simulations investigated the impact of the rotational direction of the actuator in combination with veering inflow, no wind veer, and backing inflow on the wake of a single wind turbine. The parameter study investigated the streamwise dependency of the wake on wind speed, directional shear, and rotational frequency. For a comparison of the  
 15 simulated results with the expected results from analysis in Fig. ?? for a downstream distance of  $7D$ , Fig. 18 is plotted for  $90^\circ$  bottom and top sectors ranging from  $0 \text{ m} < r \leq 50 \text{ m}$  (Fig. 1). Figure 2 represents the results at  $y=0D$  and  $z=75 \text{ m}$  as the bottom part of the rotor disk and at  $y=0D$ . The 'ref' case presents the relation between CR and CCR.  $P(CR_\alpha)/P(CR)-1$  is plotted on the x-axis and  $P(CCR_\alpha)/P(CR)-1$  on the y-axis. As the value is above the black 1:1 line, the 'ref' case results in a larger power output of a downwind turbine at  $7D$  and  $z=125 \text{ m}$   
 20 as the top of the rotor disk. The general structure (slope, sign-changing point), however, is independent of the vertical location in the analysis. Only the magnitude of the spanwise inflow  $v_f$  at  $x_{down} > x_\xi$  and of the spanwise vortex component  $v_v$  at  $x_{down} < x_\xi$  are affected in Fig. 2, as  $v_f$  is height dependent and asymmetric to the rotor center and  $v_v$  has a radial dependency. Therefore, the panels of Fig. 18 are directly comparable to those of Fig. 2 regarding the difference in  $\Delta u_g$ ,  $\Delta ds$ , and  $\Delta \Omega$  between low, moderate, and high value cases.

25 Comparing the non-veering simulations CR\_NV and CCR\_NV (Fig. 18(b)) to the analysis prediction (Fig. 2(b)),  $v > 0$  in the top sector and  $v < 0$  in the bottom sector both with a clockwise rotating rotor. In the case of a counterclockwise rotating rotor,  $v$  in the top sector corresponds to  $v$  in the bottom sector of a clockwise rotating simulation and vice versa. Only the downwind

slope for  $x_{down} < x_{\epsilon}$  is much smaller. This results from a different radial distribution and a smaller absolute value of the wind-turbine forces applied in the numerical simulations (Eq. 1) in comparison to the Rankine vortex applied in the theoretical analysis (Eqs. 15, 16). Further, the smaller slope in the numerical simulations can be related to the resolved turbulence and the resulting wake recovery.

Comparing the simulation with moderate-veering inflow CR and CCR (Fig. 7. In 'ref', the power output in case of CCR in comparison to CR is 11.5% larger. This is the vertical difference of 'ref' from the 1:1 line. The point 'b' represents the relation between  $P(CR_b)/P(CR)-1$  on the x-axis and  $P(CCR_b)/P(CR)-1$  on the y-axis. Here,  $P(CR_b) < P(CCR_b)$  with  $\Delta P = -11.5\%$  (distance from 'b' to 1:1 line 18(e)) to the analysis predictions (Fig. 2(e)), the acceleration in the case of a counterclockwise rotating rotor and the weakening in the case of a clockwise rotating rotor up to  $x_{down} \approx 10D$  are prevalent. The smaller slope-values has the same reason as in the non-veering case. The different slope-values between the simulations and the analysis predictions simply results in an upwind shift of the sign-changing location in the wake. An increase of  $\Omega$  (Fig. 18(i)) approaches the structure predicted by analysis (steeper slope, flow reversion behind the rotor, downwind shift of the sign-changing point) of Fig. 2(b). The points representing the cases  $CR_v_{SH}$  and  $CR_{SH}$  are almost identical with  $CR_b$  and  $CR$  and therefore with 'b' and 'ref' values of  $\Omega$  applied in the BEM method to calculate the wind-turbine forces (Eq. 1) are the same as the values of  $\omega$  applied in the Rankine vortex (Eq. 15). Due to the differences in the calculation of the spanwise flow field between the BEM method and the Rankine vortex, the near wake absolute values are not comparable in Fig. 2 and Fig. 18. Considering the backing inflow simulation (Fig. 18(h)) and exchanging clockwise and counterclockwise and likewise top and bottom, it corresponds to the veering inflow in Fig. 18(e), which is predicted by Fig. 2(h) and (e).

The point 'th15' represents a power increase by 4% at 7 analytic model predicts the same impact of the geostrophic wind and the directional shear on the spanwise wake structure (Fig. 2(a) vs. (d) and (c) vs. (f)). The general structure at  $x_{down} \approx 7D$  for  $CCR_{th15}$  in comparison to  $CR_{th15}$ . Further, in comparison to 'ref', the power output of a downwind turbine in case of  $CR_{th15}$  would be larger than for  $CR$  with a difference of 7% ( $\Delta < P$  on x-axis). Likewise,  $x_{\epsilon}$  is comparable in the power output of a downwind turbine in case of  $CCR_{th15}$  would be slightly smaller than for  $CCR$  with a difference of 1% ( $\Delta$  numerical simulations with  $u_g$  P on y-axis). Considering 'th60', a counterclockwise rotating rotor results in a 23% higher power output for a hypothetical downwind turbine placed at  $x = 7D$ . Compared to 'ref' ( $6 \text{ m s}^{-1}$  and 'th15')  $ds = 0.08^\circ \text{ m}^{-1}$  (Fig. 18(a)) and  $u_g = 10 \text{ m s}^{-1}$  and  $ds = 0.04^\circ \text{ m}^{-1}$  (Fig. 18(d)) and likewise with  $u_g = 14 \text{ m s}^{-1}$  and  $ds = 0.08^\circ \text{ m}^{-1}$  (Fig. 18(c)) and  $u_g = 10 \text{ m s}^{-1}$  and  $ds = 0.12^\circ \text{ m}^{-1}$  (Fig. 18(f)). Minor differences exist e.g., the power difference in compare the difference between clockwise and counterclockwise rotating simulations at  $x = 7D$  in Fig. 18(a) and (d). The larger difference between  $CR_{ds4}$  and  $CCR_{ds4}$  in Fig. 18(d) can be related to a decrease of  $\frac{\partial v_f}{\partial z}$  and a smaller amount of resolved turbulence generated by the inflow with  $ds = 0.04^\circ \text{ m}^{-1}$  (Fig. 18(d)) in comparison to  $ds = 0.08^\circ \text{ m}^{-1}$  (Fig. 18(a)), whereas the change in  $u_g$  has

30 no influence on  $\frac{\partial v_f}{\partial z}$ . Changing the wind speed and the directional shear has a significant impact on  $|v|$  further downwind at  $x_{down} > x_\xi$ , e.g.  $v_{20D}$  in Fig. 18(f)  $\approx 2 \cdot v_{20D}$  in Fig. 18(d). This corresponds to the differences between Fig. 2(f) and (d) at  $x_{down} > x_\xi$ .

Changing the rotational frequency of the vortex has its largest impact on the spanwise wake velocity directly behind the rotor, whereas an increase of the spanwise vortex component  $v_v$  results in a larger amplification of  $|v|$  in the case of a clockwise  
5 blade rotation is  $\Delta P = -7\%$  ( $-14\%$ ) and in counterclockwise rotating rotor and a larger weakening of  $|v|$  in the case of a counterclockwise blade rotation  $\Delta P = 3\%$  ( $4\%$ ).

The same investigation is presented clockwise rotating rotor (Fig. 18(g), (e), (i)). This behaviour corresponds to the near wake differences in Fig. ?? for  $CR_{es}$  vs.  $CCR_{es}$  in 'es',  $CR_{ew}$  vs.  $CCR_{ew}$  in 'ew',  $CR_{ls}$  vs.  $CCR_{ls}$  in 'ls', and  $CR_{lm}$  vs.  $CCR_{lm}$  in 'lm' and  $CR_{u14}$  vs.  $CCR_{u14}$  and  $CR_{es_u14}$  vs.  $CCR_{es_u14}$ .

10 In 2(g), (e), (i). For large enough values of the rotational frequency, the spanwise wake component reverses sign in the simulation  $CR_{\Omega h}$  directly behind the rotor (Fig. ??, squared markers represent cases of strong entrainment processes in the wake of the upwind turbine e.g. 'th15' weak stably stratified regime, 'es' strong wind veer over the whole rotor, 'ls' strong wind veer limited to the lower rotor part. Circles represent moderate forcings and entrainment processes like 'ref' (th30 moderate stably stratified regime and *em* moderate wind veer over the entire rotor) and triangles represent weak entrainment processes in  
15 18(i)).

The comparison of the wake e.g. 'th60' strong stably stratified regime, 'ew' weak wind veer over the whole rotor. The differences in the entrainment rate can be seen in Figs. ?? and ??. From simulation results with the analysis predictions can be summarized as follows:

– The simulated amplification or weakening/reversion of the spanwise inflow wind component in the wake follows the  
20 theoretical analysis in the case of no wind veer, a veering inflow, and a backing inflow for clockwise and counterclockwise rotating discs. It can be understood and described by the superposition of the rotational flow induced by the disk and the vertical shear of the incoming wind.

– The agreement of the simulation results with the analysis predictions proves that the impact of the rotational direction on the spanwise wake field is determined by the mean values of the inflow wind field and influenced by the resulting  
25 turbulence.

– The inflow parameters (wind speed and directional shear) and the rotation rate of the rotor are two counteracting processes. The individual magnitudes determine the differences in the spanwise wake component between clockwise

and counterclockwise rotating actuators. The difference increases (decreases) for increasing (decreasing) values of  $u_g$ ,  $ds$ , and  $\Omega$ .

The rotational direction impact on the spanwise velocity component in the wake also modifies the streamwise flow component. The streamwise velocity components in the wake are shown in Fig. 19 for the same sectors and simulations as in Fig. ?? it can be concluded that the potential power output of a downwind turbine at 7D would be larger in case of weak and moderate entrainment of ambient air into the wake. In case of strong entrainment, the difference 18. The larger values in the top sector in comparison to the bottom sector result from the height-dependent streamwise velocity (Eq. 6) with larger values in the upper rotor half. In the case of no wind direction change with height (NV, Fig. 19(b)), the  $\bar{u}$  values are independent of the rotational direction of the actuator. In the case of a veering (backing) inflow (Fig. 19(e) (Fig. 19(b))), the streamwise wake velocity is larger in case of CCR (CR\_b) in comparison to CR (CCR\_b) in both sectors. The parameters under veering inflow impact the difference  $\Delta\bar{u}$  between counterclockwise and clockwise rotating blades diminishes approaching the 1:1 line. Further, for a weaker mixing in the wake, the potential power output of a downwind turbine decreases in case of clockwise rotating blades (triangles vs. circles). In case of counterclockwise rotating blades (squares vs. circles), the power output of a hypothetical downwind turbine also decreases for decreasing the strength of veer. By changing the atmospheric stratification, the difference for counterclockwise rotating blades is rather small (see Fig. ??(a)), with a slight increase for a stronger stratification corresponding to weaker mixing.

actuators in the corresponding sector (Fig. 19 left and right column). An increase of  $u_g$ ,  $ds$ , or  $\Omega$  result in larger  $\Delta\bar{u}$ -values (Fig. 19 right column), whereas smaller parameter values decrease  $\Delta\bar{u}$  (Fig. 19(b) left column).

The rotational direction impact on the wake can be summarized:

- A rotational direction impact on the streamwise velocity components in the wake exists only in the case of a veering (or backing) inflow.
- In the case of veering inflow in the NH the spanwise wake width ( $\Delta L_y$ ) as well as the wake deflection angle ( $\Delta\epsilon$ ) are larger in case of a counterclockwise rotating actuator CCR (Fig. 20). This behaviour is independent of the magnitude of the parameters.
- Increasing the magnitudes of the directional shear  $ds$  or the rotation rate  $\Omega$  increase the spanwise wake width difference ( $\Delta L_y$ ) and the wake deflection angle difference ( $\Delta\epsilon$ ) between a counterclockwise and a clockwise rotating actuator. The impact of the geostrophic wind  $u_g$  is much less pronounced.

- An increase of  $u_g$  or likewise a decrease of  $\Omega$  result in a more rapid wake recovery. Increasing  $ds$ , there is no wake difference between a clockwise and a counterclockwise rotating actuator for a specific directional shear  $ds_c$ . If  $ds < ds_c$ , the streamwise velocity is larger in the case of a counterclockwise rotating rotor, whereas for  $ds > ds_c$ , the streamwise velocity is larger in the case of a clockwise rotating rotor. Approaching smaller or larger values of the directional shear,  $\Delta\bar{u}$  increases between a clockwise and a counterclockwise rotating actuator.

## 5 6 Conclusions

~~were performed to investigate the rotational direction impact~~ We investigate the impact of the rotational direction on the wake of a wind turbine ~~in a stably stratified flow~~ for veering and backing ~~winds in the and the~~ inflow conditions, as well as in the case of no wind veer in both hemispheres, using idealized LES in comparison to a simple analytic model. In addition, the ~~difference of a counterclockwise rotating rotor instead of a common clockwise rotating one under veering~~ impact of the geostrophic wind and the directional shear as well as the impact of the rotational frequency on the wake differences between clockwise and counterclockwise rotating wind turbines was investigated in the case of veering inflow.

The rotational direction of a wind turbine has only a minor impact on the wake in the case of no wind veer. This result from the numerical experiments is consistent with previous investigations by Vermeer et al. (2003), Shen et al. (2007), Sande (2009), Kumar et al. (2013), Hu et al. (2013), Yuan et al. (2014), Mühle et al. (2017), and Englberger et al. (2019). An inflow without wind veer is a typical daytime situation and also occurs in the evening transition of the diurnal boundary layer evolution, where the flow is still influenced by daytime turbulence.

In the case of veering or backing inflow, however, the wake characteristics (streamwise wake elongation, spanwise wake width, wake deflection angle) depend significantly on the rotational direction. Veering and backing inflow are characteristic nighttime situations of the boundary layer flow if no other processes as topographically induced circulations or large scale weather systems prevent the establishment of an SBL regime. ~~Veering within the wind conditions in the is investigated for the strength of stratification, the strength and the type of the veering wind and its wind speed~~ turbine rotor layer has been observed with several field campaigns with towers and lidars (Walter et al., 2009; Sanchez Gomez and Lundquist, 2020b; Bodini et al., 2019, 2020), and veer throughout the boundary layer has been observed globally using radiosonde datasets (Lindvall and Svensson, 2019).

~~The paper raises the question: 'Should wind turbines rotate in the opposite direction?'. In the , the power increases for counterclockwise rotating blades~~ Under veering inflow in the NH (backing inflow in the SH), the spanwise wake width and the wake deflection angle are larger for a counterclockwise (clockwise) rotating actuator in comparison to ~~clockwise rotating ones in almost all nighttime configurations with a veering wind investigated in this work. As the simulated conditions are~~

typical for the night ( $\approx 10$  h a day) a clockwise rotating one. An increase (decrease) of the directional shear in the atmospheric flow or of the rotational frequency of the rotor increases (decreases) the differences in the spanwise wake width and the wake deflection angle. The wind speed does not impact these wake characteristics significantly. In locations with veering inflow in the NH (backing inflow in the SH) and during veered inflow (76% of the nights according to Walter et al. (2009)), and regarding the significant power gain up to 23% under strongly stably stratified conditions and up to 13% under a weakly veering wind the answer 'yes' to this question should seriously be considered for waked wind turbines. In the directional shear values  $ds < ds_c$  with  $0.12^\circ \text{ m}^{-1} < ds_c < 0.16^\circ \text{ m}^{-1}$ , the situation is directly the opposite due to the different sign of the Coriolis force. Therefore, in the , the common clockwise rotational direction of wind turbines is the recommended rotational direction to extract the maximum power when turbines are likely to be waked. streamwise velocity is larger in the case of a counterclockwise (clockwise) rotating rotor. These differences apply to the wake ranging from  $x = 4D$  to at least  $x = 10D$  downwind. For less common higher values of the directional shear  $ds > ds_c$ , the streamwise velocity is larger in the case of a clockwise (counterclockwise) rotating rotor in the NH (SH).

Different operating conditions (e.g. yaw control) of upwind turbines are already applied to mitigate downwind impacts in wind parks (Fleming et al., 2019). This work suggests that counterclockwise rotating blades in the case of veering inflow and clockwise rotating blades in the case of backing inflow in the NH (and vice versa in the SH) could have benefits as well. The wake deflection angle becomes larger if the spanwise flow component is amplified by the vortex induced by the rotating wind turbine. This process occurs independent of the magnitude of the parameter values applied in the numerical simulations.

The practicalities of implementing different rotational directions present significant challenges. Choosing opposite rotational directions in the and the , with changing the current rotational direction in the , would have some significant implications for the possibility to share inventory between the wind turbines. For example, the gearbox has many micro-geometry modifications that are based on deformation of the gearbox under loaded conditions. Therefore, it is not possible to make a mirror image gearbox for the . It would take a significant amount of modifications to gear tooth profiles, etc. , to allow the gearbox to be used in a turbine that rotates in the opposite direction in the (John Bosche (AreVera), personal communication, 2019).

As the results show a significant improvement of wind conditions for a hypothetical downwind turbine by changing the rotational direction of the blades in the , it would have a large impact on the produced power (up to 23% difference with the conditions applied in this work), considering the cumulative installed wind capacity in 2017 of 516497 MW (96%) in

As the numerical results of this study arise from an idealized parameter study employing specific assumptions, they have limitations. For example, the turbulent perturbations applied in the numerical simulations are incorporated via a simple turbulence parametrization. The imposed turbulence parameters were retrieved from precursor LES and no real-time wind and potential temperature profiles are applied. Particularly, the impact of the (Asia, Europe, North America, Africa and Middle

30 ~~East) compared to 539581 MW world-wide (GWEC, 2018). Therefore, rotational direction on a wind-turbine wake under veering (or backing) inflow results from basic analytical predictions and was compared with the numerical model. However, the impact of rotational directions has never been measured, as no counterclockwise rotating wind turbines currently exist. Despite the limitations of this numerical study, the market on the could be large enough to justify designing a special turbine for the , including mirrored blades, gearbox etc. In the , the preferential rotational direction is clockwise, and therefore the common~~  
5 ~~wind turbines should result in the maximum produced power at night.~~ simple analysis as well as the idealized parameter study show a consistent and clear impact of the rotational direction of a wind turbine on the wake flow during conditions for which the wind direction turns with height.

~~Concluding, a possible extraction of more energy from wind turbines in the by simply changing the rotational direction of the blades, could be taken into account in the future~~ To explore a more comprehensive assessment of the wake impact, further  
10 ~~investigations would be interesting. The investigation of the non-linearity of the interaction process, numerical simulations applying the turbulence of a SBL precursor simulation for different strengths of stratification and directional shears, or even considering a low-level jet at the rotor height. Topography could influence the wake dynamic explored here. We have assessed the wake of an individual turbine, but these results could be extended to a large farm in which the presence of upwind turbines could affect turbulence intensity, which probably affects the magnitude. However, an important point will be to prove~~  
15 ~~the theoretically predicted effect resulting from superposition of inflow veer with the vortex component on the wake with measurements.~~

Finally, the overall assessment of the impact of these results depends on the frequency of occurrence of veering inflow. Only limited sets of long-term observations provide an assessment of the frequency of veering (Walter et al., 2009; Sanchez Gomez and Lundquist  
in the wind turbine rotor layer. The global climatology of veer throughout the atmospheric boundary layer based on radiosonde  
20 data (Lindvall and Svensson, 2019) suggest that veer occurs broadly in mid-latitudes and polar regions, but further investigation is required to assess if that boundary-layer veer broadly affects wind energy generation.

## Appendix A: Turbulence parametrization

The turbulence parametrization of Englberger and Dörnbrack (2018a) is applied in the simulations of this work. The main part is conducted with  $\alpha = 0.3$ ,  $\alpha_u = 0.15$ ,  $\alpha_v = 0.24$ , and  $\alpha_w = 0.13$ . This values are nighttime representations following Table 1  
25 of Englberger and Dörnbrack (2018b). Figure A1 presents the reference CR and CCR wind-turbine simulation applied in this work at  $z = 125$  m in (a) and (b), for  $z = 100$  m in (e) and (f) and at  $z = 125$  m at (i) and (j). Further, simulation results  $\alpha = 0.3$  and  $\alpha_{i^*,j,k} = 0$  are presented at  $z = 125$  m in (c) and (d), for  $z = 100$  m in (g) and (h) and at  $z = 125$  m at (k) and (l). Panels

(a) and (b) are the reference simulations CR and CCR with veering inflow. Panel (c) and (d) correspond to  $\alpha = 0.3$ , panel (e) and (f) to  $\alpha = 0.5$ , and panel (g) and (h) to  $\alpha = 0.7$ , with  $\alpha_{i^*,j,k} = 0$  in all three cases. The streamwise velocity at hub height, as well as in the lower and the upper rotor half show similar characteristics of the near wake velocity deficit maximum, the streamwise wake elongation, the spanwise wake width, and the wake deflection angle. Only the strength of occurrence of these wake characteristics depends on the turbulent intensity, which is larger in the case of  $\alpha_{i^*,j,k} = 0$ . This reinforces the assumption that wake characteristic differences depend on the mean wind profile, which is the same in all simulations of Fig. A1, and is no effect of the applied turbulence parametrization.

*Author contributions.* All authors designed the idea. A. Englberger performed the simulations and prepared the manuscript with contributions from both co-authors.

*Competing interests.* The authors declare that they have no conflict of interest.

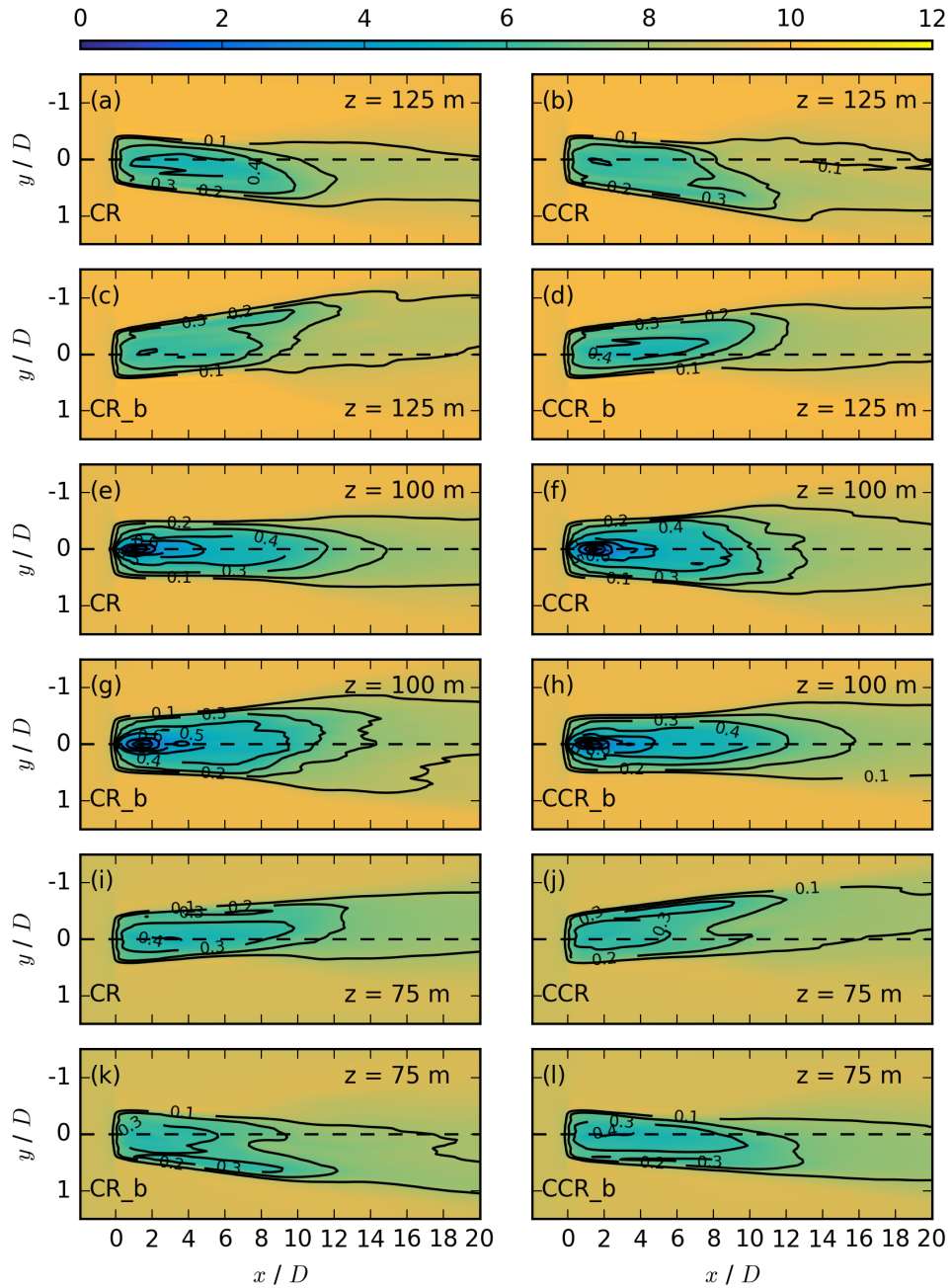
10 *Acknowledgements.* The authors gratefully acknowledge the Gauss Centre for Supercomputing e.V. ([www.gauss-centre.eu](http://www.gauss-centre.eu)) for funding this project by providing computing time on the GCS Supercomputer SuperMUC at Leibniz Supercomputing Centre (LRZ, [www.lrz.de](http://www.lrz.de)).

## References

- Abkar, M. and Porté-Agel, F.: The effect of atmospheric stability on wind-turbine wakes: A large-eddy simulation study, in: *Journal of Physics: Conference Series*, vol. 524, p. 012138, IOP Publishing, <https://doi.org/10.1088/1742-6596/524/1/012138>, 2014.
- Abkar, M. and Porté-Agel, F.: Influence of the Coriolis force on the structure and evolution of wind turbine wakes, *Physical Review Fluids*, 1, 063 701, <https://doi.org/10.1103/PhysRevFluids.1.063701>, 2016.
- 5 Abkar, M., Sharifi, A., and Porté-Agel, F.: Wake flow in a wind farm during a diurnal cycle, *Journal of Turbulence*, 17, 420–441, <https://doi.org/10.1080/14685248.2015.1127379>, 2016.
- Bak, C., Zahle, F., Bitsche, R., Kim, T., Yde, A., Henriksen, L. C., Hansen, M. H., Blasques, J. P. A. A., Gaunaa, M., and Natarajan, A.: The DTU 10-MW reference wind turbine, in: *Danish Wind Power Research 2013*, 2013.
- Bhaganagar, K. and Debnath, M.: Implications of Stably Stratified Atmospheric Boundary Layer Turbulence on the Near-Wake Structure of  
10 Wind Turbines, *Energies*, 7, 5740–5763, <https://doi.org/10.3390/en7095740>, 2014.
- Blay-Carreras, E., Pino, D., Vilà-Guerau de Arellano, J., van de Boer, A., De Coster, O., Darbieu, C., Hartogensis, O., Lohou, F., Lothon, M., and Pietersen, H.: Role of the residual layer and large-scale subsidence on the development and evolution of the convective boundary layer, *Atmos Chem Phys*, 14, 4515–4530, <https://doi.org/10.5194/acp-14-4515-2014>, 2014.
- Bodini, N., Zardi, D., and Lundquist, J. K.: Three-dimensional structure of wind turbine wakes as measured by scanning lidar, *Atmospheric  
15 Measurement Techniques*, 10, 2017.
- Bodini, N., Lundquist, J. K., and Kirincich, A.: US East Coast Lidar Measurements Show Offshore Wind Turbines Will Encounter Very Low Atmospheric Turbulence, *Geophysical Research Letters*, 46, 5582–5591, <https://doi.org/10.1029/2019GL082636>, 2019.
- Bodini, N., Lundquist, J., and Kirincich, A.: Offshore Wind Turbines Will Encounter Very Low Atmospheric Turbulence, in: *Journal of Physics. Conference Series*, vol. 1452, National Renewable Energy Lab.(NREL), Golden, CO (United States), 2020.
- 20 Bromm, M., Vollmer, L., and Kühn, M.: Numerical investigation of wind turbine wake development in directionally sheared inflow, *Wind Energy*, 20, 381–395, 2017.
- Churchfield, M. J. and Sirmivas, S.: On the effects of wind turbine wake skew caused by wind veer, in: *2018 wind energy symposium*, p. 0755, 2018.
- Englberger, A. and Dörnbrack, A.: Impact of Neutral Boundary-Layer Turbulence on Wind-Turbine Wakes: A Numerical Modelling Study,  
25 *Boundary-Layer Meteorology*, 162, 427–449, <https://doi.org/10.1007/s10546-016-0208-z>, 2017.
- Englberger, A. and Dörnbrack, A.: Impact of the diurnal cycle of the atmospheric boundary layer on wind-turbine wakes: a numerical modelling study, *Boundary-layer meteorology*, 166, 423–448, <https://doi.org/10.1007/s10546-017-0309-3>, 2018a.
- Englberger, A. and Dörnbrack, A.: A Numerically Efficient Parametrization of Turbulent Wind-Turbine Flows for Different Thermal Stratifications, *Boundary-layer meteorology*, 169, 505–536, <https://doi.org/10.1007/s10546-018-0377-z>, 2018b.
- 30 Englberger, A. and Lundquist, J. K.: How does inflow veer affect the veer of a wind-turbine wake?, in: *Journal of Physics: Conference Series*, vol. 1452, p. 012068, 2020.
- Englberger, A., Dörnbrack, A., and Lundquist, J. K.: Does the rotational direction of a wind turbine impact the wake in a stably stratified atmospheric boundary layer?, *Wind Energy Science Discussions*, 2019, 1–24, <https://doi.org/10.5194/wes-2019-45>, <https://www.wind-energ-sci-discuss.net/wes-2019-45/>, 2019.

- 35 Fleming, P., King, J., Dykes, K., Simley, E., Roadman, J., Scholbrock, A., Murphy, P., Lundquist, J. K., Moriarty, P., Fleming, K., et al.: Initial results from a field campaign of wake steering applied at a commercial wind farm–Part 1, *Wind Energy Science*, 4, 273–285, <https://doi.org/10.5194/wes-4-273-2019>, 2019.
- Fröhlich, J.: *Large Eddy Simulation turbulenter Strömungen*, Teubner Verlag / GWV Fachverlage GmbH, Wiesbaden, 414 pp, 2006.
- Gaumond, M., Réthoré, P.-E., Ott, S., Pena, A., Bechmann, A., and Hansen, K. S.: Evaluation of the wind direction uncertainty and its impact on wake modeling at the Horns Rev offshore wind farm, *Wind Energy*, 17, 1169–1178, 2014.
- 5 Grinstein, F. F., Margolin, L. G., and Rider, W. J.: *Implicit Large Eddy Simulation*, Cambridge university press, 546 pp, 2007.
- GWEC, G. W. S.: *Global wind statistics 2017*, FEBRUARY, 2018.
- Hu, H., Yuan, W., Ozbay, A., and Tian, W.: An experimental investigation on the effects of turbine rotation directions on the wake interference of wind turbines, in: *51st AIAA Aerospace Sciences Meeting including the New Horizons Forum and Aerospace Exposition*, p. 607, 2013.
- 10 Kumar, P. S., Abraham, A., Bensingh, R. J., and Ilangovan, S.: *Computational and experimental analysis of a counter-rotating wind turbine system*, 2013.
- Lindvall, J. and Svensson, G.: Wind turning in the atmospheric boundary layer over land, *Quarterly Journal of the Royal Meteorological Society*, 145, 3074–3088, 2019.
- Maegaard, P., Krenz, A., and Palz, W.: *Wind power for the world: the rise of modern wind energy*, Jenny Stanford, 2013.
- 15 Manwell, J., McGowan, J., and Roger, A.: *Wind Energy Explained: Theory, Design and Application*, Wiley: New York, NY, USA, 134 pp, 2002.
- Margolin, L. G., Smolarkiewicz, P. K., and Sorbjan, Z.: Large-eddy simulations of convective boundary layers using nonoscillatory differencing, *Phys D Nonlin Phenom*, 133, 390–397, [https://doi.org/10.1016/S0167-2789\(99\)00083-4](https://doi.org/10.1016/S0167-2789(99)00083-4), 1999.
- Mühle, F., Adaramola, M. S., and Sætran, L.: The effect of rotational direction on the wake of a wind turbine rotor—a comparison study of aligned co-and counter rotating turbine arrays, *Energy Procedia*, 137, 238–245, <https://doi.org/10.1016/j.egypro.2017.10.346>, 2017.
- 20 Prusa, J. M., Smolarkiewicz, P. K., and Wyszogrodzki, A. A.: EULAG, a computational model for multiscale flows, *Computers & Fluids*, 37, 1193–1207, <https://doi.org/10.1016/j.compfluid.2007.12.001>, 2008.
- Rhodes, M. E. and Lundquist, J. K.: The effect of wind-turbine wakes on summertime US Midwest atmospheric wind profiles as observed with ground-based doppler lidar, *Boundary-Layer Meteorol*, 149, 85–103, <https://doi.org/10.1007/s10546-013-9834-x>, 2013.
- 25 Sanchez Gomez, M. and Lundquist, J.: The Effects of Wind Veer During the Morning and Evening Transitions, in: *Journal of Physics: Conference Series*, vol. 1452, p. 012075, 2020a.
- Sanchez Gomez, M. and Lundquist, J. K.: The effect of wind direction shear on turbine performance in a wind farm in central Iowa, *Wind Energy Science (Online)*, 5, 2020b.
- Sanderse, B.: Aerodynamics of wind turbine wakes, Energy Research Center of the Netherlands (ECN), ECN-E-09-016, Petten, The Netherlands, Tech. Rep, 5, 153, 2009.
- 30 Schmidt, H. and Schumann, U.: Coherent structure of the convective boundary layer derived from large-eddy simulations, *J Fluid Mech*, 200, 511–562, <https://doi.org/10.1017/S0022112089000753>, 1989.
- Shapiro, A. and Fedorovich, E.: Analytical description of a nocturnal low-level jet, *Quarterly Journal of the Royal Meteorological Society*, 136, 1255–1262, 2010.
- 35 Shen, W. Z., Zakkam, V. A. K., Sørensen, J. N., and Appa, K.: Analysis of counter-rotating wind turbines, in: *Journal of Physics: Conference Series*, vol. 75, p. 012003, IOP Publishing, <https://doi.org/10.1088/1742-6596/75/1/012003>, 2007.

- Smolarkiewicz, P. K. and Margolin, L. G.: MPDATA: A Finite-Difference Solver for Geophysical Flows, *J Comput Phys*, 140, 459–480, <https://doi.org/10.1006/jcph.1998.5901>, 1998.
- Smolarkiewicz, P. K., Sharman, R., Weil, J., Perry, S. G., Heist, D., and Bowker, G.: Building resolving large-eddy simulations and comparison with wind tunnel experiments, *J Comput Phys*, 227, 633–653, <https://doi.org/10.1016/j.jcp.2007.08.005>, 2007.
- Stull, R. B.: *An Introduction of Boundary Layer Meteorology*, Dordrecht, Kluwer Academic, 1988.
- 5 Tomaszewski, J. M., Lundquist, J. K., Churchfield, M. J., and Moriarty, P. J.: Do wind turbines pose roll hazards to light aircraft?, *Wind Energy Science (Online)*, 3, 2018.
- Vasel-Be-Hagh, A. and Archer, C. L.: Wind farms with counter-rotating wind turbines, *Sustainable Energy Technologies and Assessments*, 24, 19–30, 2017.
- Vermeer, L., Sørensen, J. N., and Crespo, A.: Wind turbine wake aerodynamics, *Progress in aerospace sciences*, 39, 467–510, [https://doi.org/10.1016/S0376-0421\(03\)00078-2](https://doi.org/10.1016/S0376-0421(03)00078-2), 2003.
- 10 Vollmer, L., Steinfeld, G., Heinemann, D., and Kühn, M.: Estimating the wake deflection downstream of a wind turbine in different atmospheric stabilities: An LES study, *Wind Energy Science*, 1, 129–141, 2016.
- Vollmer, L., Lee, J. C., Steinfeld, G., and Lundquist, J.: A wind turbine wake in changing atmospheric conditions: LES and lidar measurements, in: *Journal of Physics: Conference Series*, vol. 854, p. 012050, IOP Publishing, <https://doi.org/10.1088/1742-6596/75/1/012003>,  
15 2017.
- Walter, K., Weiss, C. C., Swift, A. H., Chapman, J., and Kelley, N. D.: Speed and direction shear in the stable nocturnal boundary layer, *Journal of Solar Energy Engineering*, 131, 011 013, <https://doi.org/10.1115/1.3035818>, 2009.
- Yuan, W., Tian, W., Ozbay, A., and Hu, H.: An experimental study on the effects of relative rotation direction on the wake interferences among tandem wind turbines, *Science China Physics, Mechanics & Astronomy*, 57, 935–949, 2014.
- 20 Zhang, W., Markfort, C. D., and Porté-Agel, F.: Near-wake flow structure downwind of a wind turbine in a turbulent boundary layer, *Exp Fluids*, 52, 1219–1235, <https://doi.org/10.1007/s00348-011-1250-8>, 2012.



Coloured contours-

**Figure 9.** Contours of the streamwise velocity  $\overline{u_{i,j,k_h}} - \overline{u_{i,j,k_e}}$  in  $\text{m s}^{-1}$  at hub height  $k_h$ , averaged over the last 10 min, for *CR\_th15* in (a), *CCR\_th15*  $z = 125$  m in (b) the first two rows, *CR* in (e) at  $z = 100$  m the the third and fourth row, *CCR* and at  $z = 75$  m in (d) the last two rows for the simulations *CR*, *CR\_th60* in (e) *CCR*, *CR\_b* and *CCR\_th60* in (f) *CCR\_b*, each averaged over 30 min. The black contours represent the velocity deficit  $\overline{VD_{i,j,k_h}} - \overline{VD_{i,j,k_e}}$  at the same vertical location.

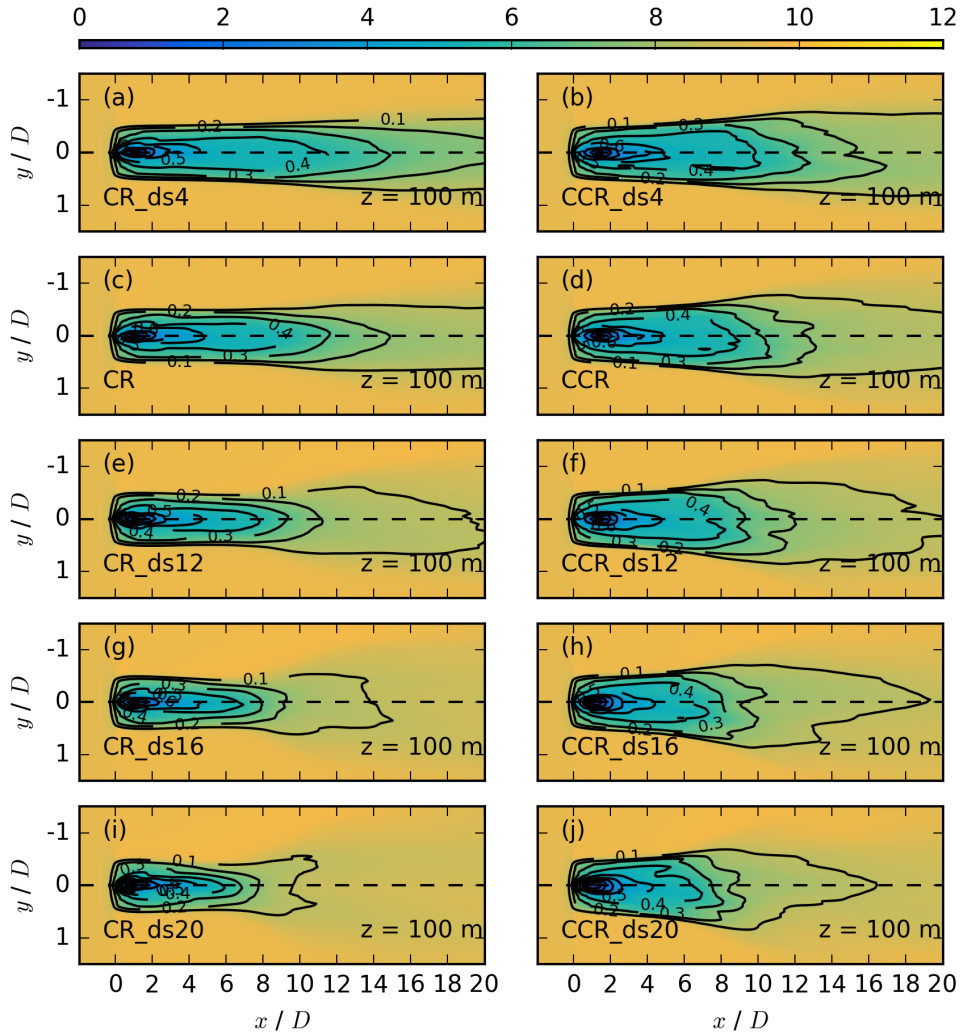


**Figure 10.** Contours of the streamwise velocity  $\overline{u_{i,j,k}}$  in  $\text{m s}^{-1}$  for different directional shears at  $z = 100$  m for CR\_ds4 in (a), CCR\_ds4 in (b), CR in (c), CCR in (d), CR\_ds12 in (e), CCR\_ds12 in (f), CR\_ds16 in (g), CCR\_ds16 in (h), CR\_ds20 in (i), and CCR\_ds20 in (j), each averaged over 30 min. The black contours represent the velocity deficit  $VD_{i,j,k}$  at the same vertical location.

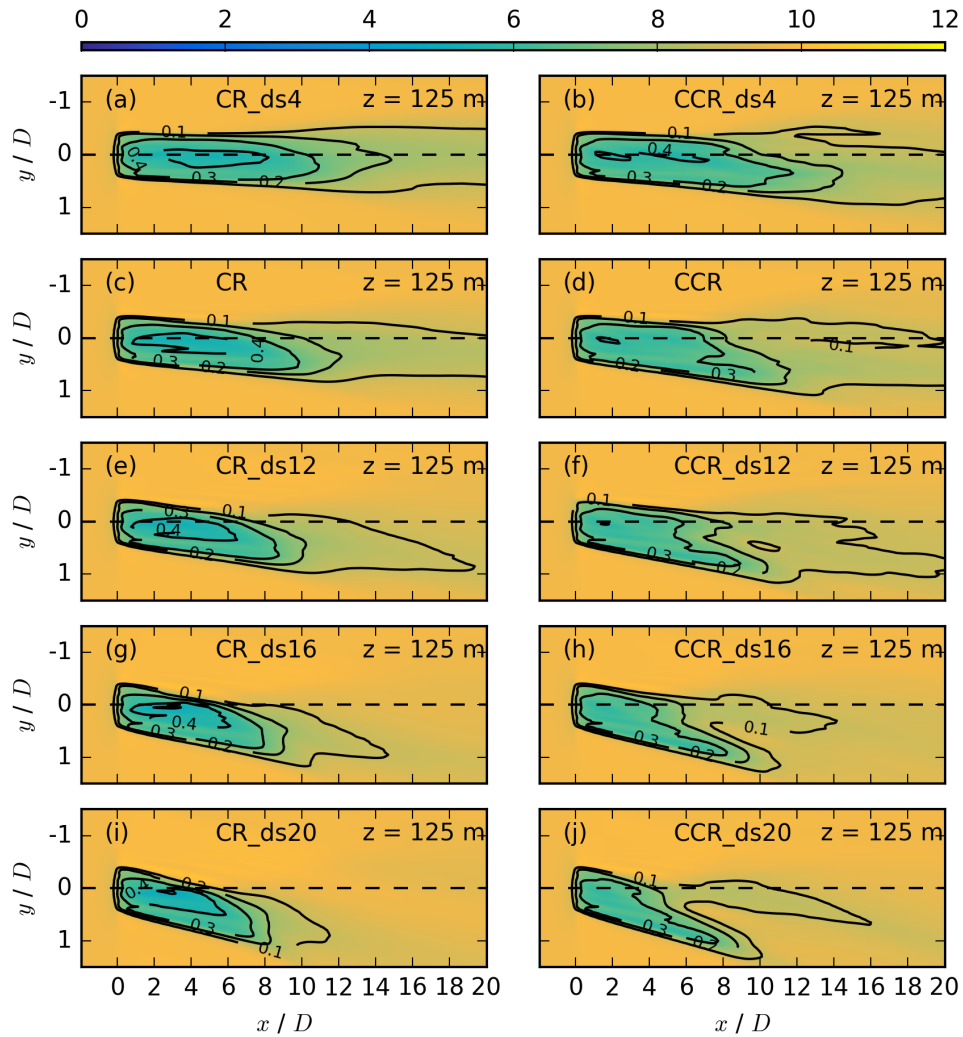


**Figure 11.** Contours of the streamwise velocity  $\overline{u_{i,j,k^*}}$  in  $\text{m s}^{-1}$  for different directional shears at  $z = 125 \text{ m}$  for the same simulations as in Fig. 10. The black contours represent the velocity deficit  $VD_{i,j,k^*}$  at the same vertical location.

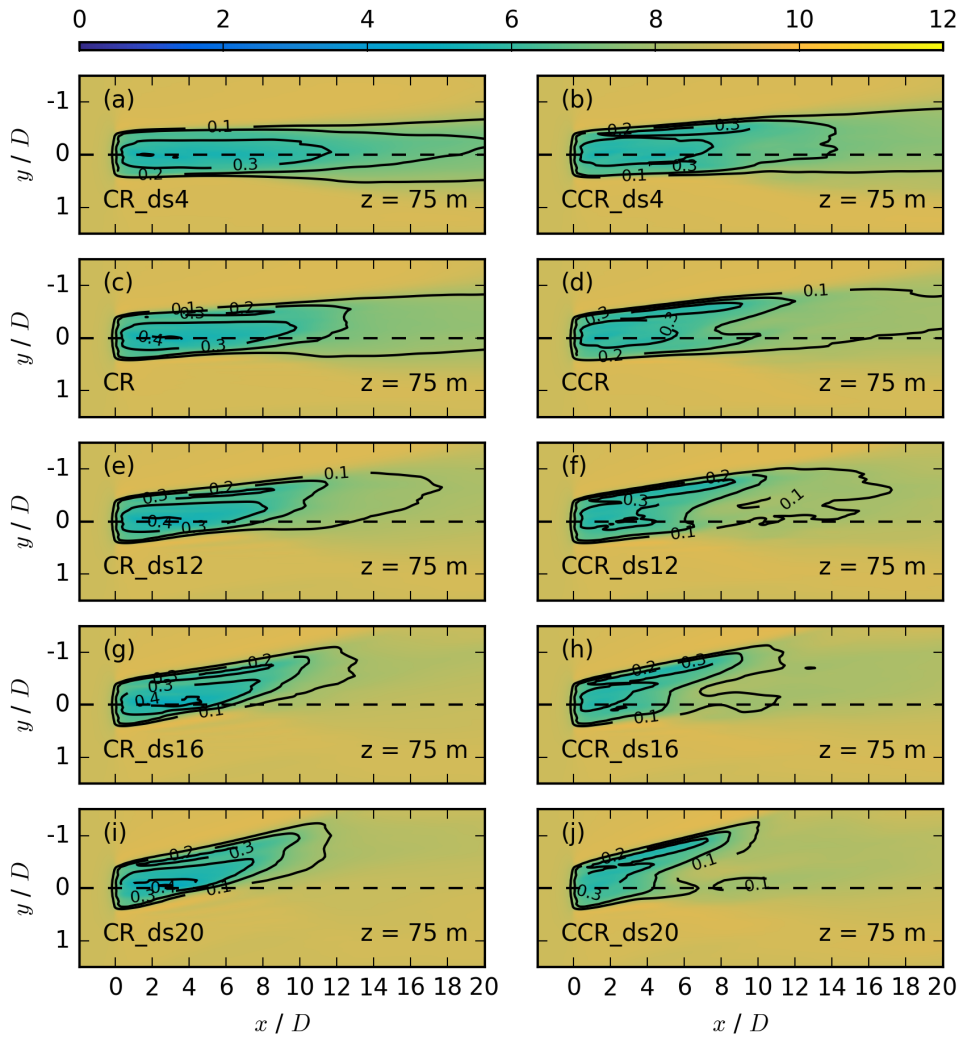


**Figure 12.** Contours of the streamwise velocity  $\overline{u_{i,j,k}}$  in  $\text{m s}^{-1}$  for different directional shears at  $z = 75 \text{ m}$  for the same simulations as in Fig. 10. The black contours represent the velocity deficit  $VD_{i,j,k}$  at the same vertical location.

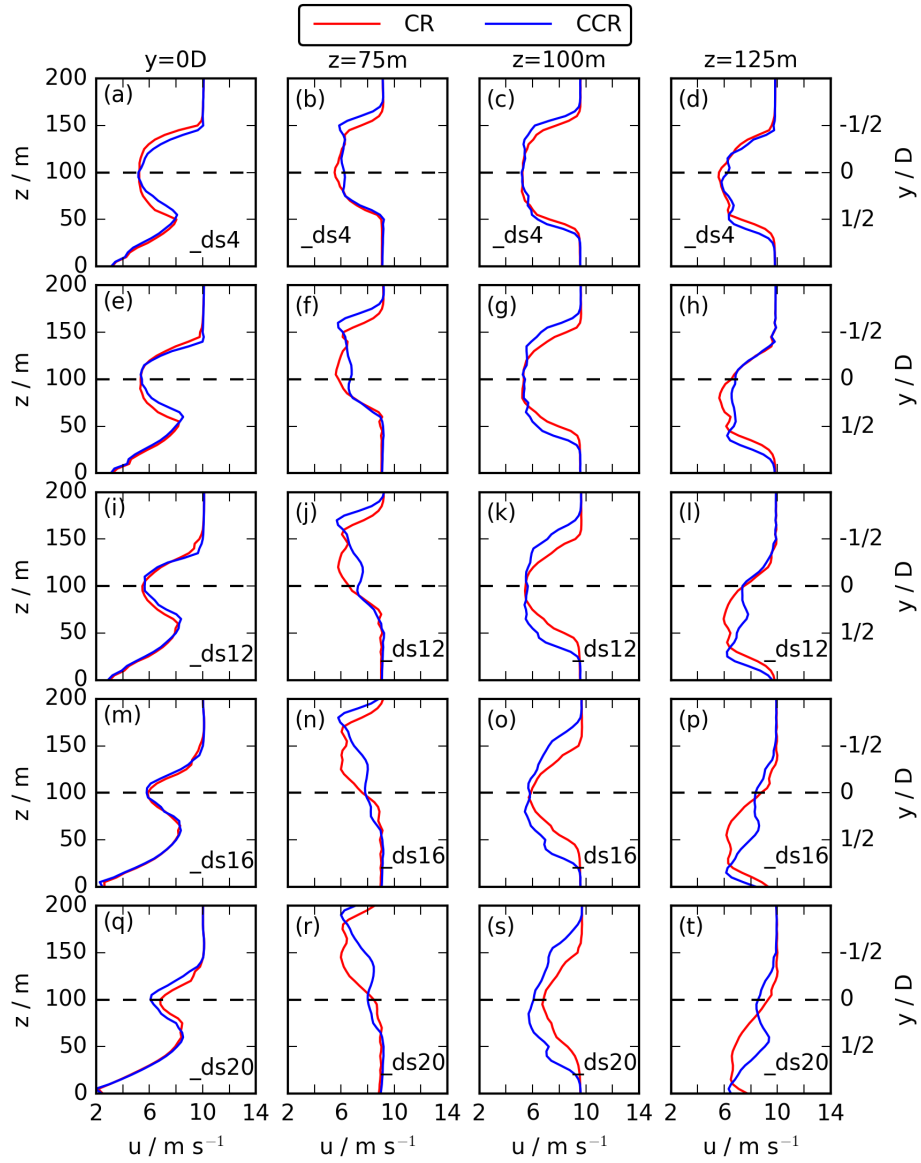


**Figure 13.** Vertical (first column) and horizontal profiles at  $z=75$  m (second column),  $z=100$  m (third column), and  $z=125$  m (fourth column) of the 30 min averaged streamwise velocity at  $x=7D$  downwind of the actuator for a directional shear of  $0.04^\circ \text{ m}^{-1}$  in (a)-(d),  $0.08^\circ \text{ m}^{-1}$  in (e)-(h),  $0.12^\circ \text{ m}^{-1}$  in (i)-(l),  $0.16^\circ \text{ m}^{-1}$  in (m)-(p), and  $0.20^\circ \text{ m}^{-1}$  in (q)-(t).

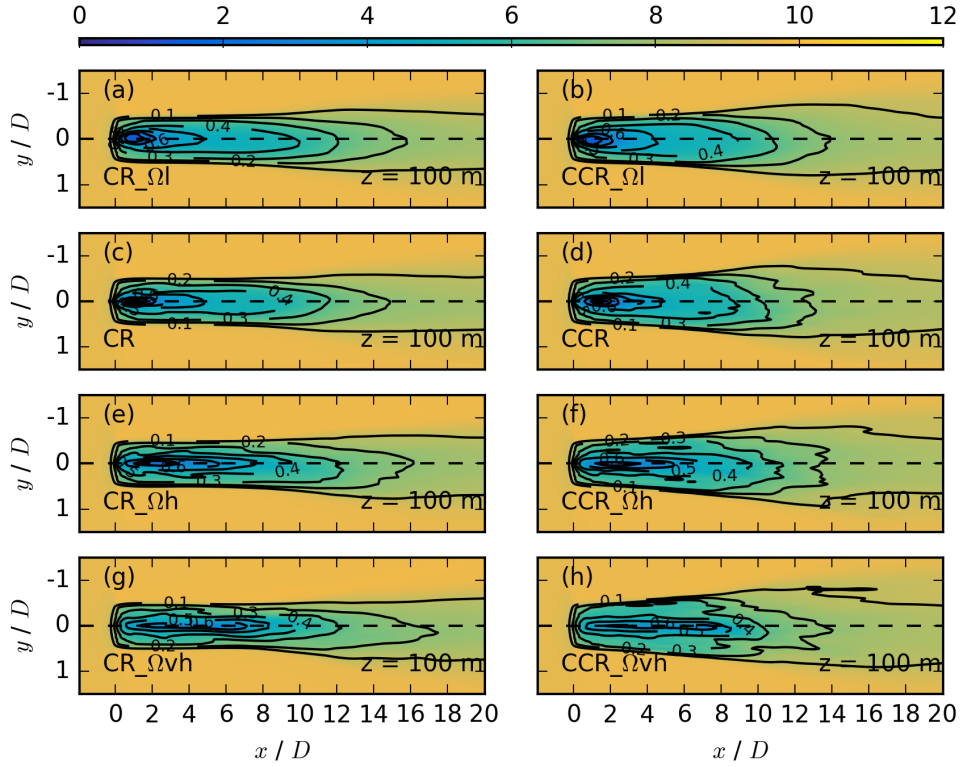


**Figure 14.** Contours of the streamwise velocity  $\overline{u_{i,j,k}}$  in  $\text{m s}^{-1}$  for different rotational frequencies at  $z = 100 \text{ m}$  for CR\_Ωl in (a), CCR\_Ωl in (b), CR in (c), CCR in (d), CR\_Ωh in (e), CCR\_Ωh in (f), CR\_Ωvh in (g), and CCR\_Ωvh in (h), each averaged over 30 min. The black contours represent the velocity deficit  $VD_{i,j,k}$  at the same vertical location.

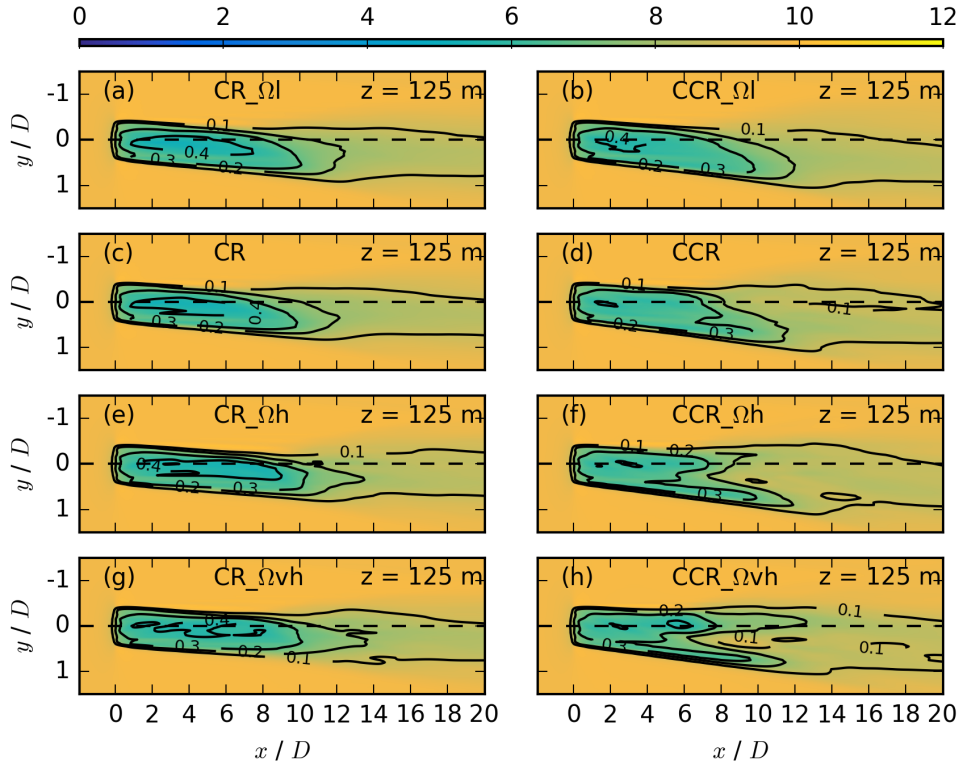


**Figure 15.** Contours of the streamwise velocity  $\overline{u_{i,j,k}}$  in  $\text{m s}^{-1}$  for different rotational frequencies at  $z = 125 \text{ m}$  for the same simulations as in Fig. 14. The black contours represent the velocity deficit  $VD_{i,j,k}$  at the same vertical location.

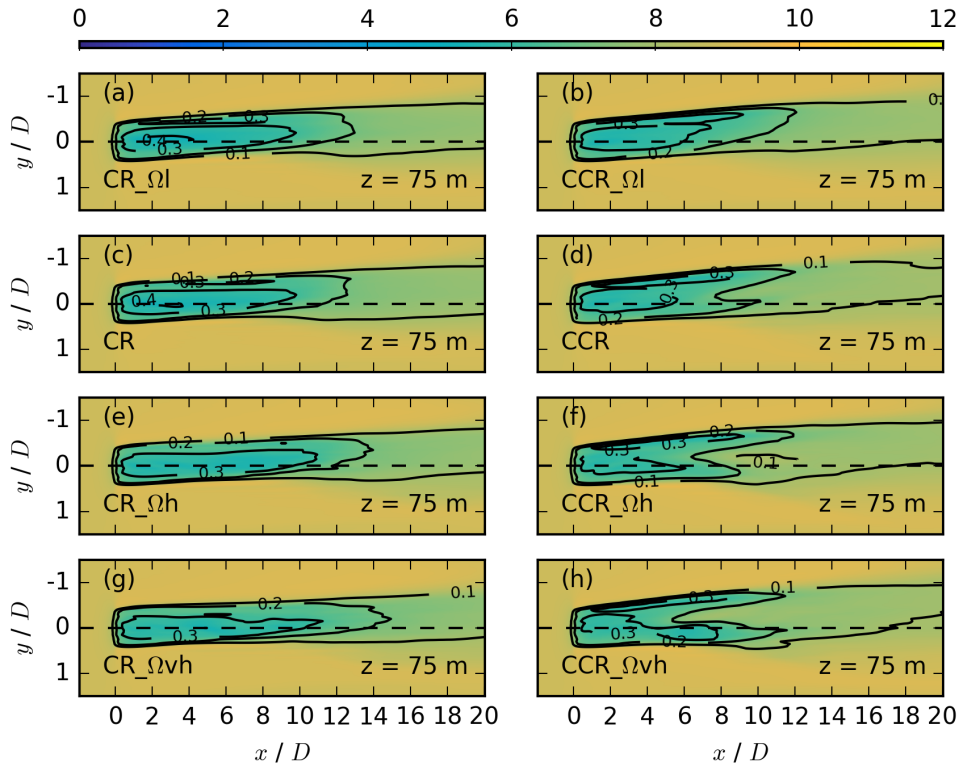


**Figure 16.** Contours of the streamwise velocity  $\overline{u_{i,j,k}}$  in  $\text{m s}^{-1}$  for different rotational frequencies at  $z = 75 \text{ m}$  for the same simulations as in Fig. 14. The black contours represent the velocity deficit  $VD_{i,j,k}$  at the same vertical location.

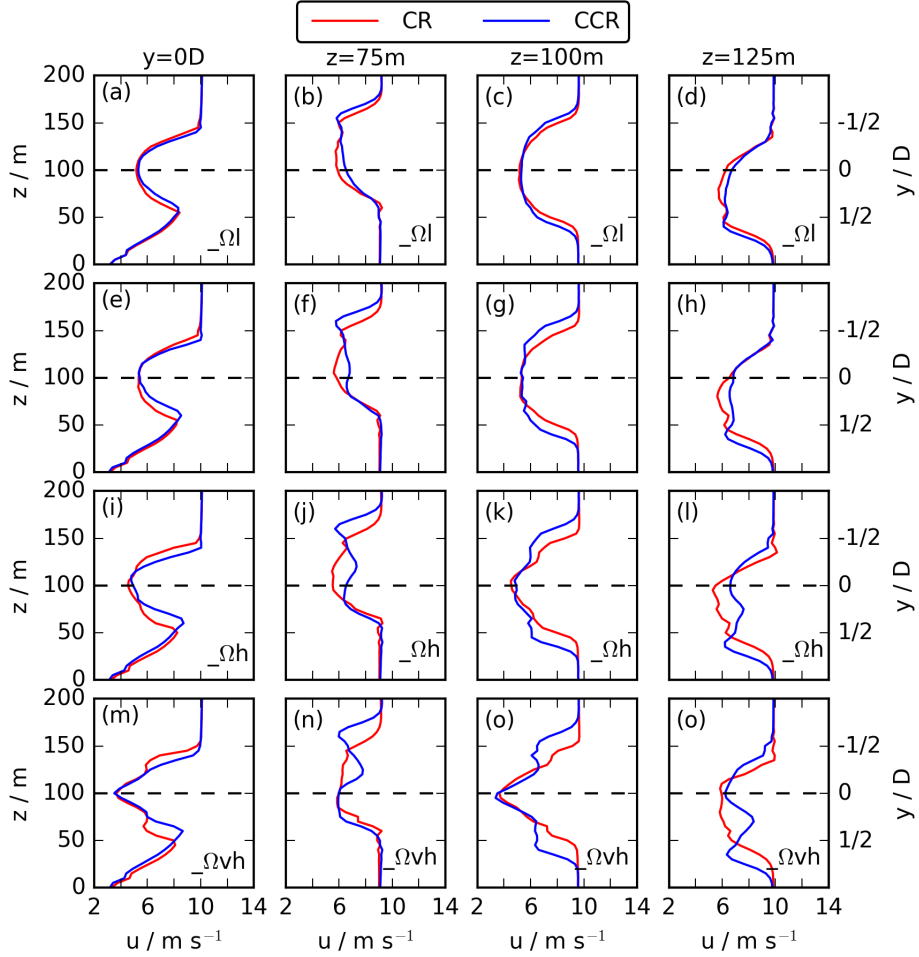


**Figure 17.** Vertical (first column) and horizontal profiles at  $z=75$  m (second column),  $z=100$  m (third column), and  $z=125$  m (fourth column) of the 30 min averaged streamwise velocity at  $x=7D$  downwind of the actuator for a rotational frequency of  $\Omega=0.058^\circ \text{ s}^{-1}$  in (a)-(d),  $\Omega=0.12^\circ \text{ s}^{-1}$  in (e)-(g),  $\Omega=0.175^\circ \text{ s}^{-1}$  in (i)-(l), and  $\Omega=0.23^\circ \text{ s}^{-1}$  in (m)-(o).

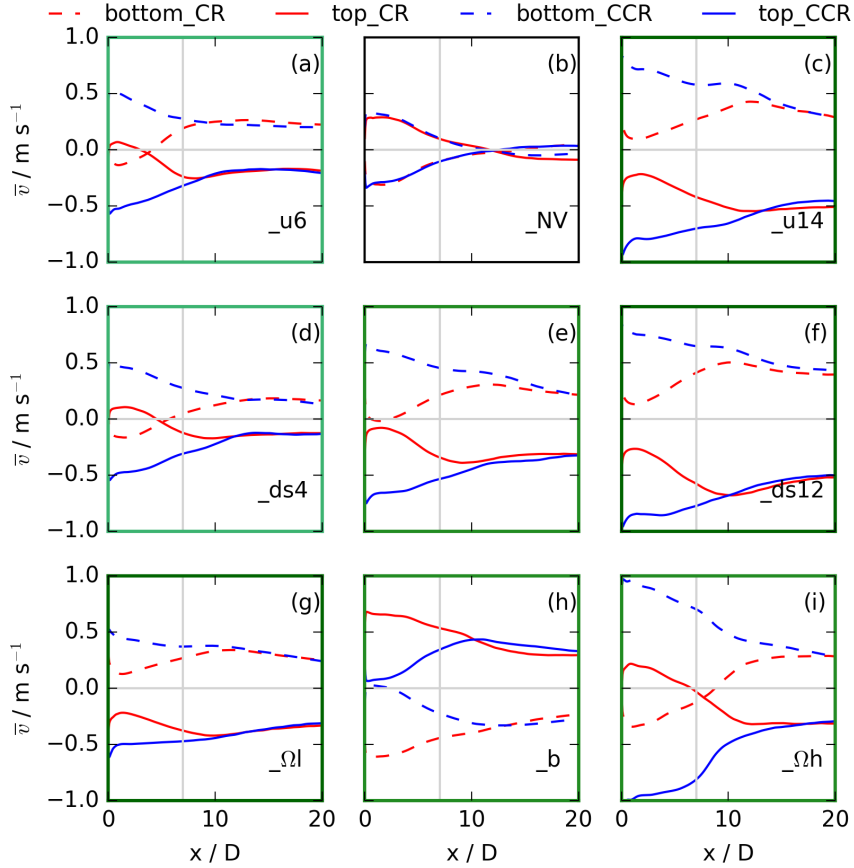


**Figure 18.** Sector averages of  $\bar{v}$  representing the top and bottom  $90^\circ$ -sectors for  $0 \text{ m} < r < 50 \text{ m}$  for clockwise and counterclockwise rotating actuators in the corresponding simulation of no veer in (b), a veering wind in (e) and a backing wind in (h). In the case of a veering wind in (c), moderate parameters of  $u_g = 10 \text{ m s}^{-1}$ ,  $ds = 0.08^\circ \text{ m}^{-1}$ , and  $\Omega = 0.12^\circ \text{ s}^{-1}$  are applied. In the left and right column, only one parameter is changes compared to the veering wind situation in (e). Applying low parameters  $u_g = 6 \text{ m s}^{-1}$  in (a),  $ds = 0.04^\circ \text{ m}^{-1}$  in (d), and  $\Omega = 0.058^\circ \text{ s}^{-1}$  in (g), and applying high parameters  $u_g = 14 \text{ m s}^{-1}$  in (c),  $ds = 0.12^\circ \text{ m}^{-1}$  in (f), and  $\Omega = 0.175^\circ \text{ s}^{-1}$  in (i). The plot is directly comparable to Fig. 2 considering the configurations.

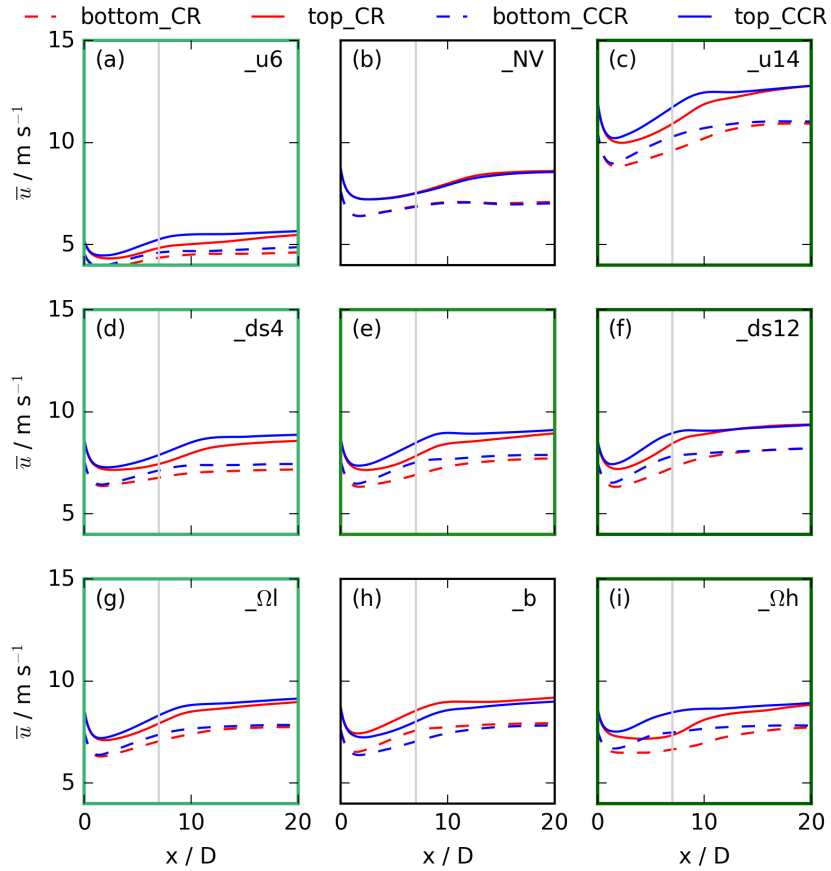


**Figure 19.** Sector averages of  $\bar{u}$  representing the top and bottom  $90^\circ$ -sectors for  $0 \text{ m} < r \leq 50 \text{ m}$  for clockwise and counterclockwise rotating actuators for the same simulations as in Fig. 18.

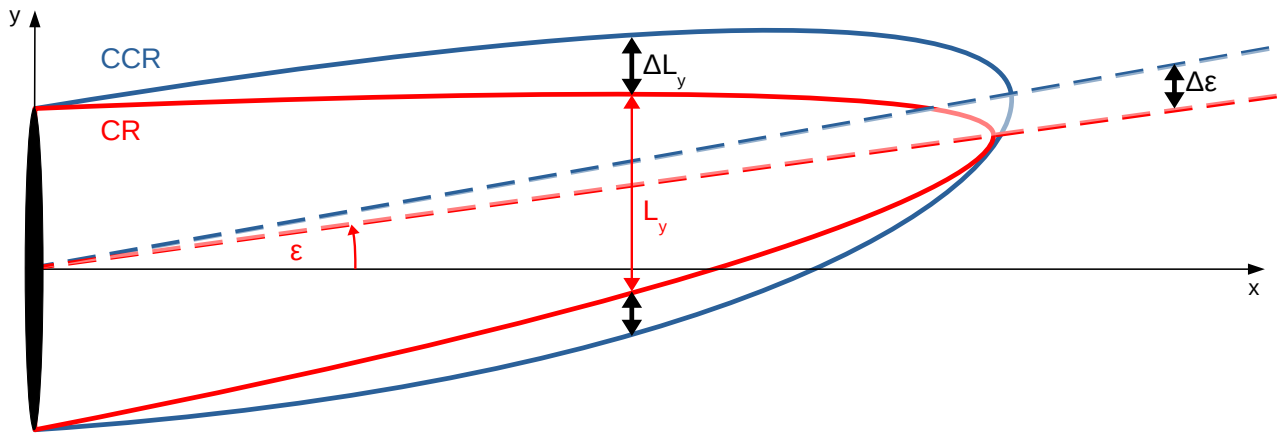


**Figure 20.** Schematic illustration of the difference in the spanwise wake width ( $L_y$ ) and the wake deflection angle ( $\epsilon$ ) between clockwise CR and counterclockwise CCR rotating actuators. The parameter impact on these wake differences is represented by  $\Delta L_y$  and  $\Delta \epsilon$ .

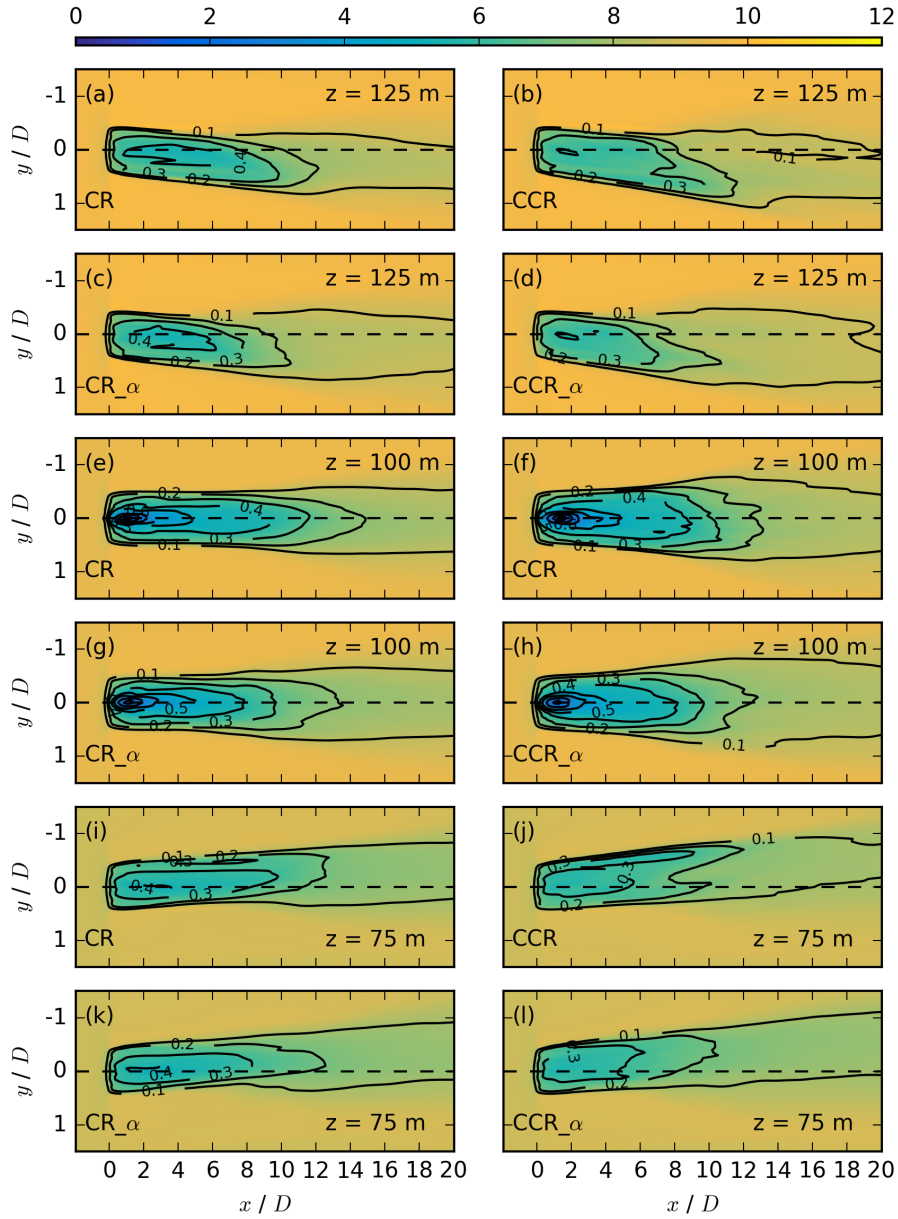


**Figure A1.** Contours of the streamwise velocity  $\overline{u_{i,j,k^*}}$  in  $\text{m s}^{-1}$  at  $z = 125$  m in the first two rows, at  $z = 100$  m the the third and fourth row, and at  $z = 75$  m in the last two rows for the simulations CR, CCR, CR $_{\alpha}$  and CCR $_{\alpha}$ , each averaged over 30 min. The black contours represent the velocity deficit  $VD_{i,j,k^*}$  at the same vertical location.